INTERACTION NOTES

Note 224

February 1975

A NEW INTEGRAL EQUATION SOLUTION OF ELECTROMAGNETIC APERTURE COUPLING AND THIN PLATE SCATTERING PROBLEMS

Y. Rahmat-Samii
R. Mittra

University of Illinois

ABSTRACT

The problems of aperture diffraction in an infinite screen, aperture coupling into a two-parallel-plate region, and scattering by infinitely thin planar scatterers in intermediate and low frequency regions are investigated in a unified fashion. Dyadic Green's functions for a two-parallel-plate region and a semi-infinite space are constructed, using the theory of images. By employing the dyadic formalism and enforcing the continuity of the tangential derivative of the normal E-field and the normal derivative of the tangential E-field, a new set of integral equations is derived to formulate the aperture diffraction and coupling phenomena. In these integral equations, not possessing any differential operator, the tangential components of the aperture E-field are decoupled. Furthermore, the interaction of the aperture rim with the incident field is accounted for by introducing a special set of homogeneous terms in the formulation. The application of the so-called edge condition is eliminated and, instead, the unique solution of the problem is determined by imposing the obvious condition that the tangential component of the E-field at the rim is zero. Similar integral equations are constructed for the scattering problem of infinitely thin and planar

scatterers using vector potential formulation and enforcing the condition that both the E-tangential and H-normal are zero on the structure.

The structurally simple nature of the new integral equations makes them numerically attractive. The method of moments is used as a basic technique of digitizing the integral equations for numerical solution. Numerical results for diffracted fields of an aperture in a single screen and in a two-parallel-plate region are presented for various aperture dimensions and incident fields, and compared with other available numerical and experimental data. The time domain response of apertures, subject to an EMP, is also computed. In addition, some numerical results are presented for the induced current and RCS computation of rectangular scatterers. These results are compared with other RCS computations using the geometrical theory of diffraction, physical optics, and variational methods.

The new integral equations are quite suitable for low-frequency diffraction problems. The resolution of these problems is reduced to solving a sequence of successive integral equations which possess an electrostatic-type kernel. The first few terms of the Rayleigh series expansion are determined analytically for a circular aperture illuminated by an obliquely incident plane wave. The low frequency results of rectangular apertures are computed and their similarities with those of circular apertures are shown.

ACKNOWLEDGMENT

This research was supported by Harry Diamond Laboratories, Washington, D.C.

TABLE OF CONTENTS

LIST OF FIGURES

LIST OF TABLES

1. INTRODUCTION

The diffraction problem has received considerable attention in the existing literature on the theory of electromagnetism. Advances in understanding this problem span almost one century and clearly show the inherent consistency between the laws of electromagnetism dictated by nature and the abstract mathematical formulations expressed through Maxwell's equations. Mathematically speaking, electromagnetic diffraction problems are classified as well-posed boundary value problems of the second order. Since there is not a universal approach for rigorously solving these boundary-value problems in a general case, a variety of analytical and approximate methods has been studied by researchers depending on the technological needs and facilities of their eras. These methods are best presented for description if the domain of the interaction between monochromatic electromagnetic fields and the material realm is divided into three regions: (i) high frequency region, where the wavelengths considered are small compared with the characteristic dimensions of the diffracting aperture (obstacle), (ii) intermediate (resonance) frequency region, where the wavelengths used are of the same order as the aperture (obstacle) dimensions, and finally (iii) low frequency region, where the wavelengths considered are long compared with the aperture (obstacle) dimensions.

The number of publications that have appeared either as scientific papers or books in analyzing the diffraction phenomenon in the above three regions is so voluminous that listing them alone may fill up a book. This, of course, does not indicate that the subject is closed and that everything has been done, but instead, reveals the vast number of theoretical attempts in relation to time as technology progresses, and

as science undertakes to fulfill the current technological needs. A brief discussion of each of the three previously mentioned regions is now given.

In the high frequency region, Kirchhoff's mathematical formulation of Huygens' principle (1891) pioneered the first reasonably rigorous mathematical description of the aperture diffraction problem. However, because of its scalar nature, this formulation did not account for the polarization of the incident field, and hence there has been an extensive amount of work which modified Kirchhoff's formulation. For instance, Kottler (see Baker and Copson, 1953) introduced certain contour integrals along the rim of the aperture to take into account the vector characteristic of the diffraction phenomenon, and the vector equivalents of Kirchhoff's formulation have been discussed in the literature, e.g., Jackson (1962). Most of these modifications are poor substitutes for the rigorous diffraction theory because they do not correctly describe the field in the vicinity of the aperture and the edge. Currently, the high frequency diffraction problems are treated by an application of one of the several different asymptotic methods that are available in the literature. Notable among these are physical optics, edge wave theory (Ufimtsev, 1962) and the geometric theory of diffraction (Keller, 1962). A review of ray techniques, including Keller's Geometric Theory of Diffraction, is given by Deschamps (1972). The interested reader is referred to the excellent bibliographies assembled by Uslenghi (1972) on this subject.

In the low frequency region, Lord Rayleigh (1897) was able to establish the first quasistatic solution for the diffraction problem. His method was based on the application of a series, named after him,

the Rayleigh series. Later, Bethe (1944), Stevenson (1953), Bouwkamp (1953, 1970), Kleinman (1967) and others used Rayleigh's series to analyze the low frequency diffraction problems. It has been found that the low frequency analysis offers much insight into the diffraction phenomenon. The interested reader is referred to the bibliographies given by Eggiman (1961) and those prepared by Van Bladel (1974).

In the intermediate (resonance) frequency region, application of the integral equation method has attracted considerable attention. The integral equation is compact, has the important feature that the boundary, as well as radiation condition, are incorporated into its formulation. Classically, integral equations were solved by employing various approximate techniques, e.g., variational method (Levine and Schwinger, 1950), and successive approximations (Suzuki, 1956). However, the advent of high-speed computers has changed the philosophy of attacking these problems considerably. Most of the current numerical techniques are essentially based on the application of the method of moments (Harrington, 1968) which has been shown to be an effective technique in solving the integral equations encountered in the theory of electromagnetism (Mittra, 1973). Although much has been written in this area concerning the linear antennas and closed scatterers, very little has been done for aperture coupling problems and scattering by infinitely thin open structures. The primary difficulties in handling these problems are the applications of the conventional integral equations, which have been found unsuitable when applying numerical techniques.

The purpose of this work is to study the aperture diffraction problem, aperture coupling into a two-parallel-plate region, and scattering by infinitely thin planar structures in the intermediate and low fre-

quency regions in a unified fashion. The method of investigation is based on a new set of integral equations which describes the diffraction phenomenon completely, but is structurally simpler than conventional ones. Results are presented for circular and rectangular geometries as two representative examples. A brief summary of the discussions covered in each chapter is given in the following paragraphs.

In Chapter 2, the mathematical description of the problem of electromagnetic coupling via apertures into a homogeneously filled cavity region is presented. Using dyadic formulation, a complete set of mathematical formulas is constructed to determine the diffracted field that would exist in the inner and outer regions of the cavity if the cavity were illuminated by an incident electromagnetic field. It is shown that the knowledge of the tangential E-field in the apertures will be sufficient for determining the diffracted fields everywhere. Furthermore, the mathematical procedure for deriving the dyadic Green's function for a two-parallel-plate region is demonstrated. This construction is then simplified to give the well-known half-space dyadic Green's function.

The problem of diffraction by apertures in a perfectly conducting screen is formulated in Chapter 3. By using the dyadic representation and enforcing the condition that the tangential components of E- and H-fields must be continuous in crossing the aperture, a new set of integral equations is constructed to determine the tangential E-field in the aperture. These equations are structurally simple and quite suitable for numerical applications. Another important feature of these integral equations is that the necessity of accounting for the so-called edge condition is eliminated and, instead, the obvious requirement that the field induced in the aperture must have no component tangential at the

edge is enforced. Although the formulation obtained in this chapter is valid for any aperture shape, the numerical results are primarily calculated for rectangular apertures. Previously, these geometries had not been investigated thoroughly, though they have significant practical applications. Numerical computations are carried out, applying the method of moments, which reduces the integral equations to matrix equations. Results are presented for the E-field distribution in the aperture and the diffracted field of the aperture for a variety of aperture sizes and incident field. Comparison is made with available experimental and theoretical results. Finally, some numerical results for the diffracted field due to an EMP (electromagnetic pulse) incident field are constructed by applying the FFT (fast Fourier transformation) algorithm, which converts the frequency domain data into the corresponding time domain data.

Since the understanding of diffraction of electromagnetic waves by electrically small apertures does provide considerable insight into the diffraction phenomenon, Chapter 4 is concerned with this investigation. The analysis, which employs the integral equations constructed in Chapter 3, demonstrates that these integral equations are indeed in a very suitable form when the low frequency limits are considered. Using the well-known Rayleigh series expansion, the solution of the integral equations is reduced to solving a sequence of successive integral equations which possess an electrostatic-type kernel. As an example, the classical problem of diffraction by an electrically small circular aperture is investigated in detail. For this geometry, analytical solutions are constructed in a systematic fashion, and results are presented for the first few terms of the Rayleigh series expansion. The computational

procedure for obtaining the electric and magnetic dipole moments is also discussed. This chapter finally closes by presenting some results describing the behavior of the induced and diffracted fields of an electrically small, rectangular aperture.

Chapter 5 is concerned with the problem of scattering of electromagnetic waves by infinitely thin and perfectly conducting scatterers. These structures are considered electromagnetically complementary to apertures perforated in an infinitely conducting screen. Though it is possible to apply Babinet's principle and construct the mathematical formulas that describe the behavior of the induced current in the structure, an alternative approach is presented in this chapter. This approach is based on the application of the vector potential, and in contrast to the conventional derivations, incorporates the fact that both E-tangential and H-normal must be zero on the structure. A set of integral equations, which are structurally similar to those obtained in Chapter 3, is derived. These equations are solved in conjunction with the condition that the normal component of the current distribution must be zero at the rim of the structure to determine the unique solution of the problem. Numerical results are presented for the induced current distribution on rectangular scatterers of different sizes due to the variety of incident fields. Finally, numerical results for the RCS (radar cross section) computation are given and compared with those based on GTD (geometrical theory of diffraction), PO (physical optics), and variational methods.

The problem of electromagnetic coupling by apertures into a two-parallel-plate cavity region is considered in Chapter 6. By using the dyadic formulation established in Chapter 2 and following the procedure

developed in Chapter 3, a set of integral equations is derived to determine the induced tangential E-field in the aperture. Due to the complexity of the kernel of the integral equation, its behavior around the resonant separations of the two parallel plates is investigated in detail. Numerical results finally demonstrate the behavior of the aperture E-field and the diffracted field in the two-parallel-plate region for different aperture sizes and different two-parallel-plate separations.

2. MATHEMATICAL FORMULATION OF THE ELECTROMAGNETIC DIFFRACTION BY APERTURES INTO CAVITIES

2.1 Introduction

This chapter is concerned with the behavior of the electromagnetic fields in the presence of perfectly conducting structures. The discussion is mainly devoted to investigation of the proper mathematical formulation which governs the behavior of electromagnetic fields diffracted by apertures into cavity regions. This problem may be considered as a subclass of the vector boundary value problems that appear in different branches of mathematical physics. This class deals with vector sources and vector boundary conditions. Since a vector source radiates a vector field, the relationship between them is best described by employing the dyadic formalism. Thus, in this chapter, the complete formulation of the problem will be demonstrated by using the dyadic formalism as a mathematical tool. The reader is referred to the works of Levine and Schwinger (1950), Morse and Feschbach (1953), Van Bladel (1964), Jones (1964), Tai (1971), and others who have applied the dyadic formulation within the theory of electromagnetism. In this chapter, the construction of the dyadic Green's function for the two-parallel-plate region will also be presented. In conclusion, this construction will then be used to generate the dyadic Green's function of the semi-infinite space.

2.2 Statement of the General Problem

The geometry of the structure under consideration in this section, which is shown in Figure 2.1, is a cavity with an aperture in its shell. Letter A is used to designate an open set containing the points in the aperture resulting from an obvious extension of the shell, and symbol $\bar{A}$

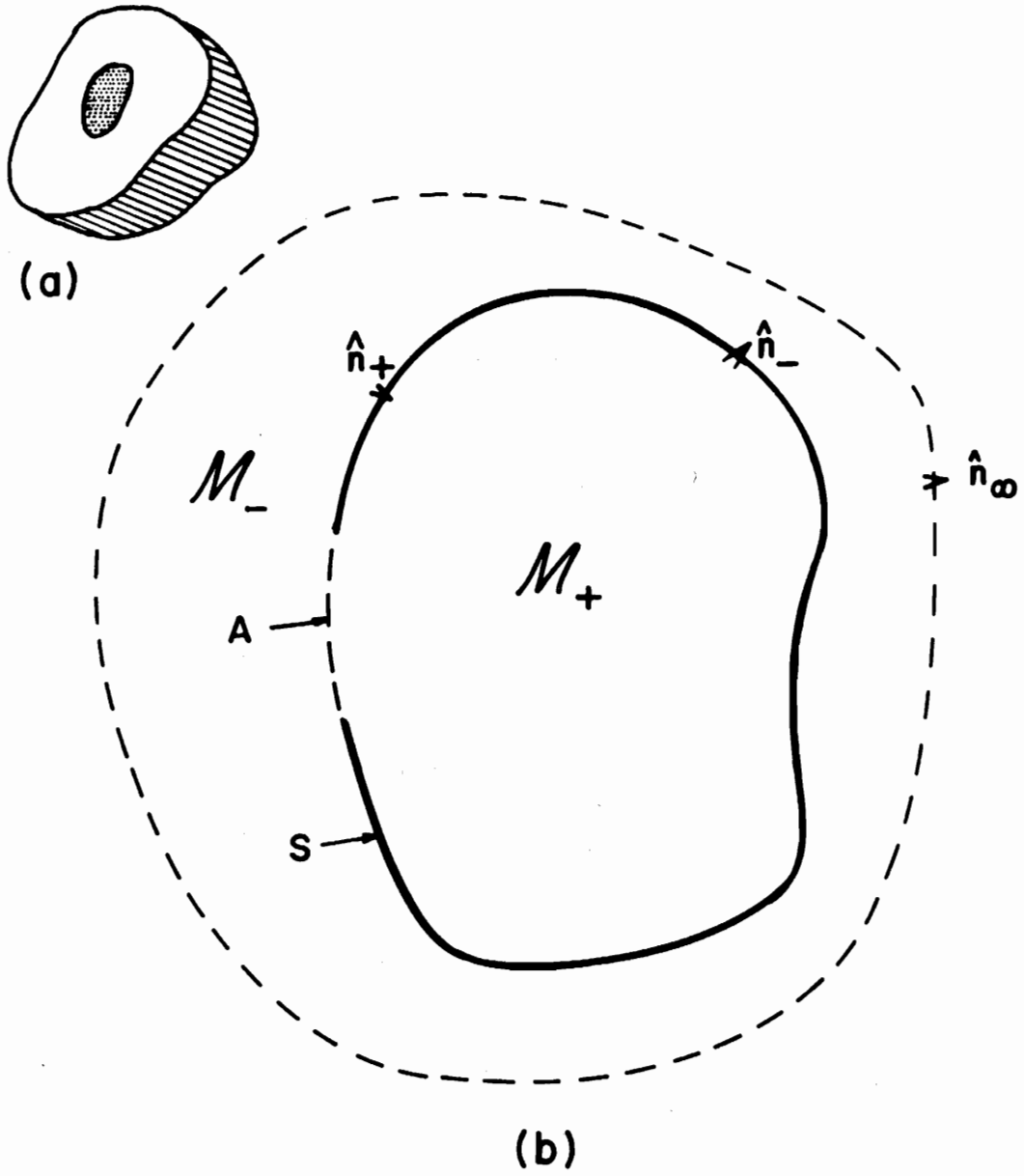

Figure 2.1. (a) Aperture in a cavity. (b) Cross-sectional view of (a) where $\mathcal{M}_-$ and $\mathcal{M}_+$ are exterior and interior regions, respectively; A is the aperture and S is the surface of the cavity.

is used to specify a closed set, constructed from A and its rim. The shell itself is denoted by S, which is an open set. Letter C is used to designate all the points belonging to the rim. Therefore, the entire manifold $\mathcal{M}$ may be defined as

$$\mathcal{M} = A \cup C \cup S = \bar{A} \cup S \quad . \tag{2.1}$$

Symbols $\mathcal{M}_-$ and $\mathcal{M}_+$ are used to indicate the exterior and interior regions of the manifold, respectively. It is assumed that $\mathcal{M}_-$ and $\mathcal{M}_+$ are filled with a homogeneous and isotropic medium, and that S is made of a perfectly conducting material.

Having described the necessary parameters that define the geometry of the structure, the general problem can then be stated as follows: What information is necessary about the electromagnetic fields in $\bar{A}$ so that one can determine the fields in $\mathcal{M}_-$ and $\mathcal{M}_+$ due to an incident electromagnetic field? The answer to this question will be clear in the next section, where one proceeds to learn that the knowledge of the tangential E-field in $\bar{A}$ will be sufficient for determining the electromagnetic fields in $\mathcal{M}_-$ and $\mathcal{M}_+$.

2.3 Formulation of the General Problem

The starting point of this section is Maxwell's equations. Perhaps these equations are one of the most celebrated sets of equations appearing in mathematical physics. These equations enable one to predict almost all possible behaviorsof the electromagnetic fields occurring at the present time. In the flat space geometry, Maxwell's equations are expressed as

$$\begin{pmatrix} \nabla x & j\omega\mu \\ -j\omega\varepsilon & \nabla x \end{pmatrix} \begin{pmatrix} \vec{E} \\ \vec{H} \end{pmatrix} = \begin{pmatrix} -\vec{K} \\ +\vec{J} \end{pmatrix} \tag{2.2}$$

where ε and μ are permittivity and permeability of the medium, respectively, and the time dependence $e^{j\omega t}$ is suppressed in the formulation. It will be more convenient for later discussions to eliminate, for instance, the H-field between the coupled-equation (2.2), and to derive the following inhomogeneous vector wave equation for the E-field:

$$(\nabla \times \nabla \times -k^2)\ \vec{E} = -\nabla \times \vec{K} - j\omega\mu\vec{J} \quad . \tag{2.3}$$

The above vector partial differential equation with a proper set of boundary conditions must be solved to give the unique solution to any problem appearing in the theory of electromagnetism. In fact, the problem is not as simple as stated here, and all the available materials in the theory of electromagnetism have been written for prescribing different techniques in order to solve Equation (2.3) for the cases of interest.

In this work, the dyadic Green's function technique is used to set up an integral representation to solve Equation (2.3), subject to the proper boundary conditions. These boundary conditions will be introduced shortly. The dyadic Green's function $\bar{\bar{G}}(\vec{R}|\vec{R}')$ is defined as a solution of the following inhomogeneous vector wave equation

$$(\nabla \times \nabla \times -k^2)\ \bar{\bar{G}}(\vec{R}|\vec{R}') = \bar{\bar{I}}\delta(\vec{R} - \vec{R}') \tag{2.4}$$

where $\bar{\bar{I}}$ is the unit dyadic and δ is the Dirac delta distribution. It is noted that $\nabla \cdot \bar{\bar{G}}(\vec{R}|\vec{R}') \neq 0$, and hence $\bar{\bar{G}}(\vec{R}|\vec{R}')$ does not satisfy the inhomogeneous Helmholtz equation, viz.,

$$(\nabla^2 + k^2)\ \bar{\bar{G}}(\vec{R}|\vec{R}') \neq -\bar{\bar{I}}\delta(\vec{R} - \vec{R}') \quad . \tag{2.5}$$

For more detailed discussion regarding the application of the proper dyadic Green's function, the reader is referred to the work done by Rahmat-Samii (1974).

In order to establish a relationship between $\vec{E}$ and $\bar{\bar{G}}$, the Green's theorem in dyadic notation is used. This theorem may be best presented by introducing the following formula:

$$\iiint_V [\vec{E} \cdot \nabla \times \nabla \times \bar{\bar{G}} - \nabla \times \nabla \times \vec{E} \cdot \bar{\bar{G}}] \, dv = -\iint_{\partial V} \hat{n} \cdot [\vec{E} \times \nabla \times \bar{\bar{G}} + (\nabla \times \vec{E}) \times \bar{\bar{G}}] \, da \tag{2.6}$$

where, in Equation (2.6), V denotes the domain of volume integration, ∂V designates the closed surface surrounding the volume V and $\hat{n}$ is the outward unit normal to the boundary ∂V. The proof of the above theorem and application of some useful operations on dyadics are discussed in Appendix A.

Given the Green's dyadic formula, the reader is now referred to the geometry shown in Figure 2.1. For a complete analysis concerning the derivation of an integral representation, two different cases will be discussed in the following sections. First, Green's theorem will be applied to the region $\mathcal{M}_+$, which is a bounded region. Second, Green's theorem will be applied to the region $\mathcal{M}_-$, which is an unbounded region. This analysis will finally lend itself to the introduction of the proper boundary condition on the dyadic Green's function.

2.3.1 Field analysis in the interior region $\mathcal{M}_+$

In this section, the domain of analysis is restricted to the points $\{\vec{R}: \ (x,y,z) \in \mathcal{M}_+\}$. Let us introduce $\bar{\bar{G}}_+$, $\bar{E}_+$ and $\hat{n}_-$ as an interior dyadic Green's function, the interior electric field, and the outward unit normal, respectively. In applying Equation (2.6), the volume of

integration V becomes $\mathcal{M}_+$ and the surface ∂V becomes $\mathcal{M}$. Substituting Equations (2.3) and (2.4) in (2.6) and simplifying the resulting equation, one obtains

$$\vec{E}_+(\vec{R}) = \iiint_{\mathcal{M}_+} [-\nabla' \times \vec{K}_+ - j\omega\mu\vec{J}_+] \cdot \bar{\bar{G}}_+(\vec{R}'|\vec{R})\, dv'$$

$$- \iint_{\mathcal{M}} \hat{n}_- \cdot [\vec{E}_+ \times \nabla' \times \bar{\bar{G}}_+(\vec{R}'|\vec{R}) + (\nabla' \times \vec{E}_+) \times \bar{\bar{G}}_+(\vec{R}'|\vec{R})]\, da' \qquad (2.7)$$

where, as one recalls, $\mathcal{M} = \partial\mathcal{M}_+$. In the above equation the prime symbol is used to indicate the operations on the prime coordinates, i.e., source coordinates.

Since the shell S is assumed to be a perfectly conducting material, $\vec{E}_+$ will satisfy the following boundary condition:

$$\hat{n}_- \times \vec{E}_+ = 0 \qquad \{\vec{R}: \ (x,y,z) \in S\} \ . \qquad (2.8)$$

Now there is enough information to make a proper decision about the boundary condition of $\bar{\bar{G}}_+(\vec{R}'|\vec{R})$. Because, in general, the term $\nabla' \times \vec{E}_+$, defined in Equation (2.7), is not known on $\mathcal{M}$, it will be desirable to eliminate this term. This can be done by imposing the following boundary condition on the dyadic Green's function, i.e.,

$$\hat{n}_- \times \bar{\bar{G}}_+(\vec{R}|\vec{R}') = 0 \qquad \{\vec{R}: \ (x,y,z) \in \mathcal{M}\} \ . \qquad (2.9)$$

Substituting (2.8) and (2.9) into (2.7) one finally derives the desirable equation for the computation of the E-field in the interior region as follows:

$$\vec{E}_+(\vec{R}) = \iiint_{\mathcal{M}_+} [-\nabla' \times \vec{K}_+ - j\omega\mu\vec{J}_+] \cdot \bar{\bar{G}}_+(\vec{R}'|\vec{R})\, dv'$$

$$- \iint_{\bar{A}} (\hat{n}_- \times \vec{E}_+) \cdot \nabla' \times \bar{\bar{G}}_+(\vec{R}'|\vec{R})\, da' \qquad \{\vec{R} : (x,y,z) \in \mathcal{M}_+\} \quad . \tag{2.10}$$

It is noted that the surface integration on the right-hand side of the above equation is performed only on the aperture region $\bar{A}$ (without affecting the result, the region of integration may be considered as A or $\bar{A}$). Perhaps the most significant characteristic of Equation (2.10) may be stated as follows: for a given source distribution $\vec{J}_+$ and $\vec{K}_+$ in the interior region $\mathcal{M}_+$, the knowledge of the tangential E-field $\hat{n}_- \times \vec{E}_+$ on the aperture $\bar{A}$ is sufficient to determine the field uniquely in the entire interior region $\mathcal{M}_+$. This result will be used in the next chapters where one deals with more specific problems.

2.3.2 Field analysis in the exterior region $\mathcal{M}_-$

In this section, the domain of analysis is restricted to the exterior points, namely, $\{\vec{R}: (x,y,z) \in \mathcal{M}_-\}$. Let $\bar{\bar{G}}_-$, $\vec{E}_-$, and $\hat{n}_+$ denote the exterior dyadic Green's function, the exterior electric field, and the outward unit normal, respectively. In order to be able to employ the dyadic Green's theorem, one must deal with a closed region. This is actually done by introducing the fictitious boundary $\mathcal{M}_\infty$, indicated by the dotted surface in Figure 2.1, to enclose the exterior region $\mathcal{M}_-$. Using Green's theorem (2.6) and denoting the exterior sources by $\vec{J}_-$ and $\vec{K}_-$, one obtains

$$\vec{E}_-(\vec{R}) = \iiint_{\mathcal{V}_-} [-\nabla' \times \vec{K}_- - j\omega\mu\vec{J}_-] \cdot \bar{\bar{G}}_-(\vec{R}'|\vec{R})\, dv'$$

$$- \iint_{\mathcal{M}} \hat{n}_+ \cdot [\vec{E}_- \times \nabla' \times \bar{\bar{G}}_-(\vec{R}'|\vec{R}) + \nabla' \times \vec{E}_- \times \bar{\bar{G}}_-(\vec{R}'|\vec{R})]\, da'$$

$$- \iint_{\mathcal{M}_\infty} \hat{n}_\infty \cdot [\vec{E}_- \times \nabla' \times \bar{\bar{G}}_-(\vec{R}'|\vec{R}) + \nabla' \times \vec{E}_- \times \bar{\bar{G}}_-(\vec{R}'|\vec{R})]\, da' \quad . \tag{2.11}$$

Comparing Equations (2.7) and (2.11) it appears that an extra surface integral must be performed in Equation (2.11).

In order to be able to evaluate the surface integral over $\mathcal{M}_\infty$, one must know the proper behavior of the E-field at infinity. It is generally known that the unique solution of Maxwell's equation can be determined by imposing the Sommerfeld radiation conditions on the electromagnetic fields as follows:

$$\lim_{R\to\infty} R\,[\nabla \times \vec{E}_- + jk\hat{R} \times \vec{E}_-] = 0 \tag{2.12}$$

which signifies that the electromagnetic fields behave as a plane wave at infinity. Condition (2.12) is actually stronger than what is really needed for fulfilling the uniqueness argument. The reader is referred to the works of Sommerfeld (1967), Wilcox (1956), Werner (1963), Van Bladel (1964), Muller (1969), and Tai (1971).

Substituting (2.12) into the surface integration as defined in Equation (2.11) and performing the integration in a spherical coordinate system one derives:

$$\iint_{\mathcal{M}_\infty} \hat{n}_\infty \cdot [\vec{E}_- \times \nabla' \times \bar{\bar{G}}_-(\vec{R}'|\vec{R}) + \nabla' \times \vec{E}_- \times \bar{\bar{G}}_-(\vec{R}'|\vec{R})]\, da'$$

$$= \lim_{R'\to\infty} \int_0^{2\pi} \int_0^{\pi} \hat{R}' \times \vec{E}_- \cdot [R'\nabla' \times \bar{\bar{G}}_-(\vec{R}'|\vec{R}) + jkR'\hat{R}' \times \bar{\bar{G}}_-(\vec{R}'|\vec{R})]\, R' \sin\theta'\, d\theta'\, d\phi', \tag{2.13}$$

The limit of the right-hand side in the above equation is zero provided the dyadic Green's function satisfies

$$\lim_{R\to\infty} R\,[\nabla \times \bar{\bar{G}}_-(\vec{R}|\vec{R}') + jk\hat{R} \times \bar{\bar{G}}_-(\vec{R}|\vec{R}')] = 0 \quad . \qquad (2.14)$$

Using the same argument as stated in the previous section, one can determine the following boundary conditions for $\vec{E}_-$ and $\bar{\bar{G}}_-(R'|R)$ at the surface $\mathcal{M}$

$$\hat{n}_+ \times \vec{E}_- = 0 \qquad \{\vec{R}: \quad (x,y,z) \in S\} \qquad (2.15)$$

and

$$\hat{n}_+ \times \bar{\bar{G}}_-(\vec{R}|\vec{R}') = 0 \qquad \{\vec{R}: \quad (x,y,z) \in \mathcal{M}\} \quad . \qquad (2.16)$$

Substituting Equations (2.16), (2.15), (2.14), and (2.13) into Equation (2.11) one finally derives the desirable formula as follows:

$$\vec{E}_-(\vec{R}) = \iiint_{\mathcal{M}_-} [-\nabla' \times \vec{K}_- - j\omega\mu\vec{J}_-] \cdot \bar{\bar{G}}_-(\vec{R}'|\vec{R})\, dv'$$

$$- \iint_{\bar{A}} \hat{n}_+ \times \vec{E}_- \cdot \nabla' \times \bar{\bar{G}}_-(\vec{R}'|\vec{R})\, da' \qquad \{\vec{R}: \quad (x,y,z) \in \mathcal{M}_-\} \quad . \qquad (2.17)$$

Although comparison of Equations (2.10) and (2.17) reveals that $\bar{G}_-$ and $\bar{G}_+$ have the same role, it should be noted that in general they are different, since $\bar{\bar{G}}_+(\vec{R}|\vec{R}')$ must satisfy Condition (2.7) whereas $\bar{\bar{G}}_-(\vec{R}|\vec{R}')$ must satisfy Conditions (2.14) and (2.15).

Having derived the necessary equations for determining the fields in regions $\mathcal{M}_+$ and $\mathcal{M}_-$, the next section will deal with the determination of the dyadic Green's functions for the geometries of the specific interests of this work.

2.4 Construction of the Dyadic Green's Function for a Two Infinitely Parallel-Plate Structure

The geometry of the structure being considered in this section is shown in Figure 2.2. This structure consists of two perfectly conducting infinite plates with separation w located in a homogeneous and isotropic medium. In order to orient the space a Cartesian coordinate system with its z-axis normal to the plates and its x-y plane parallel to the plates is erected as shown in the figure. Plates are labeled I and II to denote the $z = 0$ and $z = w$ boundaries, respectively. The interior region $\{\vec{R}: -\infty < x < \infty, -\infty < y < \infty, 0 \leq z \leq w\}$, which is called $\mathcal{M}_+$, is viewed as a closed domain.

The dyadic Green's function $\bar{\bar{G}}_+(\vec{R}'|\vec{R})$ will now be determined for the geometry described in the previous paragraph. Because in this section only the interior region $\mathcal{M}_+$ is of special interest, $\bar{\bar{G}}_+(\vec{R}|\vec{R}')$ must satisfy Equation (2.4) accompanied by the boundary condition (2.8). This clearly is a vector partial differential equation and in general there is no systematic method for constructing its solution. However, for boundaries with separability characteristic (Mikhlin, 1967) there are available methods to obtain the solution. Tai (1971) has used the vector eigenfunction M and N, introduced by Hansen (1935), to determine the dyadic Green's functions for cylindrical geometries, and the vector potential approach is discussed by Collin (1960).

Since, in this section, one is dealing with planar boundaries that extend to infinity, an alternative method is used. This method, which is based on the application of the image theory (Jordan and Balmain, 1968), will now be discussed.

To establish the formulation, one starts by locating the current element $\vec{J}_+$, as shown in Figure 2.2, in the region $\mathcal{M}_+$ of the two parallel

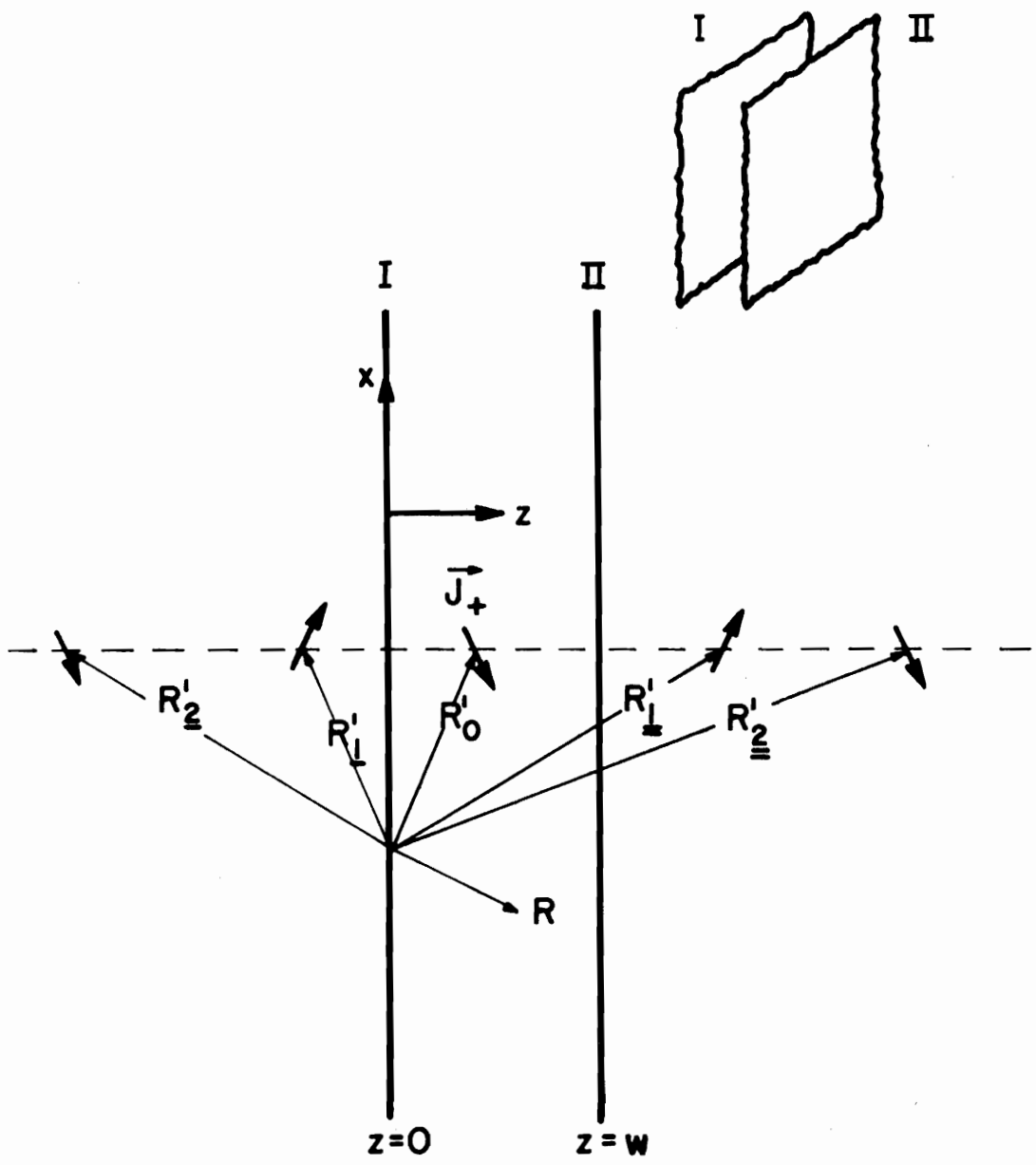

Figure 2.2. Two perfectly conducting parallel plates and the δ-current source $\vec{J}_+$; positions and orientations of image-current sources are shown for determining the dyadic Green's function.

plates. This current element may be defined as:

$$\vec{J}_+ = \vec{a}\delta(\vec{R} - \vec{R}') \tag{2.18}$$

where $\vec{a}$ is a constant vector with a_t and a_z as its transverse and longitudinal components, respectively. Vector $\vec{a}$ can then be decomposed as follows

$$\vec{a} = a_t\vec{t} + a_z\hat{z} \tag{2.19}$$

where $\vec{t}$ is a vector parallel to the x-y plane. Substituting (2.18) in (2.17) one obtains

$$\vec{E}_+(\vec{R}) = \iiint_{\mathcal{M}_+} - j\omega\mu\vec{J}_+ \cdot \bar{\bar{G}}_+(\vec{R}''|\vec{R})\, dv'' = -j\omega\mu\vec{a} \cdot \bar{\bar{G}}_+(\vec{R}'|\vec{R})$$

$$\{\vec{R}: \quad (x,y,z) \in \mathcal{M}_+\} \quad . \tag{2.20}$$

It is noted that $\vec{a}$ is an arbitrary constant vector. Since $\hat{n}_- \times \vec{E}_+ = 0$ over $\mathcal{M}$, it is possible to compute $\vec{E}_+(\vec{R})$, alternatively, by employing the theory of multiple images and vector potential technique. The E-field obtained by using this approach is then compared with the result obtained in (2.20) to determine $\bar{\bar{G}}_+(\vec{R}'|\vec{R})$.

The multiple images of the current element $\vec{J}$ with respect to the parallel plates are constructed by finding its electrical images. This construction is best understood by referring the reader to Figure 2.2. The first image of the current element (2.18) with respect to the plate I is obtained by locating an image current element in the location $\vec{R}_1'$, as shown in Figure 2.2, such that its longitudinal component is the same as the longitudinal component of the current element $\vec{J}$, and its transverse

component is the negative of the corresponding component of $\vec{J}$. This construction allows one to satisfy the boundary condition $\hat{n}_- \times \vec{E}_+ = 0$ automatically on plate I. Since the boundary condition $\hat{n}_- \times \vec{E}_+ = 0$ must also be satisfied on plate II, two more image current elements are introduced as shown in Figure 2.2. This procedure is continued until one obtains infinitely many countable current elements. The location of the current elements obtained through the imaging process and their corresponding components are listed in Table 2.1.

TABLE 2.1

CURRENT ELEMENTS DUE TO IMAGING PROCESSES

Characteristic Index of the Current Elements	Location of the Current Elements	Component of the Current Elements
0	$\vec{R}'_0 = (x',y',z')$	$\vec{a}\delta(\vec{R} - \vec{R}'_0)$
$\underline{1}$	$\vec{R}'_{\underline{1}} = (x',y',-z')$	$\vec{a}_i\delta(\vec{R} - \vec{R}'_{\underline{1}})$
$\underline{\underline{1}}$	$\vec{R}'_{+\underline{\underline{1}}} = (x',y',2w - z')$	$\vec{a}_i\delta(\vec{R} - \vec{R}'_{\underline{\underline{1}}})$
$\underline{2}$	$\vec{R}'_{\underline{2}} = (x',y',-2w + z')$	$\vec{a}\delta(\vec{R} - \vec{R}'_{\underline{2}})$
$\underline{\underline{2}}$	$\vec{R}'_{\underline{\underline{2}}} = (x',y',2w + z')$	$\vec{a}\delta(\vec{R} - \vec{R}'_{\underline{\underline{2}}})$
$\underline{3}$	$\vec{R}'_{\underline{3}} = (x',y',-2w - z')$	$\vec{a}_i\delta(\vec{R} - \vec{R}'_{\underline{3}})$
$\underline{\underline{3}}$	$\vec{R}'_{\underline{\underline{3}}} = (x',y',4w - z')$	$\vec{a}_i\delta(\vec{R} - \vec{R}'_{\underline{\underline{3}}})$
$\vdots$	$\vdots$	$\vdots$
$\underline{n}$	$\vec{R}'_{\underline{n}} = [x',y',(n - 1)(2)^{-}(1)^{-}w + (-1)^n z']$	$\vec{a}_{(i)^n}\delta(\vec{R} - \vec{R}'_{\underline{n}})$
$\underline{\underline{n}}$	$\vec{R}'_{\underline{\underline{n}}} = [x',y',(n - 1)(2)^{=}(1)^{=}w + (-1)^n z']$	$\vec{a}_{(i)^n}\delta(\vec{R} - \vec{R}'_{\underline{\underline{n}}})$
$\vdots$	$\vdots$	$\vdots$

In the above table the first column denotes a proper characteristic index for each current element. For instance, index $\underline{\underline{n}}$ indicates that the coefficient of w, defined in the second column, is $(n-1) \cdot (2)^{=} \cdot (1)^{=}$ where $(2)^{=} = 1$ and $(1)^{=} = +1$. The character '=' under number n is used to specify that this particular current element is obtained by finding the image of the current element $\underline{(n-1)}$ with respect to the plate II. Character '-' is also used to denote that the corresponding image is constructed with respect to the plate I. It is further defined that $(2)^{-} = 2$, $(1)^{-} = -1$, and $a_{(i)^n} = a_i$ for n being an odd integer and $a_{(i)^n} = a$ otherwise. In column three vector $\vec{a}$ has already been defined in Equation (2.19), and vector $\vec{a}_i$ designates its image defined as

$$\vec{a}_i = -a_t \vec{t} + a_z \hat{z} \quad . \tag{2.21}$$

Having determined all image current elements, one now proceeds to determine the E-field generated in region $\mathcal{M}_+$ by letting all the current elements radiate in the free space. Since one is dealing with a phenomenon occurring in free space, it is best to employ the vector potential method (Harrington, 1961) to determine the radiated fields. The radiating source may be defined by summing up the components introduced in the third column of Table 2-1 as follows:

$$\begin{aligned} \vec{J} = \vec{a}[\delta(\vec{R} - \vec{R}'_0) + \delta(\vec{R} - \vec{R}'_{\underline{2}}) + \delta(\vec{R} - \vec{R}'_{\underline{\underline{2}}}) + \ldots] \\ + \vec{a}_i[\delta(\vec{R} - \vec{R}'_{\underline{1}}) + \delta(\vec{R} - \vec{R}'_{\underline{\underline{1}}}) + \ldots] \quad . \end{aligned} \tag{2.22}$$

Vector potential $\vec{A}$ is now defined by simply convolving the scalar free-space Green's function $g_0(\vec{R}'|\vec{R})$ with the source distribution $\vec{J}$ in the following way

$$\vec{A}(\vec{R}) = \mu \iiint \vec{J}(\vec{R}')\, g_0(\vec{R}'|\vec{R})\, dv' \tag{2.23}$$

where

$$g_0(\vec{R}|\vec{R}') = \frac{e^{-jk|\vec{R}-\vec{R}'|}}{4\pi|\vec{R} - \vec{R}'|} \tag{2.24}$$

and

$$|\vec{R} - \vec{R}'| = \sqrt{(x - x')^2 + (y - y')^2 + (z - z')^2} \quad . \tag{2.25}$$

Substituting (2.22) in (2.23) and simplifying the result one obtains:

$$\vec{A}(\vec{R}) = \mu[\vec{a}G_+ + \vec{a}_i G_-] \tag{2.26}$$

where

$$G_+ = \sum_{n\in Z} \frac{e^{-jk\sqrt{(x-x')^2+(y-y')^2+(z-z'+2nw)^2}}}{4\pi\sqrt{(x - x')^2 + (y - y')^2 + (z - z' + 2nw)^2}} \tag{2.27}$$

and

$$G_- = \sum_{n\in Z} \frac{e^{-jk\sqrt{(x-x')^2+(y-y')^2+(z+z'+2nw)^2}}}{4\pi\sqrt{(x - x')^2 + (y - y')^2 + (z + z' + 2nw)^2}} \quad . \tag{2.28}$$

In Equation (2.27) and (2.28) the symbol Z is used to denote the set of positive and negative integers, including zero.

Knowing $\vec{A}$, one can then determine the E-field by readily using the following formula:

$$\vec{E}(\vec{R}) = -j\omega\left(1 + \frac{1}{k^2}\nabla\nabla\cdot\right)\vec{A}(\vec{R}) \quad . \tag{2.29}$$

Substituting (2.26) into the above equation, one finally derives the following equation for the E-field:

$$\vec{E}_+(\vec{R}) = -j\omega\mu\left(1 + \frac{1}{k^2}\nabla\nabla\cdot\right)(\vec{a}G_+ + \vec{a}_i G_-)$$

$$\{\vec{R}: \quad (x,y,z) \in \mathcal{M}_+\} \quad . \tag{2.30}$$

It should be noted that the E-field obtained in Equation (2.30) satisfies all of Maxwell's equations and the boundary condition $\hat{n}_- \times \vec{E}_+ = 0$ over $\iint$. Therefore, this is the one and only solution that can be accepted as a solution for the problem at hand. Comparing (2.30) with (2.20), one concludes that both of them are representing the same quantity, i.e., the electric field $\vec{E}_+(\vec{R})$. It is this comparison that finally enables one to determine the dyadic Green's function $\bar{\bar{G}}_+(\vec{R}'|\vec{R})$.

To determine $\bar{\bar{G}}_+(\vec{R}'|\vec{R})$ is just a matter of putting Equation (2.30) in a dyadic form with $\vec{a}$ as its interior multiplier. This can be done by performing the following manipulations. First, one observes that

$$\vec{a}G_+ + \vec{a}_i G_- = \vec{a}[G_+ - G_-] + 2\hat{z}a_z G_- = \vec{a} \cdot [\bar{\bar{I}}(G_+ - G_-) + 2\hat{z}\hat{z}G_-] \tag{2.31}$$

where $\vec{a}$ and $\vec{a}_i$ are defined in Equations (2.19) and (2.21), respectively. Second, one can easily show that

$$\nabla \cdot \vec{a}_i G_- = \nabla' \cdot \vec{a}G_- \tag{2.32}$$

and

$$\nabla \cdot \vec{a}G_+ = -\nabla' \cdot \vec{a}G_+ \quad . \tag{2.33}$$

Using the above results it may be simply shown that

$$\begin{aligned} \nabla\nabla \cdot [\vec{a}G_+ + \vec{a}_i G_-] &= \nabla[\vec{a} \cdot \nabla'(-G_+ + G_-)] \\ &= \vec{a} \cdot \nabla\nabla'(-G_+ + G_-) \quad . \end{aligned} \tag{2.34}$$

In deriving the above formula, the following expression is used

$$\nabla(\vec{a} \cdot \nabla' f) = (\vec{a} \cdot \nabla')\,\nabla f = \vec{a} \cdot \nabla'\nabla f \quad . \tag{2.35}$$

Substituting (2.35) and (2.31) into (2.30), one finally arrives at

$$\vec{E}_+(\vec{R}) = -j\omega\mu\vec{a} \cdot \left[\left(\bar{\bar{I}} - \frac{1}{k^2}\nabla'\nabla\right)(G_+ - G_-) + 2\hat{z}\hat{z}G_-\right]$$

$$\{\vec{R}: \quad (x,y,z) \in \mathcal{M}_+\} \quad . \tag{2.36}$$

The above equation is desirable in this form for direct comparison with the result obtained in (2.20). Since (2.20) and (2.36) are representing the same quantity for any arbitrary $\vec{a}$, one deduces that the dyadic Green's function will take the following form:

$$\bar{\bar{G}}_+(\vec{R}'|\vec{R}) = \left(\bar{\bar{I}} - \frac{1}{k^2}\nabla'\nabla\right)(G_+ - G_-) + 2\hat{z}\hat{z}G_- \quad , \tag{2.37}$$

where the scalar functions G_+ and G_- have been defined previously in Equations (2.27) and (2.28), respectively. It is easy to check that the dyadic Green's function satisfies the following relation, namely,

$$[\bar{\bar{G}}_+(\vec{R}'|\vec{R})]^T = \bar{\bar{G}}_+(\vec{R}|\vec{R}') \tag{2.38}$$

where the symbol "T" is used to indicate the transposed operator. Equation (2.38) is an obvious consequence of the reciprocity theorem (Stratton, 1941) which often appears in the theory of electromagnetism.

The dyadic Green's function obtained in this section will be used in Chapter 6, where the problem of aperture coupling into a parallel-plate region is discussed. It is also worth mentioning that the derivation of the dyadic Green's function can be performed by using the eigenfunction techniques described in Tai's book (1971).

2.5 Construction of the Dyadic Green's Function for Semi-Infinite Space

This section can actually be considered as a special case of the previous section and is treated in a separate section because of its special importance which will become apparent in the next chapters. The geometry of the problem under consideration can be constructed by letting plate II go to infinity along the z-axis as in Figure 2.2. According to the specification developed in Section 2.3, this structure should be considered as an exterior region. Therefore, one must solve Equation (2.4) subject to the boundary condition (2.16) and radiation condition (2.13) in order to determine the dyadic Green's function $\bar{\bar{G}}_+(\vec{R}'|\vec{R})$.

The technique developed in the previous section is used to construct the dyadic Green's function $\bar{\bar{G}}_+$. For the simple geometry considered in this section, there are only two current elements, as defined in the first two rows of Table 2.1, that make contributions in determining the dyadic Green's function. By using these two current elements and following the steps developed in the previous section one easily determines that

$$\bar{\bar{G}}_+(\vec{R}'|\vec{R}) = \left(\bar{\bar{I}} - \frac{1}{k^2}\nabla'\nabla\right)(g_+ - g_-) + 2\hat{z}\hat{z}g_- \qquad (2.39)$$

where g_+ and g_- are constructed as follows:

$$g_+ = G_+;\ g_- = G_- \qquad \text{for } n = 0 \quad . \qquad (2.40)$$

One can also readily verify that $\bar{\bar{G}}_+(\vec{R}'|\vec{R})$ satisfies the radiation condition defined in Equation (2.14).

It is well known that the free-space dyadic Green's function has a special singular behavior at the source region (Van Bladel, 1961; Rahmat-Samii, 1974). This phenomenon is also observable for the case developed in this section, since $\left(\bar{\bar{I}} - \frac{1}{k^2} \nabla'\nabla\right) g_+$ represents the free-space dyadic Green's function and g_- does not have any singularity in region $\mathcal{M}_+$.

3. DIFFRACTION BY AN APERTURE IN A PERFECTLY CONDUCTING SCREEN

3.1 Introduction

The problem of diffraction by an aperture in a perfectly conducting screen is one which has drawn much attention, thus necessitating a great deal of work since the era of Maxwell (1879;1904) or even earlier. Mathematicians, physicists and engineers have used many different analytical techniques and methods for solving this problem. Kirchhoff (1891) and Lord Rayleigh (1897) were able to design the first mathematical formulations of the high and low frequency behavior of the diffracted field, respectively. Kirchhoff's mathematical formulation is based on the application of Huygens' principle (Baker and Copson, 1953) and Green's theorem. This approach, which considers that the aperture field is essentially the same as the incident field, uses this information to determine the diffracted field. The basic idea of Lord Rayleigh's formulation is that, in the vicinity of the aperture, the electromagnetic field distribution can be calculated as though the wavelength were infinite.

Advances in the early 1950's in microwave techniques led to a renewal of interest in the diffraction of electromagnetic waves by an aperture in a conducting screen. In particular, the experimental work of Andrews (1950) and Robinson (1953), who measured the field within, and in the neighborhood of, circular openings, gave a good basis for comparing the results obtained from the existing theoretical formulation and experimental data. It was found that most of the existing methods were incomplete for determining the field distribution in the aperture and neighboring points, when the aperture size was comparable to the

wavelength. Bouwkamp (1953) then made a critical review of previous work and was able to show the incompleteness of the formulation obtained by Bethe (1944) and Copson (1946). Levine and Schwinger (1950) used Green's theorem approach and applied a variational technique to formulate the diffraction problem for circular apertures. Keller et al. (1957) have applied the geometrical theory of diffraction to determine the diffracted field. In the latter studies, the authors have also made an interesting comparison among different existing theorems in the high frequency domain. Suzuki (1956) has applied a variational technique and the method of successive approximations to solve the diffraction problem of a narrow slit in a conducting screen. Neither of the above techniques were suitable for solving the diffraction problem for nonseparable geometries, as with rectangular apertures in the medium frequency regime, i.e., where the size of aperture is comparable to the wavelength.

Recent advancement in computer technology has given new insight to researchers in applying numerical techniques. Although it was first thought that by using the computer all unsolved problems could be solved numerically, it was soon discovered that that was not the case, and very special care should be taken to obtain a proper solution. Researchers' experiences have revealed that the choice of a suitable mathematical formulation and a proper approximation technique is a very vital step in successfully determining the numerical solutions. For instance, recent publications about the numerical investigation of linear antennas are good examples in displaying the difficulties which occur in the numerical domain. Aperture diffraction has recently been treated numerically via application of different formulations. For instance,

the conventional E-type integral equation has been used by Spiegel and Young (1973), and the wire-grid model has been employed by Lin et al. (1974). It has been found that these techniques are not completely satisfactory either to determine the E-field distribution due to an obliquely incident field or to compute the near field of the aperture.

In this chapter, a formulation is developed for the aperture diffraction problem which has many desirable characteristics. This formulation is based on the application of a new set of structurally simple integral equations which formulates the aperture diffraction problem completely and provides good numerical behavior. Numerical computation is mainly devoted to determining the diffracted field by a rectangular aperture, a geometry that has not been investigated thoroughly and is very important from practical considerations. Results are then compared with those of available experimental and theoretical data.

3.2 An Investigation of the Vector Integral Equation

The geometry of the structure considered in this section is shown in Figure 3.1. The notations introduced in Chapter 2 are assumed here with no changes. Symbol $\mathcal{M}_+$ is used to denote the exterior region in the right-hand side of the screen shown in Figure 3.1, and symbol $\mathcal{M}_-$ designates the exterior region in the left-hand side of the screen. Therefore, all the fields appearing in the region $\mathcal{M}_+$ and $\mathcal{M}_-$ will have indices "+" and "-", respectively. It is further assumed that a monochromatic wave $\vec{E}^i$, $\vec{H}^i$, originating from a source situated in the half-space $\mathcal{M}_-$, is incident upon the screen. In this section, an integral equation is constructed to compute the tangential E-field in the aperture.

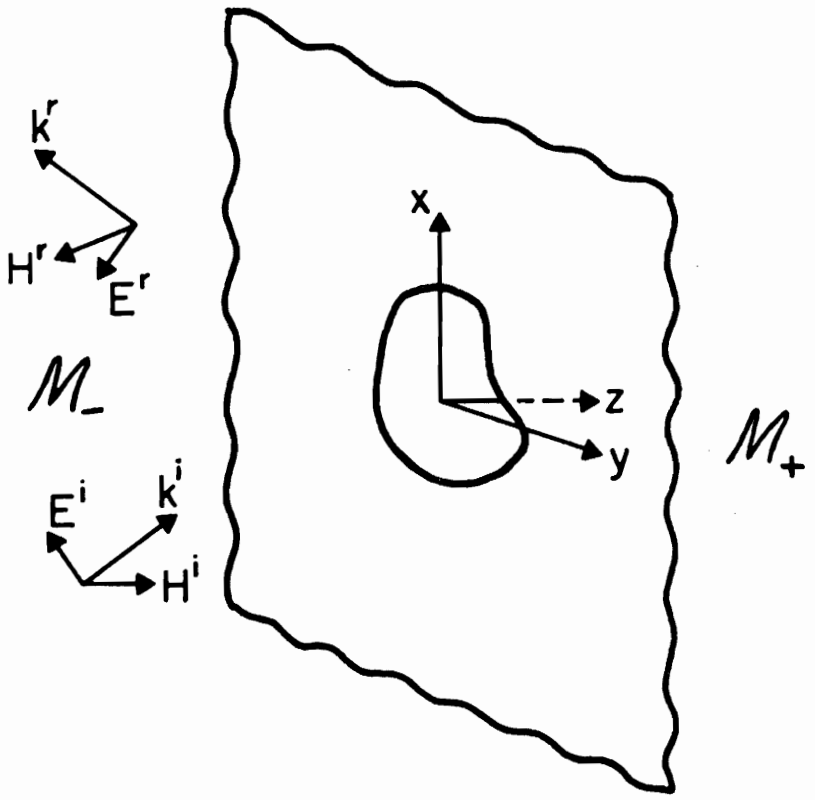

Figure 3.1. Aperture in a perfectly conducting screen illuminated by a plane wave.

The electromagnetic field $\vec{E}$, $\vec{H}$, at any point in space, is split up into an incident field $\vec{E}^i$, $\vec{H}^i$, a reflected field $\vec{E}^r$, $\vec{H}^r$ (associated with the reflected wave that exists when the screen is complete), and a diffracted field $\vec{E}^d$, $\vec{H}^d$, due to the aperture alone. It is then found that in $\mathcal{M}_-$

$$\vec{E}_- = \vec{E}_-^i + \vec{E}_-^r + \vec{E}_-^d \tag{3.1}$$

$$\vec{H}_- = \vec{H}_-^i + \vec{H}_-^r + \vec{H}_-^d \tag{3.2}$$

and in $\mathcal{M}_+$

$$\vec{E}_+ = \vec{E}_+^d \tag{3.3}$$

$$\vec{H}_+ = \vec{H}_+^d \tag{3.4}$$

the reflected field $\vec{E}_-^r$, $\vec{H}_-^r$ can, in general, be constructed from the knowledge of the incident field and the reflecting surface (Jones, 1964). To obtain the complete solution of the problem, the diffracted field must be determined.

In determining the diffracted field, one employs Equation (2.10) which reads as follows

$$\vec{E}_\pm^d(\vec{R}) = -\iint_A \hat{n}_{\mp} \times \vec{E}_0^d(\vec{R}') \cdot \nabla' \times \bar{\bar{G}}_\pm(\vec{R}'|\vec{R})\, da'$$

$$\{\vec{R}: \quad (x,y,z) \in \mathcal{M}_\pm\} \tag{3.5}$$

where $\bar{\bar{G}}_\pm(\vec{R}'|\vec{R})$, which has already been defined in Equation (2.39), takes the following form

$$\bar{\bar{G}}_\pm(\vec{R}'|\vec{R}) = \left(\bar{\bar{I}} - \frac{1}{k^2}\nabla'\nabla\right)(g_\pm - g_{\mp}) + 2\hat{z}\hat{z}g_{\mp} \quad . \tag{3.6}$$

By using the identities given in Appendix A, one easily finds that

$$\nabla' \times \bar{\bar{G}}_{\pm}(\vec{R}'|\vec{R})\Big|_{z'=\pm 0} = \left\{ \frac{\mp z}{|\vec{R} - \vec{\rho}'|}\, \hat{y}\hat{x} + \frac{\pm z}{|\vec{R} - \vec{\rho}'|}\, \hat{x}\hat{y} - \frac{x' - x}{|\vec{R} - \vec{\rho}'|}\, \hat{y}\hat{z} + \frac{y' - y}{|\vec{R} - \vec{\rho}'|}\, \hat{x}\hat{z} \right\} \cdot \left(-jk - \frac{1}{|\vec{R} - \vec{\rho}'|} \right) \cdot 2g_0(\vec{\rho}'|\vec{R}) \tag{3.7}$$

where

$$g_0(\rho'|R) = g_+(x',y',z' = 0|\vec{R}) = g_-(x',y',-z' = 0|\vec{R}) \tag{3.8}$$

and

$$\vec{\rho}' = x'\hat{x} + y'\hat{y} \quad . \tag{3.9}$$

After substituting (3.6) into (3.5) and considering (3.7), one finally obtains

$$\vec{E}^d_{\pm}(\vec{R}) = -2\nabla \times \iint_{\bar{A}} \vec{E}^d_0(\vec{\rho}') \times \hat{n}_{\pm} g_0(\vec{\rho}'|\vec{R})\, da'$$

$$\{\vec{R}: \quad (x,y,z) \in \mathcal{M}_{\pm}\} \quad . \tag{3.10}$$

The above equation, which is a manifestation of the Huygens' principle, could be constructed directly by employing this principle. Equation (3.10) was derived by Jackson (1962) using the scalar Green's function formulation.

In Appendix B, it is shown that

$$\vec{E}(\vec{\rho}) \times \hat{n}_{\pm} = \vec{E}^d_0(\vec{\rho}) \times \hat{n}_{\pm} = \lim_{z \to \pm 0} 2\hat{n}_{\pm} \times \nabla \times \iint_{\bar{A}} \vec{E}^d_0(\vec{\rho}') \times \hat{n}_{\pm} g_0(\vec{\rho}'|\vec{R})\, da' \quad . \tag{3.11}$$

In the above equation, since the limiting process is applied to a singular integral (Mikhlin, 1957), it must be defined properly and care should be exercised in evaluating the limit correctly. The details of this analysis are discussed in Appendix 3-A.

In crossing the aperture from the half-space $\mathcal{M}_-$ to the half-space $\mathcal{M}_+$, the tangential components of the E-field and H-field must remain continuous. This fact automatically states that all components of the electromagnetic field are continuous in crossing the aperture. Upon using the fact that $\lim_{z\to-0} \left(\vec{E}_-^{\,i} + \vec{E}_-^{\,r}\right) \times \hat{n} = 0$, and employing the result obtained in Equation (3.11), one can readily state

$$\lim_{z\to-0} \left\langle \left(\vec{E}_-^{\,i} + \vec{E}_-^{\,r} + \vec{E}_-^{\,d}\right) \times \hat{n} \right\rangle = \lim_{z\to+0} \left\langle \vec{E}_+^{\,d} \times \hat{n} \right\rangle \qquad (3.12)$$

where $\hat{n}$ can be viewed either as $\hat{n}_+$ or as $\hat{n}_-$. The above result is a manifestation of the continuity of the tangential E-field in crossing the aperture. It now remains to enforce the condition of continuity of the tangential H-field in crossing the aperture. To do this, one first observes that the following is true:

$$\hat{n} \times \vec{H}_\pm = -\frac{1}{j\omega\mu} \hat{n} \times \nabla \times \vec{E}_\pm \quad . \qquad (3.13)$$

Thus, continuity of the tangential H-field is achieved if one requires that the normal derivative of the tangential E-field and the tangential derivative of the normal E-field are continuous in crossing the aperture.

Because the Cartesian components of the E^d-field are needed in studying the continuity condition, one rewrites Equation (3.10) as follows

$$\vec{E}^{d}_{\pm}(\vec{R}) = \mp 2 \frac{\partial}{\partial z} \iint_{\bar{A}} (E_x \hat{x} + E_y \hat{y})\, g_0(\vec{\rho}' | \vec{R})\, da'$$

$$\pm 2\hat{z} \left(\frac{\partial}{\partial x} \iint_{\bar{A}} E_x g_0(\vec{\rho}' | \vec{R})\, da' + \frac{\partial}{\partial y} \iint_{\bar{A}} E_y g_0(\vec{\rho}' | \vec{R})\, da' \right) , \qquad (3.14)$$

where in deriving Equation (3.14) E_{0x} and E_{0y} have been replaced by E_x and E_y using Equation (3.11). Enforcing the continuity of the normal component of the E-field determines that

$$4 \left[\frac{\partial}{\partial x} \iint_{\bar{A}} E_x g_0(\vec{\rho}' | \vec{R})\, da' + \frac{\partial}{\partial y} \iint_{\bar{A}} E_y g_0(\vec{\rho}' | \vec{R})\, da' \right] \Bigg|_{z=0} = -\hat{n}_- \cdot \left(\vec{E}^{i}_{-} + \vec{E}^{r}_{-} \right) \Bigg|_{z=0}$$

$$\{\vec{R}: \quad (x,y,z = 0) \in A\} \quad . \qquad (3.15)$$

Later, the above equation will play a vital role in construction of the integral equation. One can now easily verify that the tangential derivative of the normal E-field is continuous in crossing the aperture. To constrain the continuity of the normal derivative of the tangential E-field within the aperture, the following equation must be satisfied

$$4 \left\{ \frac{\partial^2}{\partial z^2} \left[\iint_{\bar{A}} (E_x \hat{x} + E_y \hat{y})\, g_0(\vec{\rho}' | \vec{R})\, da' \right] \right\} \Bigg|_{z=0}$$

$$= \left\{ \frac{\partial}{\partial z} \left[\left(E^{i}_{-x} + E^{r}_{-x} \right) \hat{x} + \left(E^{i}_{-y} + E^{r}_{-y} \right) \hat{y} \right] \right\} \Bigg|_{z=0} \qquad \{\vec{R}: \quad (x,y,z = 0 \in A\} \quad . \qquad (3.16)$$

Equations (3.1), (3.3), and (3.14) have been employed to construct the above equation. Simultaneous satisfaction of Equations (3.15) and (3.16) by E_x and E_y guarantees that the tangential H-field is then continuous when the aperture is crossed.

By employing the limiting procedure described in Appendix B, one can readily show that the following is true.

$$\left\{\frac{\partial^2}{\partial z^2}\iint_{\bar{A}} f(\vec{\rho}')\, g_0(\vec{\rho}'|\vec{R})\, da'\right\}\Bigg|_{z=0} = -\left(\frac{\partial^2}{\partial x^2}+\frac{\partial^2}{\partial y^2}+k^2\right)\iint_{\bar{A}} f(\vec{\rho}')\, g_0(\vec{\rho}'|\vec{\rho})\, da' \tag{3.17}$$

where $f(\vec{\rho})$ is assumed to be a regular function, and $\vec{\rho} = x\hat{x} + y\hat{y}$. Using the above result, one can easily manipulate (3.16) to obtain

$$4\left(\frac{\partial^2}{\partial x^2}+\frac{\partial^2}{\partial y^2}+k^2\right)\iint_{\bar{A}} \begin{Bmatrix} E_x \\ E_y \end{Bmatrix} g_0(\vec{\rho}'|\vec{\rho})\, da' = -\frac{\partial}{\partial z}\begin{Bmatrix} E^i_{-x}+E^r_{-x} \\ E^i_{-y}+E^r_{-y} \end{Bmatrix}\Bigg|_{z=0}$$

$$\{\vec{\rho}:\ (x,y)\in A\} \quad . \tag{3.18}$$

Perhaps it is now worthwhile to describe briefly what has been done up to this point: the discussion presented above is essentially concentrated around Equations (3.15) and (3.18). The solution of these equations, tangential E-field in the aperture, obviously satisfies all of Maxwell's equations, boundary conditions, and continuity conditions; therefore, it is the unique solution of the problem. It should be noted that there are three equations for determining the two unknowns E_x and E_y in Equations (3.15) and (3.18). This may first look rather astonishing, but it has been found that the correct result can not be obtained, if one only tries to use two of them. For instance, an attempt was made to construct the solution by employing the two equations appearing in (3.18), and as expected, the obtained result did not show the correct behavior. From what has been written, it is now apparently desirable to find a set of two integral equations that incorporates the

effect of all three equations with less singular behavior. This will be exhibited in the following paragraphs.

Since in this work, the plane incident field is of primary interest, one takes

$$\vec{E}^i_- = \left(\hat{x}E^i_{0x} + \hat{y}E^i_{0y} + \hat{z}E^i_{0z}\right) e^{-jk(\alpha x+\beta y+\gamma z)} \tag{3.19}$$

where $\alpha = \sin\theta^i \cos\phi^i$, $\beta = \sin\theta^i \sin\phi^i$ and $\gamma = \cos\theta^i$ are the cosine directors of the incident wave vector, and θ^i and ϕ^i are the corresponding elevation and azimuthal angles. It can be easily verified that the reflected field $\vec{E}^r_-$ has the following form

$$\vec{E}^r_- = \left(-\hat{x}E^i_{0x} - \hat{y}E^i_{0y} + \hat{z}E^i_{0z}\right) e^{-jk(\alpha x+\beta y-\gamma z)} \quad . \tag{3.20}$$

Substituting (3.19) and (3.20) into (3.15) and (3.18), one finally obtains

$$2\frac{\partial}{\partial x}\iint_{\bar{A}} E_x(\vec{\rho}')\, g_0(\vec{\rho}'|\vec{\rho})\, da' + 2\frac{\partial}{\partial y}\iint_{\bar{A}} E_y(\vec{\rho}')\, g_0(\vec{\rho}'|\vec{\rho})\, da' = E^i_{0z}\, e^{-jk(\alpha x+\beta y)}$$

$$\{\vec{\rho}:\ (x,y) \in A\} \tag{3.21}$$

and

$$2\left(\frac{\partial^2}{\partial x^2} + \frac{\partial^2}{\partial y^2} + k^2\right) \iint_{\bar{A}} \begin{Bmatrix} E_x(\vec{\rho}') \\ E_y(\vec{\rho}') \end{Bmatrix} g_0(\vec{\rho}'|\vec{\rho})\, da' = +jk\gamma \begin{Bmatrix} E^i_{0x} \\ E^i_{0y} \end{Bmatrix} e^{-jk(\alpha x+\beta y)}$$

$$\{\vec{\rho}:\ (x,y) \in A\} \quad . \tag{3.22}$$

In order to determine the integrated form of (3.22), a form that does not contain the two-dimensional wave operator, one first extends the domain of $\{\vec{\rho}:\ (x,y) \in A\}$ to the entire screen $\{\vec{\rho}:\ (x,y) \in \mathcal{M}\}$. In this

extended domain, one then integrates (3.22) to obtain the following result:

$$2 \iint_{\bar{A}} \begin{Bmatrix} E_x(\vec{\rho}') \\ E_y(\vec{\rho}') \end{Bmatrix} g_0(\vec{\rho}'|\vec{\rho})\, da' = +jk\gamma \begin{Bmatrix} E^i_{0x} \\ E^i_{0y} \end{Bmatrix} \iint_{-\infty}^{\infty} e^{-jk(\alpha x'+\beta y')} H_0^2(k|\vec{\rho} - \vec{\rho}'|)\, da' + \begin{Bmatrix} h_x(x,y) \\ h_y(x,y) \end{Bmatrix} \tag{3.23}$$

where H_0^2 is a Hankel function of the second kind and the zeroth order, and $h_x(x,y)$ and $h_y(x,y)$ are homogeneous solutions of the two-dimensional wave operator, namely,

$$\left(\frac{\partial^2}{\partial x^2} + \frac{\partial^2}{\partial y^2} + k^2\right) \begin{Bmatrix} h_x(x,y) \\ h_y(x,y) \end{Bmatrix} = 0 \quad . \tag{3.24}$$

The final step toward construction of the integral equation is the determination of the proper homogeneous solutions h_x and h_y. One first observes that the double integral, appearing in the left-hand side of Equation (3.23), can readily be evaluated to give

$$\iint_{-\infty}^{\infty} e^{-jk(\alpha x'+\beta y')} H_0^2(k|\vec{\rho} - \vec{\rho}'|)\, da' = \frac{1}{(jk\gamma)^2} e^{-jk(\alpha x+\beta y)} \quad \text{for } \gamma \neq 0 \quad . \tag{3.25}$$

In deriving the above equation, the fact that $\alpha^2 + \beta^2 + \gamma^2 = 1$ is employed. As a proper representation for the homogeneous solutions h_x and h_y, the following expression is used:

$$\begin{Bmatrix} h_x(x,y) \\ h_y(x,y) \end{Bmatrix} = \frac{1}{k} \int_0^{2\pi} \begin{Bmatrix} C_x(\xi) \\ C_y(\xi) \end{Bmatrix} e^{jk(x\cos\xi + y\sin\xi)}\, d\xi \tag{3.26}$$

where $C_x(\xi)$ and $C_y(\xi)$ are two unknown functions yet to be determined. It will be clear shortly why the above expression is indeed a proper choice for the homogeneous solutions. One can easily show that (3.26) satisfies (3.24). Upon substituting (3.26) and (3.25) into (3.23) and requiring that Equation (3.21) must be satisfied, the following relationship between $C_x(\xi)$ and $C_y(\xi)$ can then be established:

$$C_x(\xi) \cos \xi + C_y(\xi) \sin \xi = 0 \quad . \tag{3.27}$$

In deriving the above equation, the fact that $\nabla \cdot \vec{E}^i = 0$ is applied. In order to satisfy Equation (3.27), one may define C_x and C_y to be as follows:

$$C_x(\xi) = C(\xi) \sin \xi \tag{3.28a}$$

and

$$C_y(\xi) = -C(\xi) \cos \xi \tag{3.28b}$$

where $C(\xi)$ is an unknown function yet to be determined.

Then substituting Equations (3.28), (3.26) and (3.25) into (3.23), one finally determines the most desirable form of the integral equation as presented below:

$$\iint_{\bar{A}} \begin{Bmatrix} E_x \\ E_y \end{Bmatrix} \frac{e^{-jk|\vec{\rho}-\vec{\rho}'|}}{2\pi|\vec{\rho}-\vec{\rho}'|} \, da' = \frac{1}{jk\gamma} \begin{Bmatrix} E^i_{0x} \\ E^i_{0y} \end{Bmatrix} e^{-jk(\alpha x+\beta y)} + \frac{1}{k} \int_0^{2\pi} \begin{Bmatrix} \sin \xi \\ -\cos \xi \end{Bmatrix} C(\xi) \, e^{jk(x\cos\xi+y\sin\xi)} \, d\xi$$

$$\{\vec{\rho}: \quad (x,y) \in \bar{A}\} \quad . \tag{3.29}$$

As indicated before, the information contained in Equations (3.21) and (3.22) is now confined in Equation (3.29). In other words, the solution of Equation (3.29) satisfies all of the Maxwell's equations, boundary conditions and continuity conditions. Although one is now dealing with two equations appearing in (3.29), one has already paid the price by introducing a new unknown $C(\xi)$. That is, there are two equations and three unknowns. To determine $C(\xi)$ requires the satisfaction of the edge condition (Jones, 1964; Mittra and Lee, 1971) by the tangential component of the E-field. For the structure being discussed in this section, the edge condition may be stated as:

1. The component of $\vec{E}$ parallel to the rim must be proportional to $S^{1/2}$,
2. The component of $\vec{E}$ perpendicular to the rim must be proportional to $S^{-1/2}$,

where S is the distance measured along the normal to the rim. As discussed by Flammer (1933), imposing the condition that the parallel component of $\vec{E}$ field must be zero at the rim implies that the edge condition is satisfied. Thus, to ensure the unique determination of the complete solution Equation (3.29) must be solved subject to the condition

$$\vec{E}(\vec{\rho}) \cdot \hat{\tau} = 0 , \quad \{\vec{\rho}: \ (x,y) \in C\} \ ; \tag{3.30}$$

this point will be elaborated in the next section. It is worthwhile to mention that the edge condition is satisfied directly if one solves the set of Equations (3.21) and (3.22), because these equations are dictating the laws of electromagnetism in a direct fashion. On the other hand, one needs to enforce the condition (3.30) in solving

Equation (3.29), since this equation does not manifest the law of electromagnetism properly. Equation (3.29) shows that if one does not use the condition (3.30), there will be many spurious solutions which satisfy Equation (3.29) and are not physically realizable.

An alternative form of (3.29) can be obtained by representing $C(\xi)$ in terms of a Fourier series expansion. This new form gives a clear picture of the homogeneous solution behavior introduced in (3.23). Assuming that $C(\xi)$ is a Fourier transformable function, the following must be true

$$C(\xi) = \sum_{n=-\infty}^{\infty} C_n e^{jn\xi} \quad . \tag{3.31}$$

Incorporating (3.31) into (3.29) and employing the well-known representation for Bessel's function (Abramowitz, 1970), viz.,

$$J_n(k\rho) = \frac{j^n}{2\pi} \int_0^{2\pi} e^{-jk\rho\cos\phi}\, e^{jn\phi}\, d\phi \quad , \tag{3.32}$$

one finally obtains

$$\iint_{\bar{A}} \begin{Bmatrix} E_x \\ E_y \end{Bmatrix} \frac{e^{-jk|\vec{\rho}-\vec{\rho}'|}}{2\pi|\vec{\rho}-\vec{\rho}'|}\, da' = \frac{1}{jk\gamma} \begin{Bmatrix} E^i_{0x} \\ E^i_{0y} \end{Bmatrix} e^{-jk(\alpha x+\beta y)}$$
$$+ \frac{\pi}{k} \begin{Bmatrix} -j \\ -1 \end{Bmatrix} \sum_{n=-\infty}^{\infty} C_n \Big[j^{n+1} e^{j(n+1)\phi} J_{n+1}(k\rho)$$
$$+ \begin{Bmatrix} -1 \\ 1 \end{Bmatrix} j^{n-1} e^{j(n-1)\phi} J_{n-1}(k\rho) \Big] \quad \{\vec{\rho}: \ (x,y) \in \bar{A}\} \tag{3.33}$$

where (ρ,ϕ) are the polar coordinates of the point (x,y). One could

have introduced the above homogeneous solution in solving Equation (3.23) directly, because $\sum a_n J_n(k\rho)\, e^{jn\phi}$ is a solution of Equation (3.24) when it is written in the polar coordinate system. Since E_x and E_y are square integrable functions, the left-hand side of Equation (3.33) is always bounded, which readily implies that the right-hand of Equation (3.33) is also bounded. Because the origin of the coordinate system being taken in the set $\{\vec{\rho}: \ (x,y) \in \bar{A}\}$, Hankel functions $\sum b_n H_n(k\rho)\, e^{jn\phi}$ can not be an acceptable solution for this case, since they are singular at point (0,0). Now it only remains to show that the infinite series appearing in the right-hand side of Equation (3.33) would be a convergent series, when it is subjected to the condition (3.30). No attempt is made to prove the convergence in an analytical fashion at this point, but it will be discussed in the next section, where some numerical results are presented.

Before closing this section, it is of interest to make a comparison between Equation (3.33) and that of the conventional one. It is well known that the tangential component of the incident magnetic field is not altered in the aperture (Bethe, 1944), namely,

$$\hat{n} \times \vec{H} = \hat{n} \times \vec{H}^i \qquad \{\vec{R}: \ (x,y,z) \in \bar{A}\} \quad . \tag{3.34}$$

This fact is used to write the conventional integral equation in the following form (Spiegel and Young, 1974):

$$k^2 \iint_{\bar{A}} E_y(\vec{\rho}')\, g_0(\vec{\rho}'|\vec{\rho})\, da' - \iint_{\bar{A}} \left[E_x(\vec{\rho}') \frac{\partial^2 g_0(\vec{\rho}'|\vec{\rho})}{\partial x' \partial y'} - E_y(\vec{\rho}') \frac{\partial^2 g_0(\vec{\rho}'|\vec{\rho})}{\partial x'^2} \right] da'$$

$$= \frac{\omega \mu_0}{4j} H_x^i \tag{3.35a}$$

$$-k^2 \iint_{\bar{A}} E_x(\vec{\rho}')\, g_0(\vec{\rho}'|\vec{\rho})\, da' + \iint_{\bar{A}} \left[-E_x(\vec{\rho}') \frac{\partial^2 g_0(\vec{\rho}'|\vec{\rho})}{\partial y'^2} + E_y(\vec{\rho}') \frac{\partial^2 g_0(\vec{\rho}'|\vec{\rho})}{\partial x' \partial y'} \right] da'$$

$$= \frac{\omega\mu_0}{4j} H_y^i \qquad (3.35b)$$

where H_x^i and H_y^i refer to the tangential component of the incident magnetic field existing on the surface of the aperture, and $g_0(\vec{\rho}'|\vec{\rho})$ has been defined in (2.24). First observation reveals that Equation (3.35) is highly singular when it is compared with Equation (3.33). Because of this singular behavior, Equation (3.35) also suffers numerical instability. Perhaps the reader has already recognized the resemblance between Equations (3.35) and (3.33) with Pocklington's and Hallen's integral equations (Collin, 1969) appearing in the theory of the linear antennas. It may further be observed that the x and y components of the tangential E-field are coupled directly in Equation (3.35), whereas these components are decoupled in (3.33) and coupling only occurs through the constant coefficients of the homogeneous terms. This property of Equation (3.33) leads to important and useful consequences when one analyzes the low frequency characteristics of the solution in the next chapter.

3.3 Numerical Results and Discussions

3.3.1 Reduction of integral equations to matrix equations

In this section the procedure for extracting numerical solutions of the integral equations derived in Section 3.2 will be outlined. The integral equations will be converted into matrix equations using the standard moment method (Harrington, 1968; Mittra, 1973).

For a general equation written in an operator form

$$L(e) = f \quad , \tag{3.36}$$

the matrix equation for unknown expansion coefficients E_i of the unknown e, expressed in terms of a set of basis functions e^i, is given by

$$[M]\{E\} = \{x\} \tag{3.37}$$

where

$$[M] = [m_{ij}] = \left[\langle f_j, L(e^i)\rangle\right] \tag{3.38}$$

$$\{x\} = \{x_j\} = \left\{\langle f_j, f\rangle\right\} \tag{3.39}$$

f_j = testing function

and

$$\langle f_i, f_j\rangle = \iint_{\bar{A}} f_i(\vec{\rho}')\, f_j(\vec{\rho}')\, da' \quad . \tag{3.40}$$

The next step is to employ the above technique to derive the numerical solution of the integral equation (3.33). Since there are no differential operators in the kernel of (3.33), the pulse function and δ function can be used as basis and testing elements, respectively. To do this, the aperture is subsectionalized uniformly into M x N patches as shown in Figure 3.2. The fundamental definition for the pulse approximation is given by

$$\begin{aligned} e^{mn}(x',y') &= 1 \ , \quad (x',y') \in \Delta x'_m \times \Delta y'_n \\ &= 0 \ , \quad (x',y') \notin \Delta x'_m \times \Delta y'_n \quad . \end{aligned} \tag{3.41}$$

Then employing (3.36), one finally derives a discretized version of (3.33) which reads

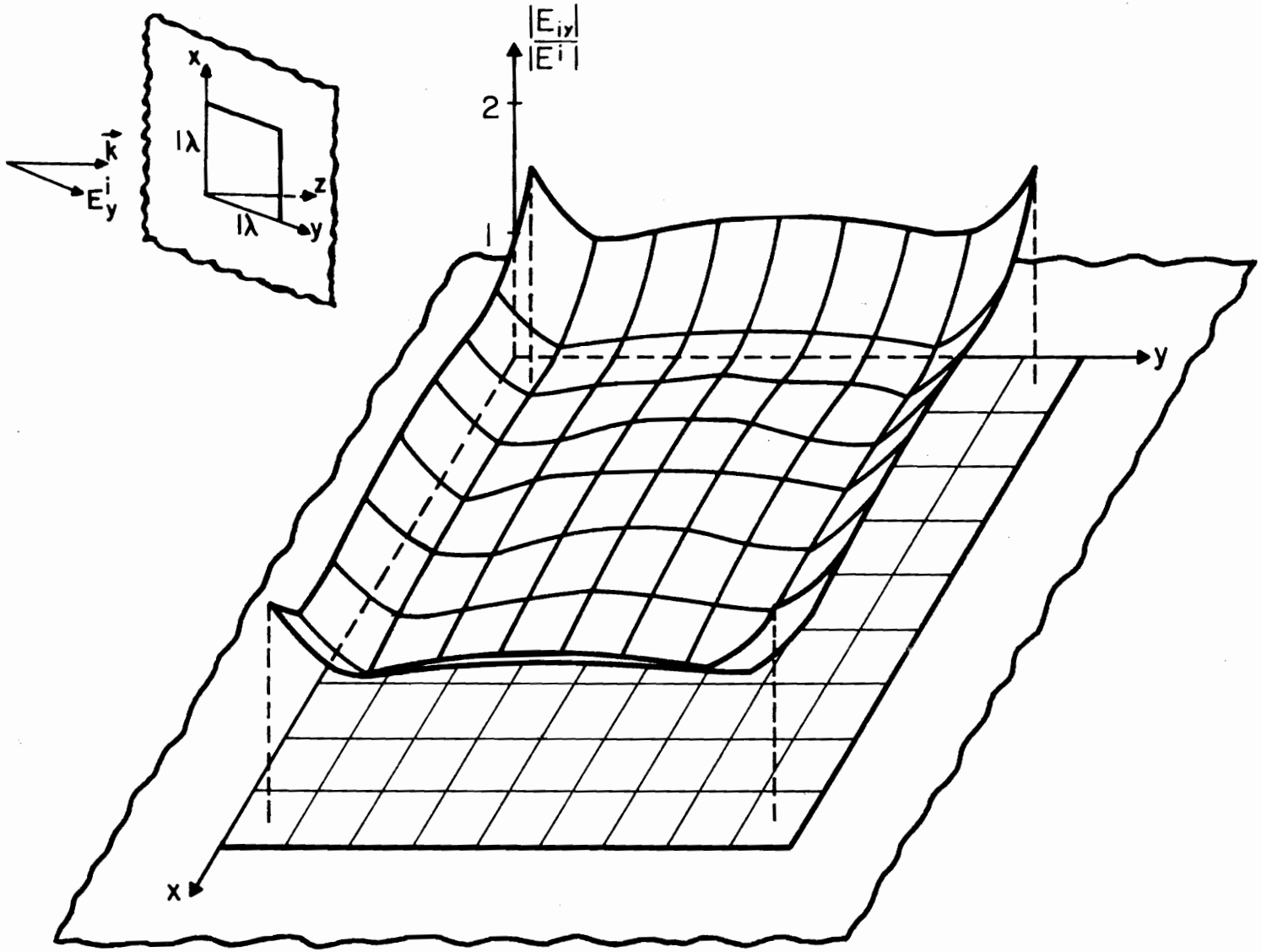

Figure 3.2. Three-dimensional representation of the amplitude distribution of the inhomogeneous portion of the E_y-field in the aperture.

$$\sum_{m=1}^{M}\sum_{n=1}^{N}\begin{Bmatrix} E_x(x'_m,y'_n) \\ E_y(x'_m,y'_n) \end{Bmatrix} 2g_0(x_\ell,y_p;x'_m,y'_n)\,\Delta x'_m\,\Delta y'_n = \frac{1}{jk\gamma}\begin{Bmatrix} E^i_{0x} \\ E^i_{0y} \end{Bmatrix} e^{-jk(\alpha x_\ell+\beta y_p)}$$

$$+\frac{\pi}{k}\begin{Bmatrix} -j \\ -1 \end{Bmatrix}\sum_{n=-L+1}^{L} C_n\left[j^{n+1}e^{j(n+1)\phi}J_{n+1}(k\rho)+\begin{Bmatrix} -1 \\ 1 \end{Bmatrix} j^{n-1}e^{j(n-1)\phi}J_{n-1}(k\rho)\right]$$

$$\ell = 1, \ldots, M;\ p = 1, \ldots, N \qquad (3.42)$$

where $\rho = \left(x_\ell^2 + y_p^2\right)^{1/2}$, $\phi = \tan^{-1}(y_p/x_\ell)$, and 2L corresponds to the total number of matching points on the rim. This procedure is followed in anticipation of the application of the boundary condition $\vec{E}\cdot\hat{\tau} = 0$, which is eventually used to determine the unknown C_n's. It should be noted that at the point $(x'_m,y'_n) = (x_\ell,y_p)$, the kernel $2g_0$ exhibits a singular behavior; therefore, special care must be exercised in evaluating the integral in the neighborhood of this singular point. This is done by noting, in the first instance, that the self-patch region may be approximated as

$$\int_{-\Delta x/2}^{\Delta x/2}\int_{-\Delta y/2}^{\Delta y/2}\frac{e^{-jk\sqrt{x'^2+y'^2}}}{2\pi\sqrt{x'^2+y'^2}}\,dx'\,dy' \approx \frac{1}{\pi}\left\{\Delta x\,\ell n\left|\tan\left(\frac{\pi}{4}+\frac{1}{2}\tan^{-1}\frac{\Delta y}{\Delta x}\right)\right| + \Delta y\,\ell n\left|\tan\left(\frac{\pi}{4}+\frac{1}{2}\tan^{-1}\frac{\Delta x}{\Delta y}\right)\right| - j\,\frac{k\Delta x\Delta y}{2}\right\}. \qquad (3.43)$$

The manipulations for the derivation of the above equation are summarized in Appendix C.

Using matrix notation, (3.42) may then be expressed in the following form:

$$\begin{cases} [g_0]\{E_x\} = \left\langle E_x^i \right\rangle + [h_x]\{C\} \\ [g_0]\{E_y\} = \left\langle E_y^i \right\rangle + [h_y]\{C\} \end{cases} \tag{3.44}$$

where $[h_x]$ and $[h_y]$ are $(M \cdot N)$ x $(2L)$ matrices defined as follows:

$$\begin{bmatrix} h_x \\ h_y \end{bmatrix} = \frac{\begin{pmatrix} -j \\ -1 \end{pmatrix} \pi}{k} \begin{bmatrix} j^{-L+2} e^{-j(-L+2)\phi_1} J_{-L+2}(k\rho_1) \mp j^{-L} e^{-jL\phi_1} J_{-L}(k\rho_1) \cdots \\ \vdots \qquad\qquad\qquad\qquad \vdots \\ je^{j\phi_1} J_1(k\rho_1) \mp j^{-1} e^{-j\phi_1} J_{-1}(k\rho_1) \cdots \\ \vdots \qquad\qquad\qquad\qquad \vdots \\ j^{L+1} e^{j(L+1)\phi_1} J_{L+1}(k\rho_1) \mp j^{L-1} e^{j(L-1)\phi_1} J_{L-1}(k\rho_1) \cdots \end{bmatrix}$$

$$\begin{bmatrix} j^{-L+2} e^{j(-L+2)\phi_{MN}} J_{-L+2}(k\rho_{MN}) \mp j^{-L} e^{-jL\phi_{MN}} J_{-L}(k\rho_{MN}) \\ \vdots \qquad\qquad\qquad\qquad \vdots \\ je^{j\phi_{MN}} J_1(k\rho_{MN}) \mp j^{-1} e^{-j\phi_{MN}} J_{-1}(k\rho_{MN}) \\ \vdots \qquad\qquad\qquad\qquad \vdots \\ j^{L+1} e^{j(L+1)\phi_{MN}} J_{L+1}(k\rho_{MN}) \mp j^{L-1} e^{j(L-1)\phi_{MN}} J_{L-1}(k\rho_{MN}) \end{bmatrix}^T \tag{3.45}$$

Note that coefficients -j and -1, shown in the r.h.s. of the above equation, are used for h_x and h_y, respectively, and "T" is used to indicate the transposed operator. Equation (3.44) is subjected to the condition $\vec{E} \cdot \hat{\tau} = 0$. This condition can also be stated in a matrix form as

$$[\tau]\left\{\begin{array}{c}\langle E_x\rangle \\ \hline \langle E_y\rangle\end{array}\right\} = \left[\begin{array}{c|c}[\tau_x] & 0 \\ \hline 0 & \tau_y\end{array}\right]\left\{\begin{array}{c}\langle E_x\rangle \\ \hline \langle E_y\rangle\end{array}\right\} = 0 \qquad (3.46)$$

where $[\tau]$ is a (2L) x (2M · N) matrix. The elements of this matrix are zero everywhere except at the prescribed edge patches where they are set equal to unity in order to fulfill the condition $\vec{E} \cdot \hat{\tau} = 0$.

Solving (3.44) for $\{E_x\}$ and $\{E_y\}$, one obtains

$$\begin{cases} \{E_x\} = [g_0]^{-1} \langle E_x^i\rangle + [g_0]^{-1}[h_x]\{C\} \\ \{E_y\} = [g_0]^{-1} \langle E_x^i\rangle + [g_0]^{-1}[h_y]\{C\} \end{cases} . \qquad (3.47)$$

Subjecting the above equation to condition (3.46), the following form is derived:

$$\begin{cases} [\tau_x][g_0]^{-1} \langle E_x^i\rangle + [\tau_x][g_0]^{-1}[h_x]\{C\} = 0 \\ [\tau_y][g_0]^{-1} \langle E_y^i\rangle + [\tau_y][g_0]^{-1}[h_y]\{C\} = 0 \end{cases} . \qquad (3.48)$$

The above equation represents a set of 2L equations for the 2L unknowns C_n's. This equation may be rewritten as

$$\left[\begin{array}{c|c}[\tau_x][g_0]^{-1} & 0 \\ \hline 0 & [\tau_y][g_0]^{-1}\end{array}\right]\left\{\begin{array}{c}\langle E_x^i\rangle \\ \hline \langle E_y^i\rangle\end{array}\right\} = -\left[\begin{array}{c}[\tau_x][g_0]^{-1}[h_x] \\ \hline [\tau_y][g_0]^{-1}[h_y]\end{array}\right]\{C\} . \qquad (3.49)$$

Equation (3.49) can now be solved to obtain

$$\{C\} = -\left[\begin{array}{c}[\tau_x][g_0]^{-1}[h_x] \\ \hline [\tau_y][g_0]^{-1}[h_y]\end{array}\right]^{-1}\left[\begin{array}{c|c}[\tau_x][g_0]^{-1} & 0 \\ \hline 0 & [\tau_y][g_0]^{-1}\end{array}\right]\left\{\begin{array}{c}\langle E_x^i\rangle \\ \hline \langle E_y^i\rangle\end{array}\right\} . \qquad (3.50)$$

After the C_n's have been determined, the tangential E-field in the aperture may be computed by substituting (3.50) into (3.46). Before doing this, $\{E_x\}$ and $\{E_y\}$ are first decomposed into the following two components:

$$\{E_x\} = \{E_{ix}\} + \{E_{hx}\} \tag{3.51a}$$

$$\{E_y\} = \{E_{iy}\} + \{E_{hx}\} \tag{3.51b}$$

where subscripts i and h refer to the inhomogeneous and homogeneous components of the field, respectively. By substituting (3.50) into (3.46) and making use of (3.51), the following formulas are finally derived:

$$\begin{Bmatrix} E_{ix} \\ iy \end{Bmatrix} = [g_0]^{-1} \begin{Bmatrix} E_x^i \\ y \end{Bmatrix} \tag{3.52}$$

$$\begin{Bmatrix} E_{hx} \\ hy \end{Bmatrix} = -[g_0]^{-1} \begin{bmatrix} h_x \\ y \end{bmatrix} \left[\begin{array}{c|c} [\tau_x][g_0]^{-1}[h_x] & \\ \hline & [\tau_y][g_0]^{-1}[h_y] \end{array}\right]^{-1} \left[\begin{array}{c|c} [\tau_x][g_0]^{-1} & 0 \\ \hline 0 & [\tau_y][g_0]^{-1} \end{array}\right] \begin{Bmatrix} \{E_x^i\} \\ \hline \{E_y^i\} \end{Bmatrix} . \tag{3.53}$$

The numerical accuracy and stability of the solution of (3.53) may be checked rather simply by verifying how well we have satisfied the boundary condition

$$\left[\begin{array}{c|c} [\tau_x] & 0 \\ \hline 0 & [\tau_y] \end{array}\right] \begin{Bmatrix} \{E_x\} \\ \{E_y\} \end{Bmatrix} = 0 \tag{3.54}$$

which requires that the tangential E-field in the aperture must be zero at the rim.

Since the elements of $\{E_x\}$ and $\{E_y\}$ are zero at the edge patches located along the x-axis and y-axis, respectively, one may then use an alternative scheme to that used in the previous paragraphs and rearrange a new matrix equation. This is done by replacing the zero elements of $\{E_x\}$ and $\{E_y\}$ by the elements of $\{C\}$ and exchanging the corresponding elements of the matrix $[g_0]$ by those of $[h_x]$ and $[h_y]$. After introducing all of the changes as described above, the matrix equation (3.43) may be rearranged to read as follows:

$$\left[[g_0],[h_x],[h_y]\right] \begin{Bmatrix} \{E_{mx}\} \\ \{E_{my}\} \\ \{C\} \end{Bmatrix} = \begin{Bmatrix} \langle E_x^i \rangle \\ \langle E_y^i \rangle \end{Bmatrix} \tag{3.55}$$

where $\left[[g_0],[h_x],[h_y]\right]$ is a $(2M \cdot N) \times (2M \cdot N)$ matrix constructed by incorporating the necessary changes, and $\{E_{mx}\}$ is the modified version of $\{E_x\}$ which is constructed by removing the zero elements of $\{E_x\}$. The same construction is true for $\{E_{my}\}$. One can then solve (3.55) and determine $\{E_{mx}\}$, $\{E_{my}\}$ and $\{C\}$. It should be mentioned that the matrix $\left[[g_0],[h_x],[h_y]\right]$ has many zero elements and therefore special care must be exercised to invert this matrix economically. The form (3.55) is of special importance in connection with the application of the singularity expansion method (SEM) (Tesche, 1973).

3.3.2 Kirchhoff approximation

The Kirchhoff approximation has been used very extensively in the high frequency domain analysis. Perhaps this approximation is one of the simplest methods for treating the aperture diffraction problem. This approximation has taken several different forms in the literature. Three different ways of formulating the Kirchhoff approximation for the

scalar wave function are described by Keller et al. (1957), and the formulation of the vector equivalents of the Kirchhoff integral is analyzed, for instance, by Jackson (1962). In this work the Kirchhoff's E-approximation will be used in order to perform some numerical comparisons.

In formulating the Kirchhoff's E-approximation, one assumes that the E-tangential field in the aperture is the same as the corresponding tangential field of the incident field at the aperture. Using this fact and employing Equation (3.10), the diffracted field in the $z > 0$ region takes the following form:

$$\vec{E}_+^d(\vec{R}) = -2\nabla \times \iint_{\bar{A}} \vec{E}^i(\vec{\rho}') \times \hat{n}_+ g_0(\vec{\rho}' | \vec{R})\, da'$$

$$\{\vec{R}: \quad (x,y,z) \in \mathcal{R}_+\} \quad . \tag{3.56}$$

In the following section some representative solutions of Equations (3.52) and (3.53) will be presented. These solutions are then compared with the results obtained from (3.56) for a number of different aperture sizes and incident fields.

3.3.3 The numerical result of the field distribution in rectangular apertures

A $1\lambda \times 1\lambda$ square aperture illuminated by a normally incident plane wave as shown in Figure 3.2 is considered as the first example. The solution is deliberately left in general format and no use is made of the anticipated symmetry of the solution for the normally incident field. This general format is also helpful in checking the accuracy of the numerical solution by verifying that the proper symmetries are exhibited in the solutions.

The aperture is subsectionalized into 9 x 9 square patches and the condition (3.46) is enforced at all of the edge patches [i.e., $2(M + N) = 36$ in Equation (3.42)]. Assuming that the incident field has the following polarization

$$\vec{E}^i = |E^i| \, \hat{y} e^{-jkz} \quad , \tag{3.57}$$

Equation (3.42) can then be solved by following steps (3.47), (3.49), (3.50) and (3.52). Figure 3.2 shows the three-dimensional representation of the amplitude of the E_{iy} field obtained by solving Equation (3.52). Note that because of the prescribed incident field (3.57), the transverse field E_{ix} is zero everywhere in the aperture. To obtain the solution of (3.52) no homogeneous terms are used and, as Figure 3.2 exhibits, this part of the solution does not, by itself, satisfy the correct edge behavior. Figure 3.3 displays the amplitude distribution of the homogeneous solution E_{hy}, obtained by solving (3.53) with the use of homogeneous terms defined in (3.42). The total solution E_y is now constructed by superimposing the two solutions as indicated in (3.51a). From Figure 3.4 it is noted that this solution does indeed exhibit the correct symmetry and edge behavior. The determination of E_x, the cross-polarized component, also follows along the same lines. It is interesting to note that E_x is identically equal to E_{hx}, the homogeneous portion of the solution, since the incident E_x field is identically zero. Figure 3.5 shows that proper symmetry and edge behavior are obtained for the x-component of the E-field also. The above discussions make it patently clear that the inclusion of the homogeneous term is essential for constructing the complete solution.

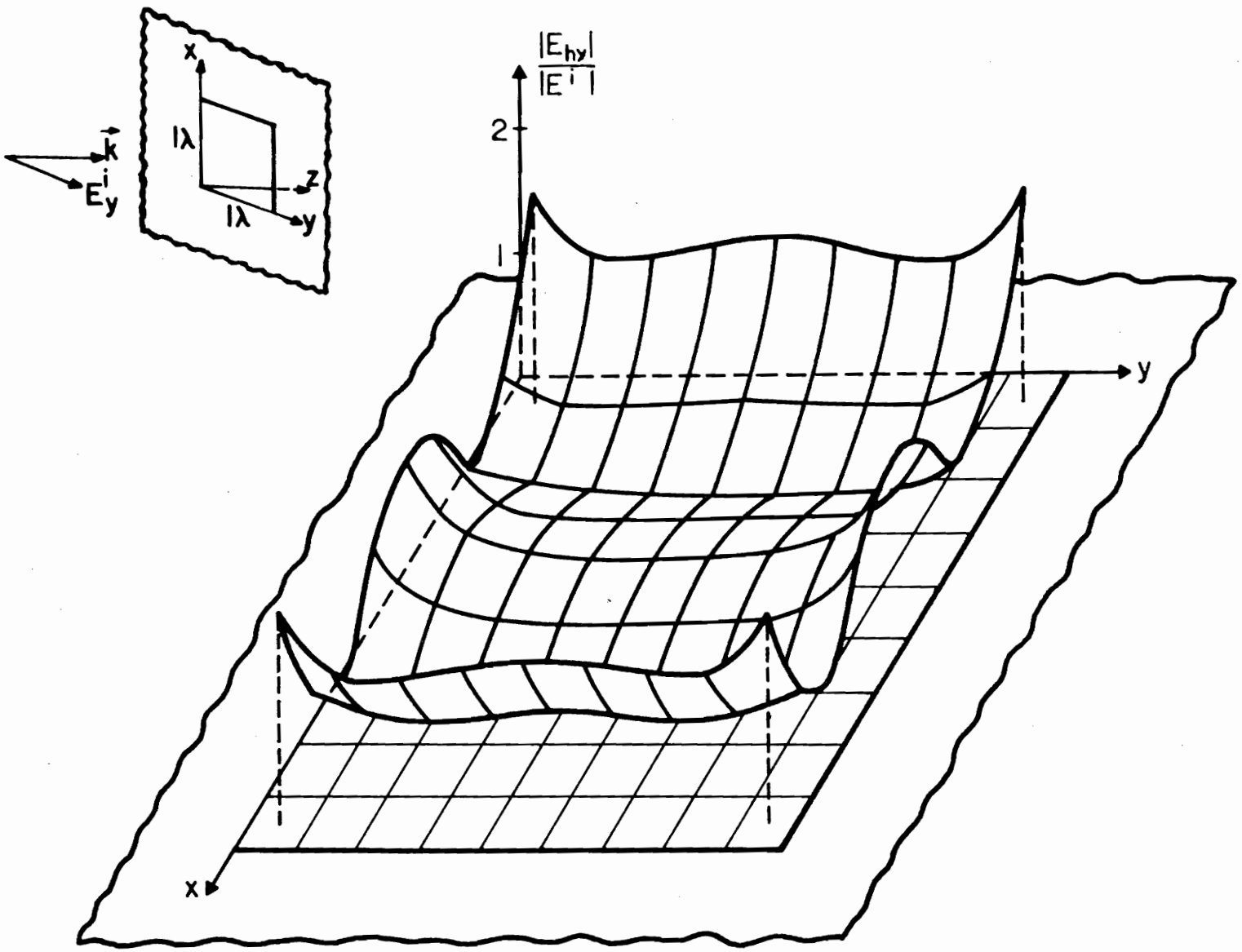

Figure 3.3. Three-dimensional representation of the amplitude distribution of the homogeneous portion of the E_y-field in the aperture.

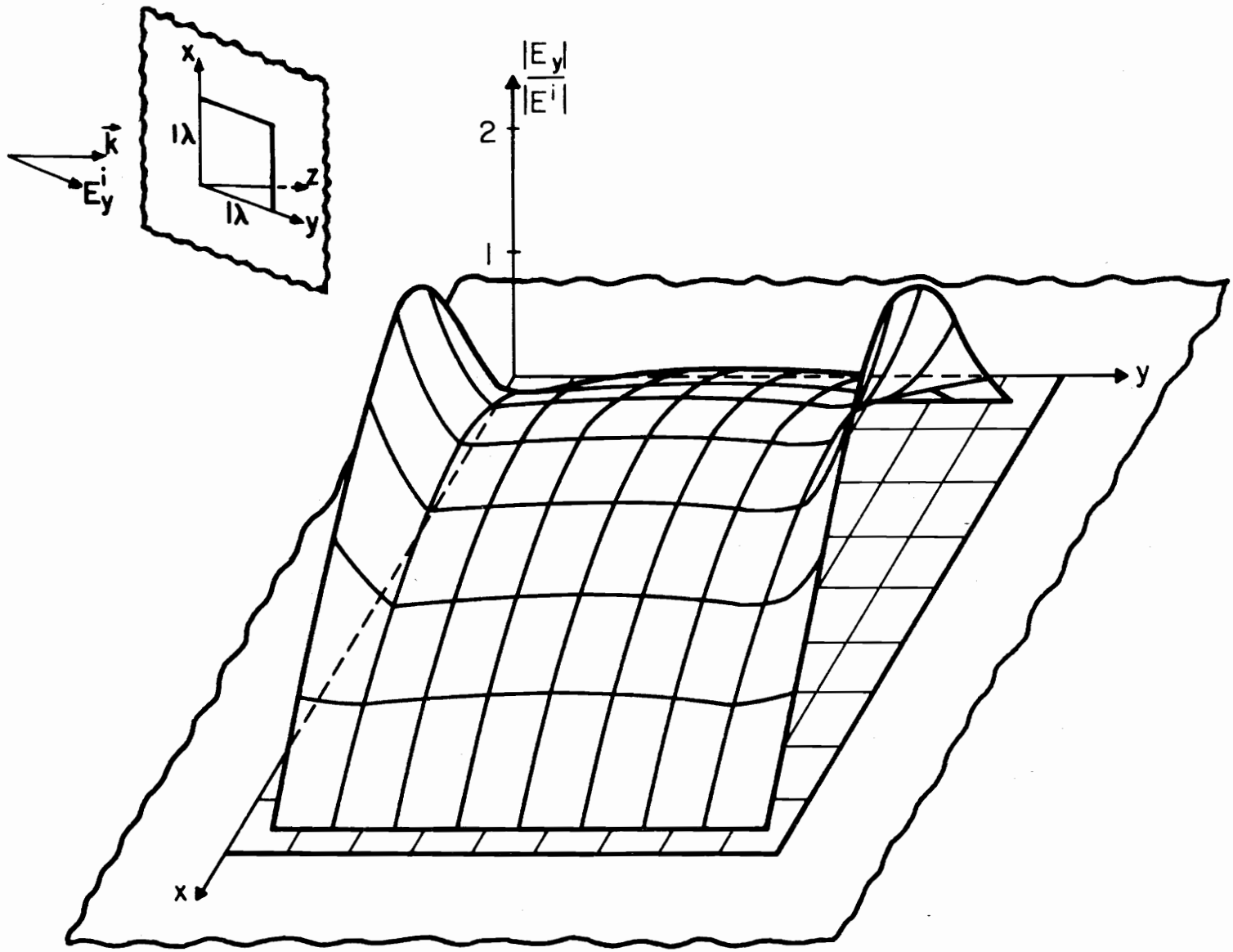

Figure 3.4. Three-dimensional representation of the amplitude distribution of the E_y-field in the aperture.

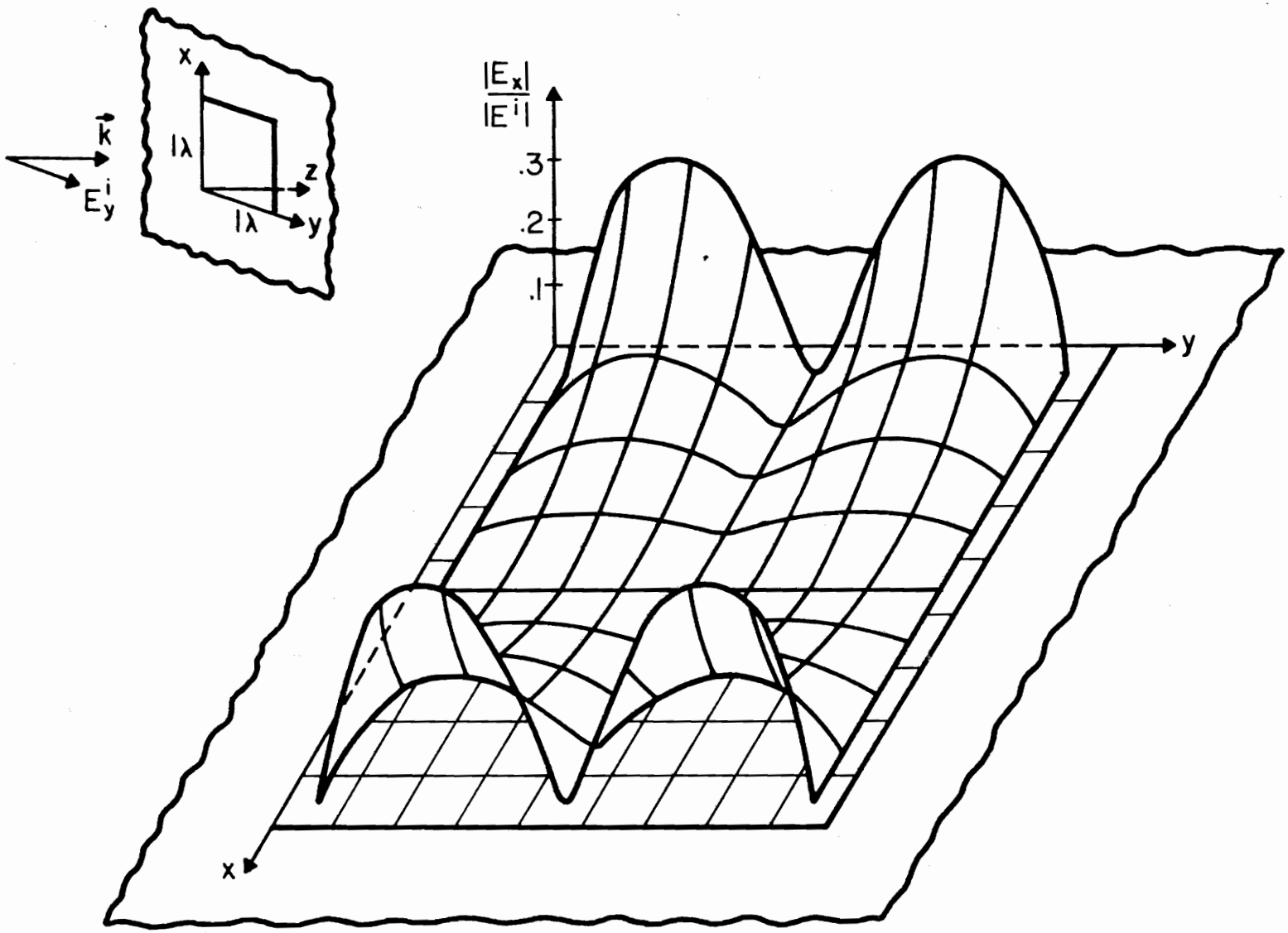

Figure 3.5. Three-dimensional representation of the amplitude distribution of the E_x-field in the aperture.

In order to check the convergence of the satisfaction of the edge behavior, E_x and E_y were recomputed by employing only 20 edge patches where the condition (3.46) was imposed. No substantial difference in the final results was observed between the 36-edge patch and 20-edge patch cases. This appears to indicate that a solution satisfying the proper edge behavior can be constructed by using substantially fewer Bessel functions than the number $2(M + N)$ indicated in (3.42). An additional convergence check on the matrix size also has been carried out. The $1\lambda \times 1\lambda$ aperture has been subsectionalized into 6 x 6 square patches, rather than the original 9 x 9, and the numerical solution has been found to be substantially unchanged. In particular, the computed fields at observation points located behind the aperture are almost identical for the two cases.

Figures 3.6a and 3.6b show the amplitude and phase distributions of the E_x and E_y fields sampled along the principal axes of a $1\lambda \times 1\lambda$ square aperture. These results are compared with the ones given by Kirchhoff's approximation, as plotted in the same figures. It is obvious that the results obtained by employing the integral equation technique exhibit the correct edge behavior, whereas those of Kirchhoff do not. The two solutions deviate even further from each other in the immediate neighborhood of the edges.

After determining the aperture field, the scattered E-field behind the aperture may be readily computed using (3.10). Figure 3.7 displays the behavior of the E-field sampled along two lines parallel to the z-axis as indicated in the same figure. Due to the fact that the incident field is polarized in the y-direction, the dominant field is the E_y-field. The plot in Figure 3.7 shows that the field has a $\frac{1}{r}$ type behavior away from the aperture.

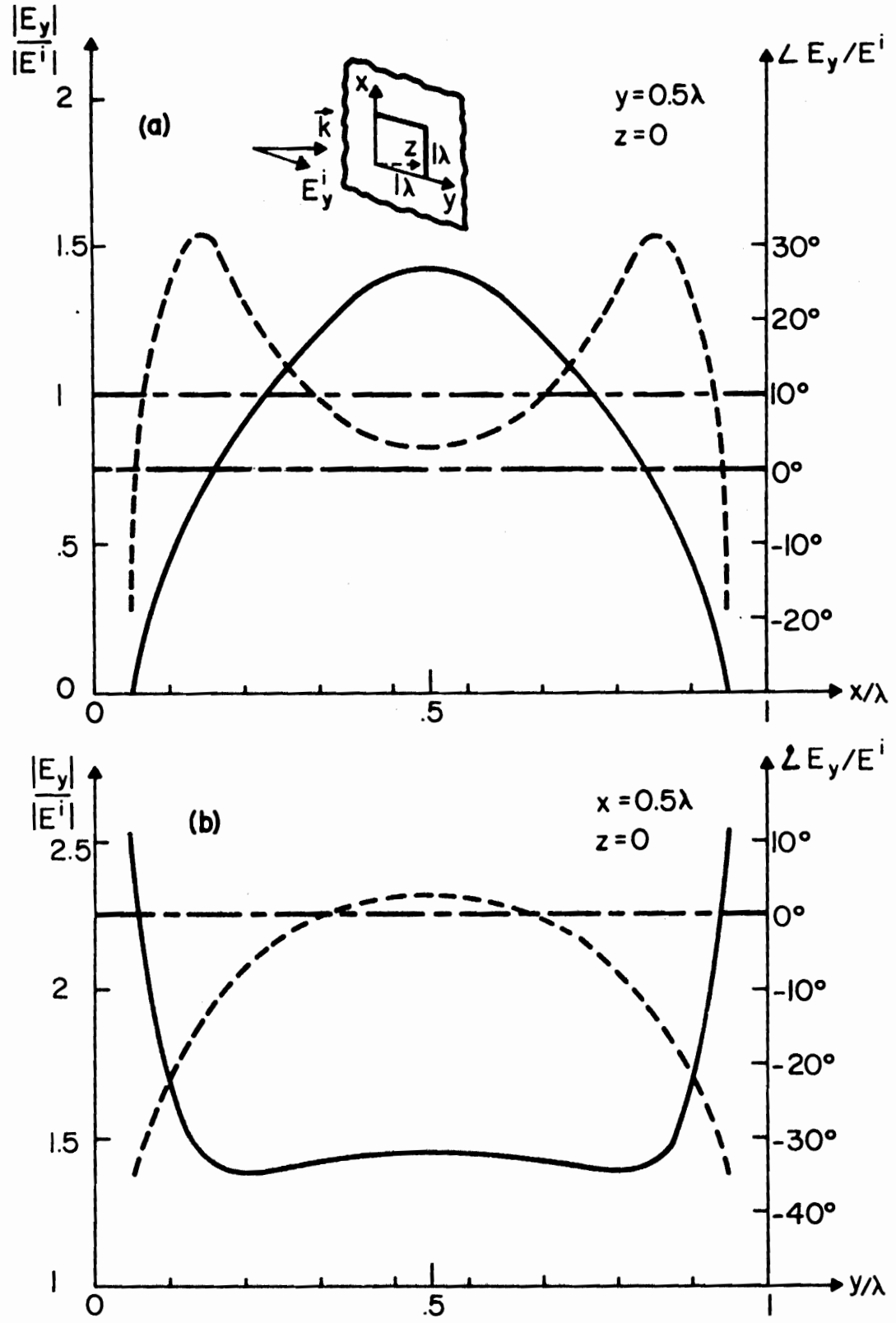

Figure 3.6. Amplitude and phase distribution of the E_y-field in a 1λ x 1λ square aperture due to a normally incident plane wave. (a) E_y-field sampled along a line parallel to the x-axes and passing through the center. (b) E_y-field sampled along a line parallel to the y-axes and passing through the center. Amplitude (——) and phase (----) of E_y from integral equation solution. Amplitude (—— -) and phase (—— --) of E_y field from Kirchhoff's approximation.

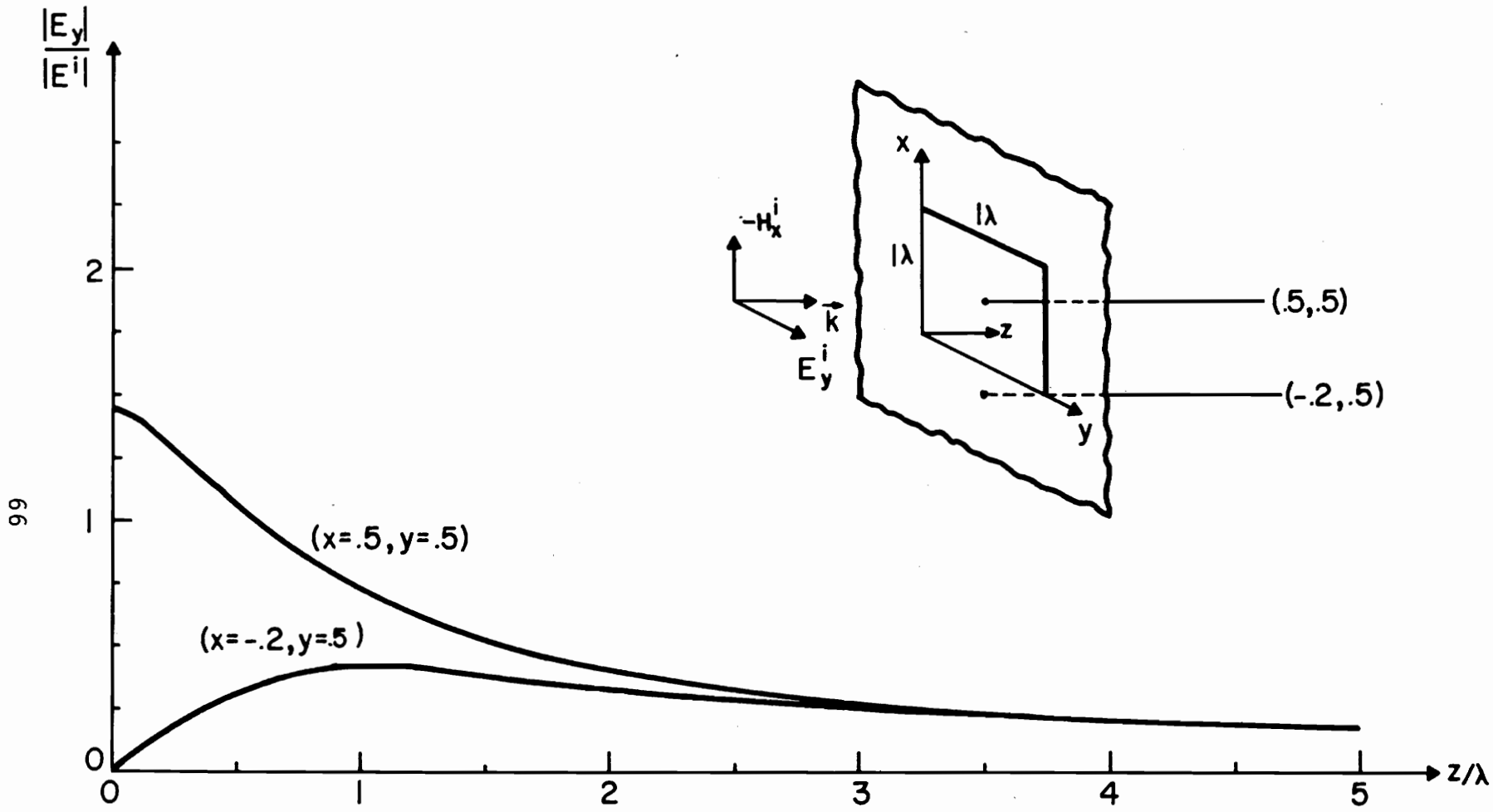

Figure 3.7. Amplitude distribution of E_y-field sampled along two lines parallel to the z-axis.

In Figure 3.8 a comparison of the square aperture results is made with those obtained experimentally by Robinson (1953) who measured the E-field across a circular aperture of one wavelength in diameter. Observation shows that the two results are quite comparable even at the edges where the field exhibits a singular behavior. It should be pointed out that this close agreement between the field distributions in circular and square apertures is obtained only when one compares the fields along the principal axes of the square aperture, a result which is not altogether unexpected. Figure 3.9 shows a comparison between the results obtained using our integral equation and Kirchhoff approximation (3.56) for the field behind the aperture, and also a plot of the experimentally measured results (Andrews, 1950) for a circular aperture. All three solutions exhibit the same type of behavior, at least 1.5λ behind the aperture. It is further noted that the integral equation solution shows a much better agreement with the experimental results than the ones based on the Kirchhoff approximation. The deviation between the integral equation solution and Kirchhoff's approximation is about 18 percent at a point located two wavelengths behind the aperture along a line which runs parallel to the z-axis and originates at the center of the square. This deviation becomes progressively smaller as one moves away from the aperture.

In order to examine the behavior of the E-field in the aperture due to an obliquely incident plane wave, the aperture is illuminated with the following incident field:

$$\vec{E}^i = |E^i| \; (-\hat{x} \sin 60° + \hat{y} \cos 60°) \; e^{-jk(x\sin 30°\cos 60° + y\sin 30°\sin 60° + z\cos 30°)} \tag{3.58}$$

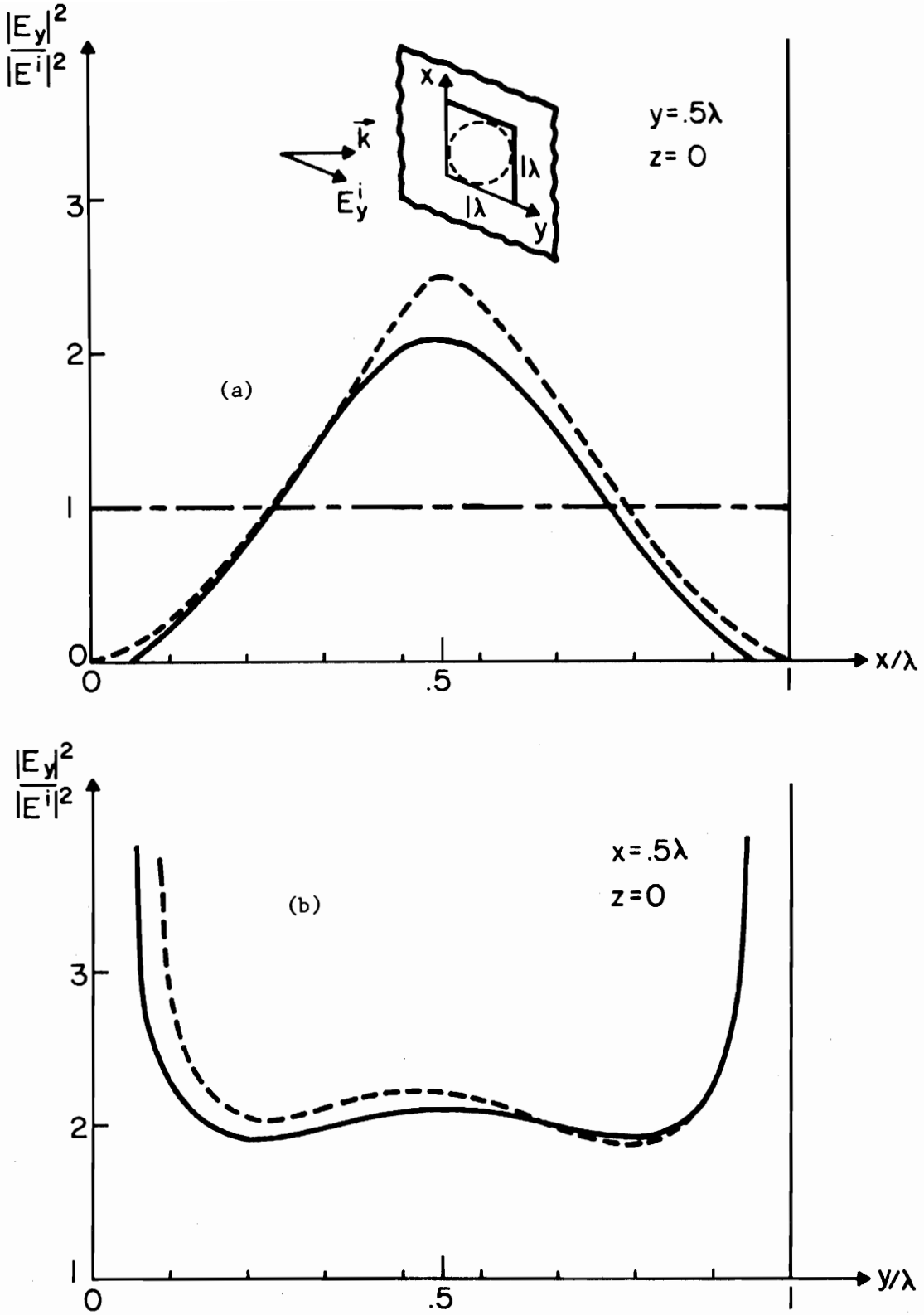

Figure 3.8. Intensity distribution of the E_y-field sampled along the principal axes of a 1λ x 1λ square aperture and a circular aperture of radius 1λ. (a) Intensity distribution sampled along a line parallel to the x-axis and passing through the center. (b) Intensity distribution sampled along a line parallel to the y-axis and passing through the center. Integral equation solution (——). Experimental results (---) from Robinson (1953).

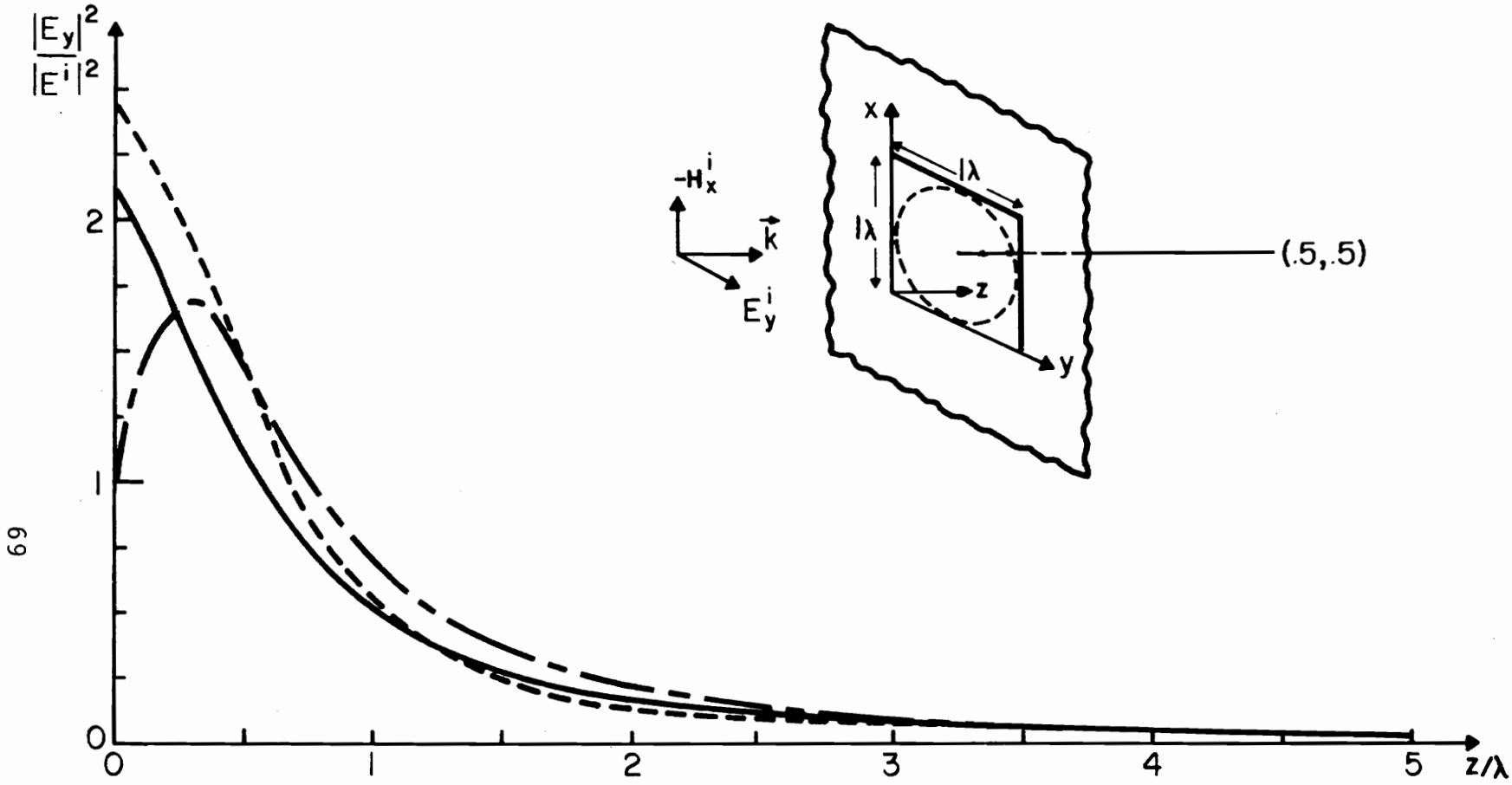

Figure 3.9. Intensity distribution of E_y-field sampled along a line parallel to the z-axis and passing through the center of square and circular apertures. Integral equation (——) solution for square aperture. Kirchhoff approximation for square aperture (—— -). Experimental result (---) for circular aperture from Andrews (1950).

The above incident field is called E-parallel since the E-field is parallel to the x-y plane which coincides with the plane of the aperture. Figure 3.10 displays the behavior of the E-field sampled along the center axes of a 1λ x 1λ aperture illuminated by the plane wave (3.58). In contrast with the case of normal incidence the solution no longer displays any kind of symmetry; however, the correct edge behavior is still evident from the plot of the aperture field in Figure 3.10. These results are again compared with those determined using the Kirchhoff approximation. One observes that for an obliquely incident field, the two results deviate more drastically than for the case of normal incidence. These aperture field distributions have once again been used to determine the E-field behind the aperture sampled along the z-axis as shown in Figure 3.11. In contrast to the case of normal incidence, all three components of the E-field have non-zero amplitudes. Although the E_z component is almost 100 times smaller than the E_x and E_y components, it shows a rather interesting behavior. Note that the E_z component is zero at the center of the aperture, indicating that the incident E_z^i-field, which is zero in this case, is not perturbed. Away from the aperture, it rises to a maximum, almost $\lambda/2$ behind the aperture, and then decays with a $1/r^2$ type behavior.

Another important problem in connection with the study of aperture diffraction is the case of grazing incidence. In contrast with a number of other techniques that have been employed for attacking this problem, no special modifications are necessary in the integral equation approach for handling this problem. Consider an H-parallel incident plane wave as follows:

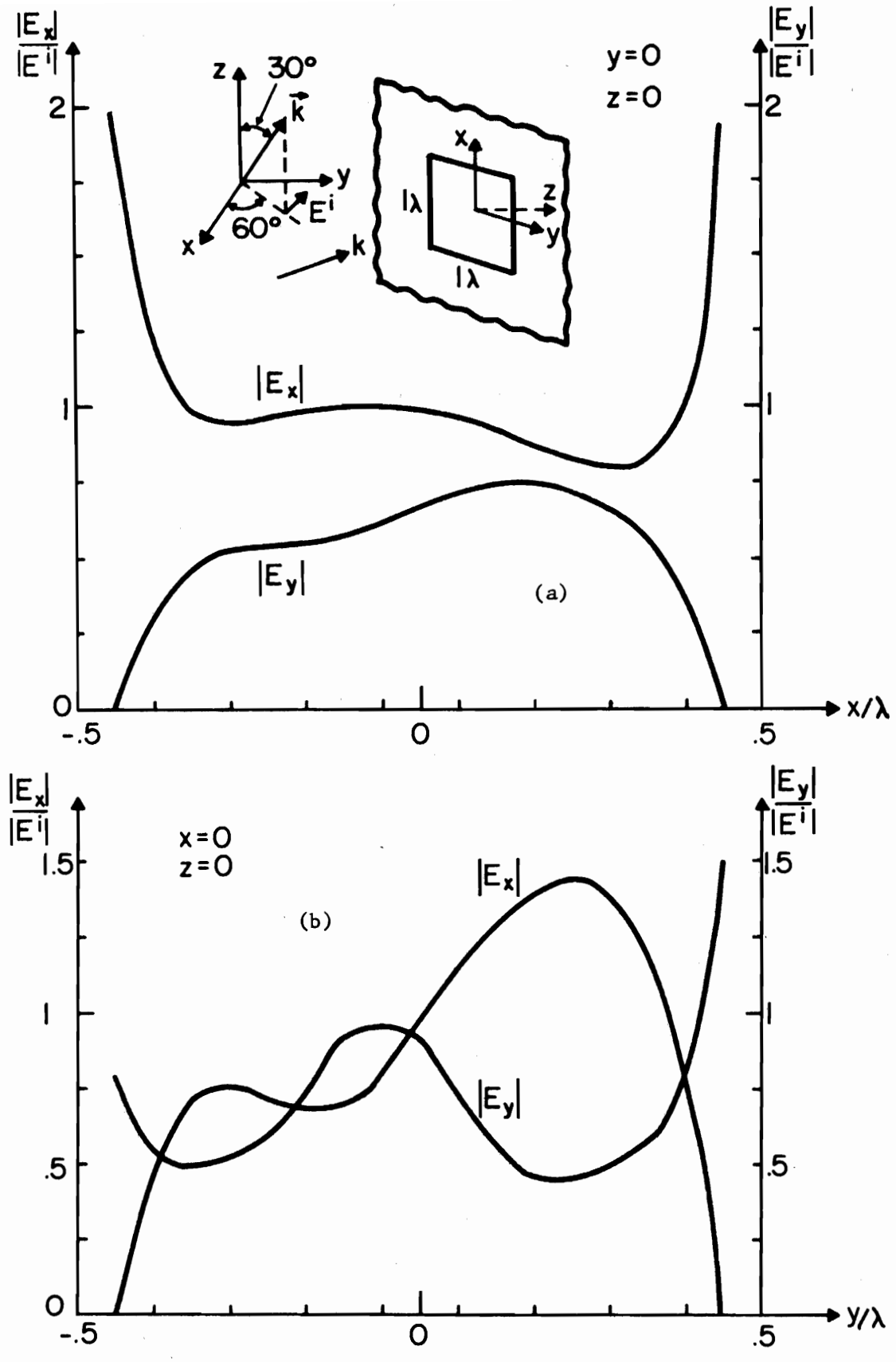

Figure 3.10. The amplitude distribution of E_x- and E_y-field in a 1λ x 1λ square aperture due to an obliquely incident plane wave. (a) E-field sampled along the x-axes. (b) E-field sampled along the y-axes.

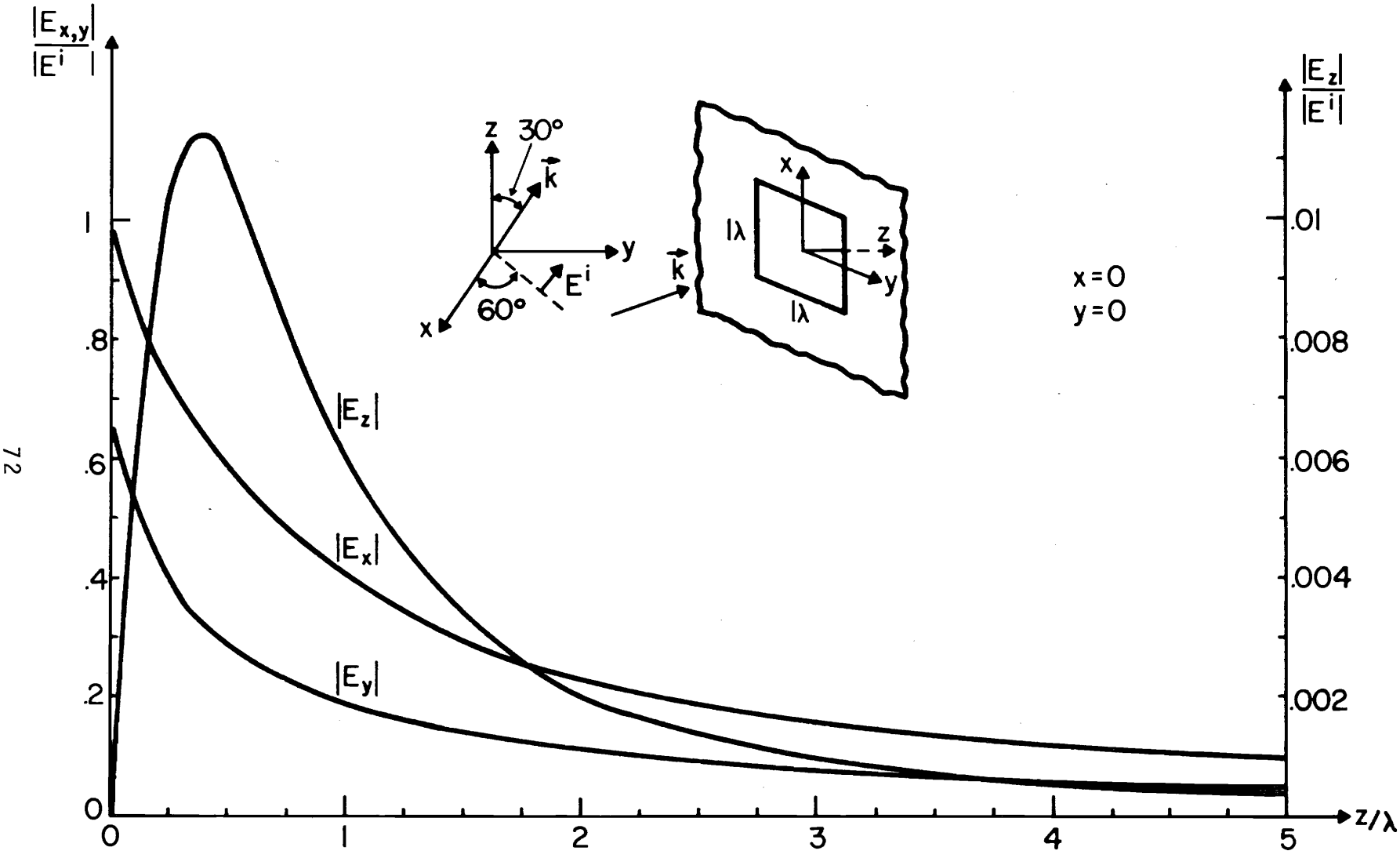

Figure 3.11. E-field distribution along the z-axis of a 1λ x 1λ square aperture illuminated by an obliquely incident plane wave.

$$E^i = |E^i|(\gamma \cos \phi^i \hat{x} + \gamma \sin \phi^i \hat{y} - \sin \theta^i \hat{z})\, e^{-jk(\alpha x+\beta y+\gamma z)} \qquad (3.59)$$

[α, β, γ, ϕ^i and θ^i have been defined earlier in Equation (3.19)]. The H-component of the incident field is now parallel to the plane of the aperture. Substituting Equation (3.59) into (3.42) and finding the limit for the grazing angle, i.e., letting $\gamma = 0$, the first term in the r.h.s. of Equation (3.42) takes the following form:

$$\lim_{\gamma \to 0} \frac{1}{jk\gamma} \begin{Bmatrix} E^i_{0x} \\ E^i_{0y} \end{Bmatrix} e^{-jk(\alpha x_\ell + \beta y_p)} = \frac{1}{jk} \begin{Bmatrix} |E^i| \cos \phi^i \\ |E^i| \sin \phi^i \end{Bmatrix} e^{-jk(\alpha x_\ell + \beta y_p)} . \qquad (3.60)$$

The field behind the aperture for the case of H-polarized grazing incidence is shown in Figure 3.12. As expected, the E_z-field takes the value of unity in the aperture which indicates that the z-component of the incident field is still unperturbed by the aperture. It is interesting to note that although near the aperture E_z has a higher amplitude than E_x, the former decays more rapidly than the latter away from the aperture. This is explained by the fact that the only nonzero components of $\vec{E}$ are transverse, and hence all of the longitudinal components must eventually approach zero.

3.4 Diffraction by a Narrow Aperture

The problem of diffraction of a plane electromagnetic wave by a narrow aperture has attracted the attention of many investigators. Among them, the work of Suzuki (1956) has received considerable attention. In his work Suzuki introduced a magnetic-type Hertzian vector and was able to construct an integral equation for the dominant component of the E-field in the aperture. He further assumed that the

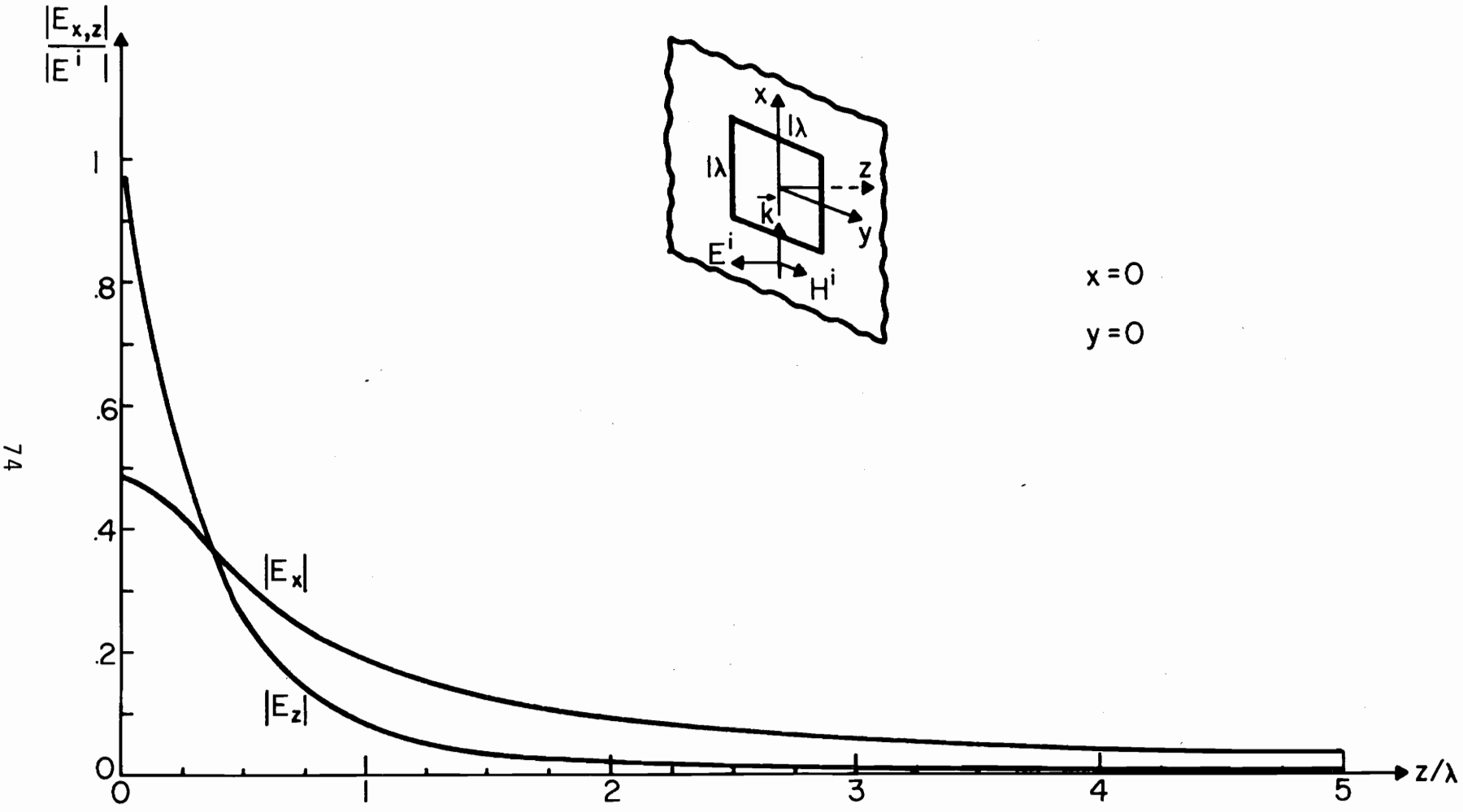

Figure 3.12. Amplitude distribution of E-field sampled along the z-axis for a 1λ x 1λ square aperture illuminated by a plane wave incident at the grazing angle.

other component of the field is zero in the entire aperture. In this section the procedure outlined in Section 3.2 will be followed and Suzuki's approximations will be incorporated in order to generate an integral equation which is quite similar to his integral equation.

Let a plane wave incident field with E_y^i polarization be illuminated normally on a very narrow rectangular aperture. The long side and the narrow side of the aperture lie along the x-axis and the y-axis, respectively. Since the incident field is polarized along the y-axis, the dominant induced field in the aperture will be along the y-axis too. It is then reasonable to assume that the E_x component of the field has zero value in the aperture. Incorporating this assumption in Equation (3.29) one obtains

$$\iint_{\bar{A}} \begin{Bmatrix} 0 \\ E_y \end{Bmatrix} \frac{e^{-jk|\vec{\rho}-\vec{\rho}'|}}{2\pi|\vec{\rho}-\vec{\rho}'|}\, da' = \frac{1}{jk} \begin{Bmatrix} 0 \\ E_{0y}^i \end{Bmatrix} + \frac{1}{k} \int_0^{2\pi} \begin{Bmatrix} \sin\xi \\ -\cos\xi \end{Bmatrix} C(\xi)\, e^{jk(x\cos\xi + y\sin\xi)}\, d\xi$$

$$\{\rho: \quad (x,y) \in \bar{A}\} \quad . \tag{3.61}$$

In order to satisfy the top equation of (3.61) it is clear that $C(\xi)$ must take the following form:

$$C(\xi) = A\delta(\xi) + B\delta(\xi - \pi) \tag{3.62}$$

where A and B are two arbitrary constants yet to be determined. Substituting Equation (3.62) into Equation (3.61) and simplifying the result, the following equation is derived:

$$\iint_{\bar{A}} E_y \frac{e^{-jk|\vec{\rho}-\vec{\rho}'|}}{2\pi|\vec{\rho}-\vec{\rho}'|}\, da' = \frac{1}{jk} E_{0y}^i + \frac{1}{k}\left(-Ae^{jkx} + Be^{-jkx}\right) \tag{3.63}$$

which can be simplified even further by utilizing the fact that the solution must exhibit symmetry along the x-axis. Incorporating the symmetry, one may rewrite Equation (3.63) as follows

$$\iint_{\bar{A}} E_y \frac{e^{-jk|\vec{\rho}-\vec{\rho}'|}}{2\pi|\vec{\rho}-\vec{\rho}'|} da' = \frac{1}{jk} E^i_{0y} + \frac{C}{k} \cos kx \qquad (3.64)$$

where C is a constant which can be determined by enforcing the condition $E_y = 0$ at the edge of the aperture parallel to the y-axis. Integral equation (3.64) is identical to the integral equation used by Suzuki (1956). This equation has the same type of characteristics as the Hallen's integral equation (Collin, 1969). Although (3.64) satisfies all of the Maxwell's equations and continuity conditions, the solution E_y obtained from this equation exhibits the correct edge behavior only when a very narrow aperture is considered.

In the following section, after defining the transmission coefficient, the complete integral equation, i.e., Equation (3.33), will be applied to determine the field distribution in a narrow aperture and hence to check the validity of the approximations employed in constructing Equation (3.64).

3.4.1 Transmission coefficient

There is a quantity of physical interest in dealing with a problem of aperture coupling known as the transmission coefficient. The transmission coefficient "T" of the aperture, which is defined as the ratio of the transmitted energy flux W through the aperture to the incident energy flux w upon the aperture, is expressed as follows:

$$T = \frac{W}{w} \quad . \qquad (3.65)$$

The suitable expression for W is derived from the real part of the Poynting vector theorem (Jordan, 1968) in a nondissipative source-free region

$$\mathrm{Re} \int \nabla \cdot \frac{1}{2} \vec{E} \times \vec{H}^* \, d\nu = 0 \tag{3.66}$$

where integration is performed in the half space in the right-hand side of the screen, and "*" denotes the conjugate operator. This integration involves the quantity

$$\vec{P} = \frac{1}{2} \vec{E} \times \vec{H}^* \quad , \tag{3.67}$$

the real part of which is the average energy flux density. After integrating Equation (3.67) throughout the shadow half space, a connection between the total energy flux at infinity and that through the aperture may be stated as:

$$W = \mathrm{Re} \iint_{\mathcal{M}_\infty} \frac{1}{2} \hat{n} \cdot \vec{E} \times \vec{H}^* \, da = \mathrm{Re} \iint_{\mathcal{M}} \frac{1}{2} \hat{z} \cdot \vec{E} \times \vec{H}^* \, da = \mathrm{Re} \iint_{\mathcal{M}} \frac{1}{2} \hat{z} \times \vec{E} \cdot \vec{H}^* \, da$$

$$= \mathrm{Re} \iint_{\bar{A}} \frac{1}{2} \hat{z} \times \vec{E} \cdot \vec{H}^* \, da \quad . \tag{3.68}$$

Since the tangential component of the magnetic field in the aperture is the same as the tangential component of the magnetic field due to the incident field, one obtains

$$W = \mathrm{Re} \iint_{\bar{A}} \frac{1}{2} \hat{z} \times \vec{E} \cdot (\vec{H}^i)^* \, da \tag{3.69}$$

where H^i is the magnetic component of the incident field.

The incident field is defined as:

$$\vec{E}^i = \vec{E}_0^i \, e^{-j\vec{k}\cdot\vec{r}} \quad . \tag{3.70}$$

Using Maxwell's equations one readily derives

$$\vec{H}^i = \sqrt{\frac{\varepsilon}{\mu}} \; \hat{k} \times \vec{E}^i \quad . \tag{3.71}$$

Employing Equations (3.70) and (3.71) one can then define the total energy flux through the aperture due to the incident field as

$$w = \mathrm{Re} \iint_{\bar{A}} \frac{1}{2} \hat{z} \cdot \vec{E}^i \times (H^i)^* \, da = \mathrm{Re} \iint_{\bar{A}} \frac{1}{2} \sqrt{\frac{\varepsilon}{\mu}} \; |E_0^i|^2 \; \hat{z} \cdot \hat{k} \, da \quad . \tag{3.72}$$

Substituting Equation (3.70) and Equation (3.72) into Equation (3.65), the transmission coefficient T takes the following expression

$$T = \frac{\mathrm{Re} \iint_{\bar{A}} \hat{z} \times \vec{E} \cdot [\hat{k} \times E^i]^* \, da}{|E_0^i|^2 \, A(\hat{z} \cdot \hat{k})} \tag{3.73}$$

where A is the area of the aperture. The above formula will be used to compute the transmission coefficient in the next section.

3.4.2 The numerical result of the field distribution and the transmission coefficient of a narrow aperture

To demonstrate the behavior of the field distribution in a narrow aperture, Equation (3.42) has been used. Figure 3.13a shows the E_y-field distribution inside a narrow aperture whose dimensions are $1\lambda \times .1\lambda$. This aperture is illuminated by a normal incident plane wave

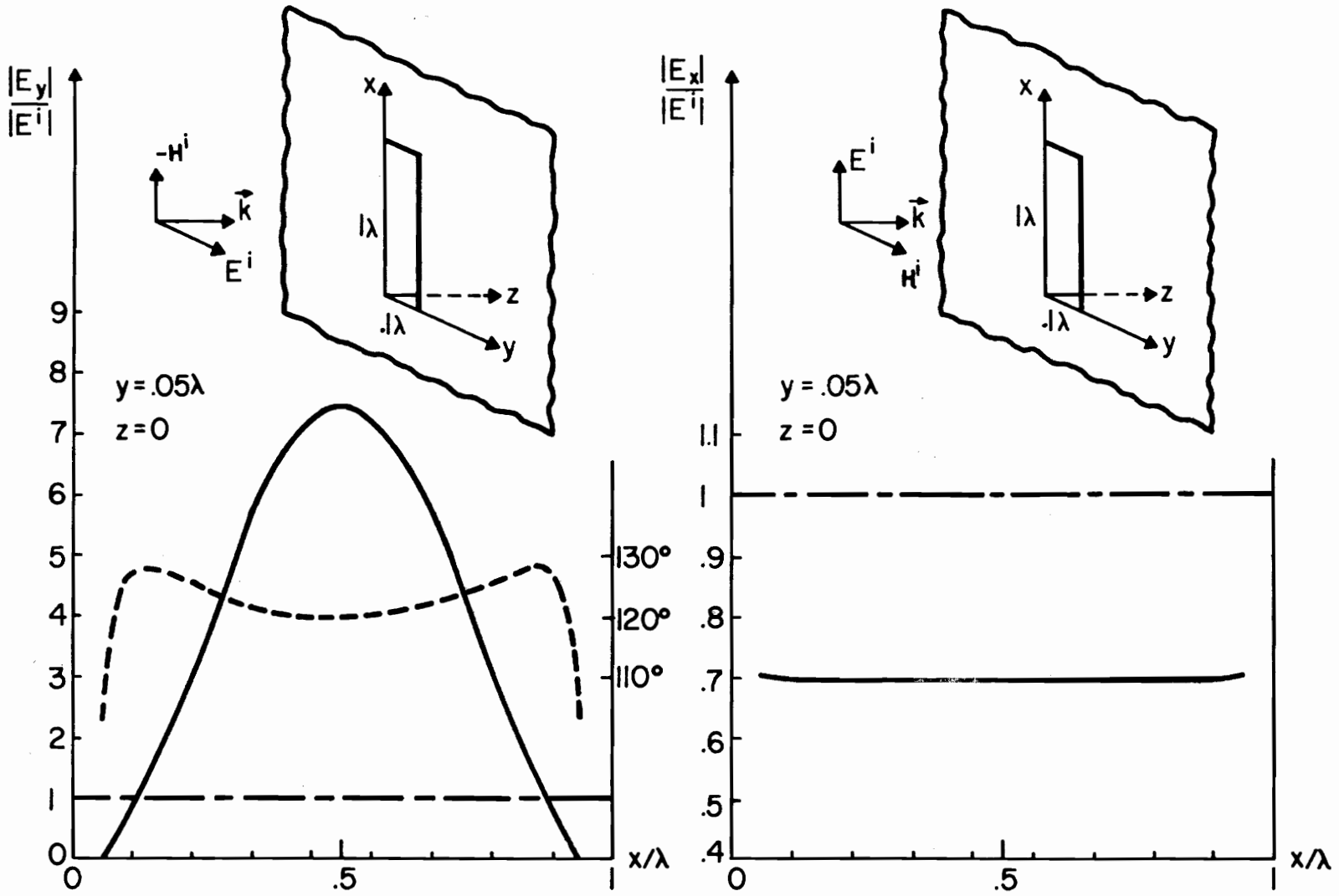

Figure 3.13. Amplitude and phase distribution of the E-field in a narrow aperture illuminated by a normally incident plane wave. (a) E_y-field sampled along a line parallel to the x-axis and passing through the center. (b) E_x-field sampled along a line parallel to the x-axis and passing through the center. Amplitude (——) and phase (----) curves are obtained from integral equation. Amplitude curve (—— -) is obtained using Kirchhoff approximation.

polarized in the y-direction. Figure 3.13 shows that the magnitude of the cross component of the field, i.e., E_x component, is at least 100 times smaller than the magnitude of the dominant component E_y. This numerical result now justifies the assumption used to construct Equation (3.64). It has been further noticed that the series appearing in the r.h.s. of Equation (3.42) does not converge fast, and exhibits an oscillatory behavior around the edge points. This indicates that applying Equation (3.64) is more desirable for very narrow apertures than using Equation (3.42). Figure 3.13b displays the behavior of the E-field in a $1\lambda \times .1\lambda$ aperture illuminated by a normal incident field with E_x polarization. This solution is obtained by solving Equation (3.42). The aperture responds weakly to the E_x polarization as compared to the E_y polarization, a result that was expected. It is further noted that the field distribution derived via the integral equation approach is substantially different from that obtained by the Kirchhoff approximation, as shown in the same figures.

The above aperture field distributions are used to evaluate the diffracted field by the narrow aperture in the region $z > 0$, results of which are shown in Figure 3.14. It is evident that the discrepancy between the two solutions grows worse as one approaches the aperture. This discrepancy is about 46 percent even at a distance of 2λ behind the aperture. This is almost three times larger than for the case of the $1\lambda \times 1\lambda$ aperture investigated earlier.

In order to study the resonance phenomenon in narrow apertures, the transmission coefficient of such apertures has been calculated by employing Equation (3.73). The result, which is shown in Figure 3.15, has been compared with that of Suzuki (1956) who solved integral

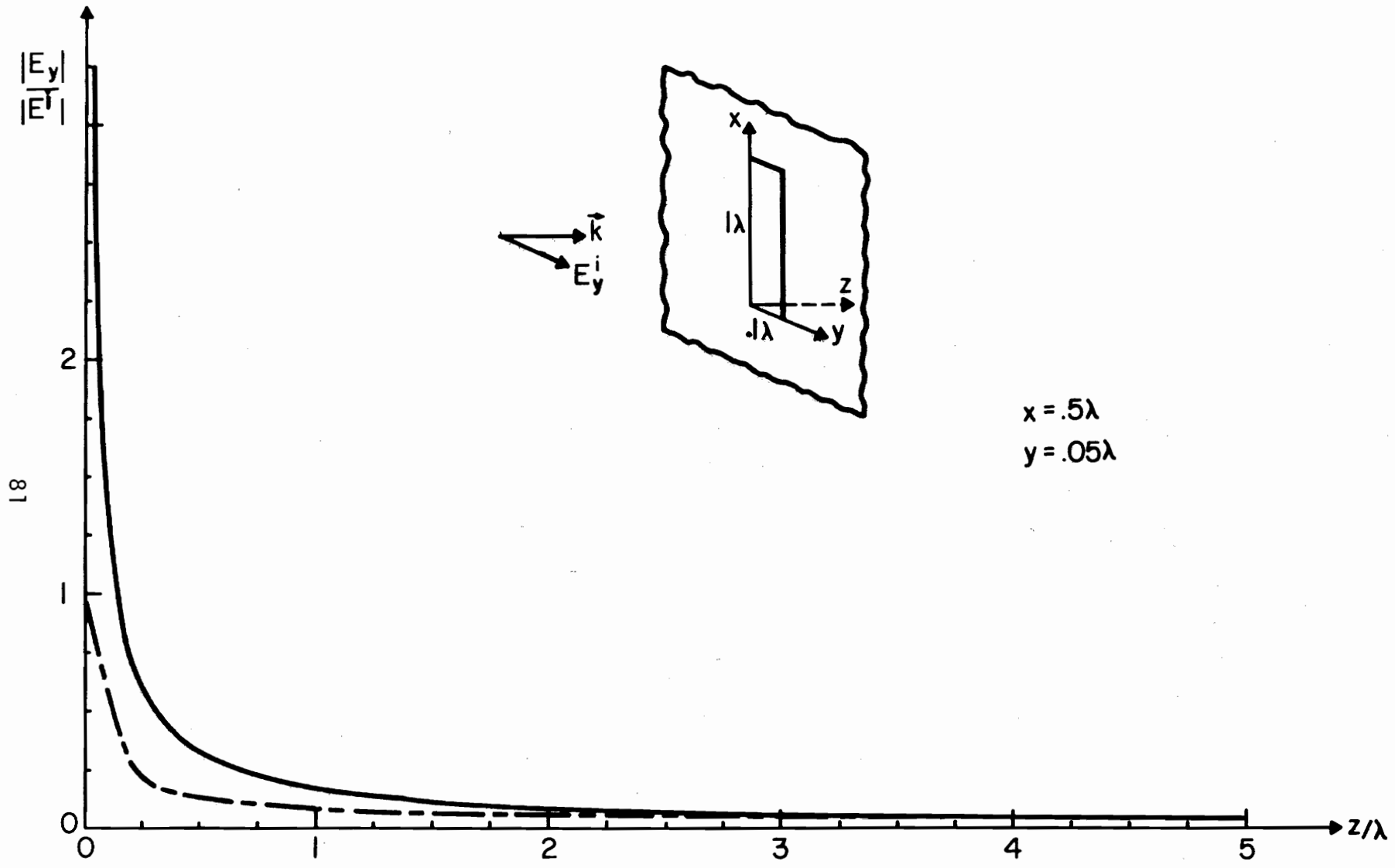

Figure 3.14. Amplitude distribution of the E_y-field sampled along a line parallel to the z-axis and passing through the center. Integral equation (——) solution. Kirchhoff approximation (—— -).

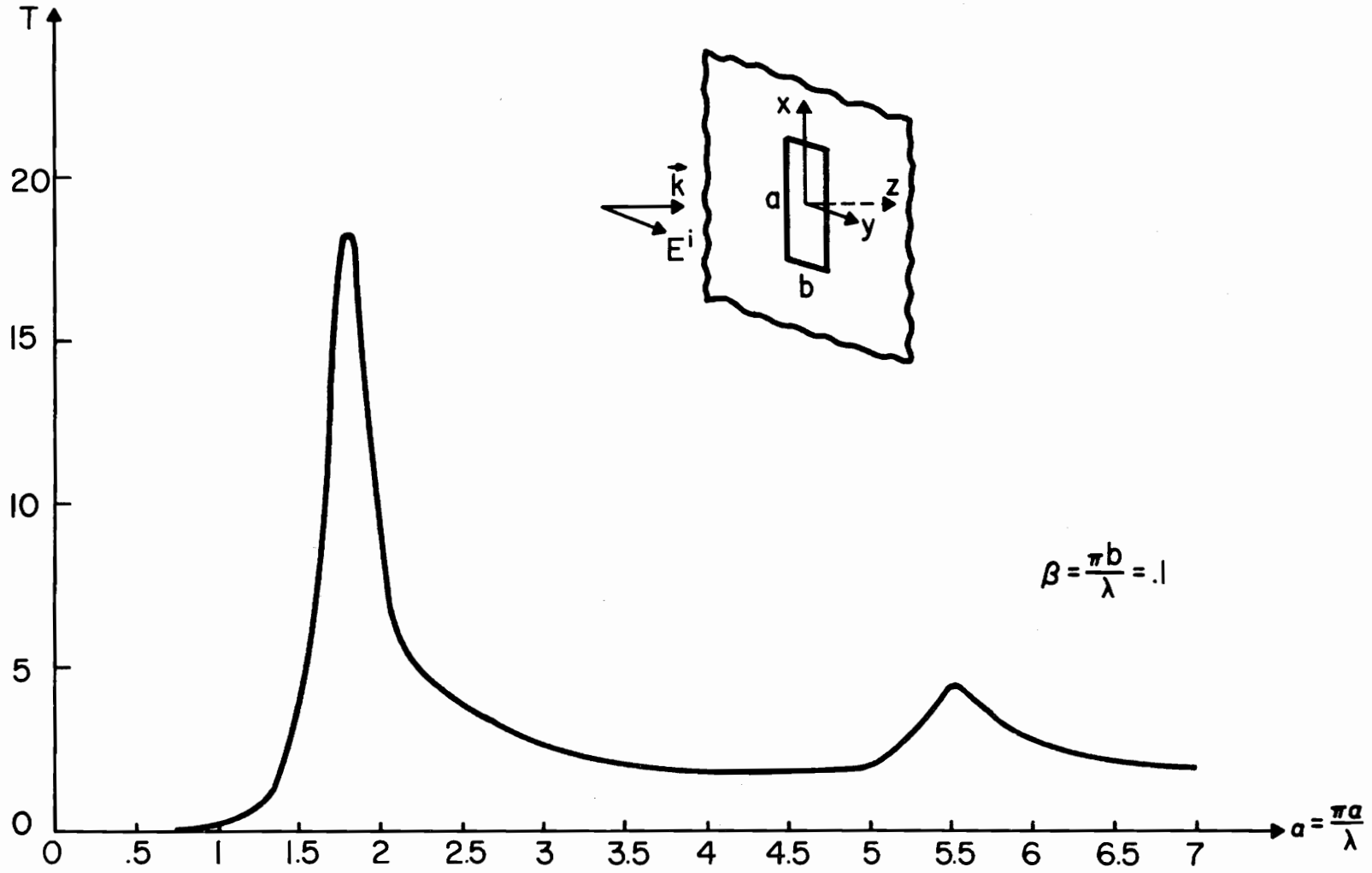

Figure 3.15. Transmission coefficient of a narrow aperture due to a normally incident field.

equation (3.65) via the application of the successive approximation approach. Good agreement between the results has been found. It is evident that the resonances occur when the length of the aperture is approximately equal to $\lambda/2$, $3\lambda/2$, $5\lambda/2$, . . .; the transmission coefficient has maxima at these points.

3.5 Transient Response of Apertures Due to an EMP

3.5.1 Formulation of the time-domain problem

In the previous sections, the problem of computing the frequency response of apertures due to a given plane wave incident on the structure has been discussed in great detail. This section will be concerned with the problem of determining the transient response of apertures illuminated by an EMP from the knowledge of their frequency domain behavior.

The incident EMP may take the following general form:

$$\vec{e}^{i}(t,\vec{R}) = \vec{e}^{i}[t - (\alpha x + \beta y + \alpha z)/c]\ \theta\ [t - (\alpha x + \beta y + \alpha z)/c] \tag{3.74}$$

where α, β, and γ are the cosine directors of the direction of the incident field, $c = \frac{1}{\sqrt{\mu\varepsilon}}$ denotes the speed of light in the medium, and θ is the unit step function. It is further assumed that Equation (3.74) satisfies Maxwell's equation in the time domain.

The Fourier transform and the inverse Fourier transform operators may be defined as follows (Sneddon, 1972):

$$\vec{E}(f,\vec{R}) = F[\vec{e}(t,R)] = \int_{-\infty}^{\infty} \vec{e}(t,\vec{R})\ e^{-j2\pi ft}\ dt \tag{3.75}$$

and

$$\vec{e}(t,\vec{R}) = F^{-1}[\vec{E}(f,\vec{R})] = \int_{-\infty}^{\infty} \vec{E}(f,\vec{R})\ e^{j2\pi ft}\ df \quad . \tag{3.76}$$

Substituting Equation (3.74) into Equation (3.75) and performing the operation results in

$$\vec{E}^i(f,\vec{R}) = F[\vec{e}^i(t,\vec{R})] = \left\{F\left[\vec{e}_0^i(t)\ \theta\ (t)\right]\right\} e^{-jk(\alpha x+\beta y+\alpha z)}$$
$$= \vec{E}_0^i(f)\ e^{-jk(\alpha x+\beta y+\gamma z)} \qquad (3.77)$$

where $k = 2\pi f/c$. Equation (3.77) clearly describes a plane-wave incident field in the frequency domain. Therefore, for any given frequency, one can solve the aperture diffraction problem by simply following the steps developed in the previous sections. This calculation enables one to obtain, for instance, the diffracted field $\vec{E}(f,\vec{R})$ in region $\mathcal{M}_+$ in the frequency domain. Having determined the frequency domain response, the time domain response $\vec{e}(t,\vec{R})$ can then be calculated by employing Equation (3.76).

Since one is dealing with a causal phenomenon, $\vec{e}(t,\vec{R})$ must fulfill the causality condition, namely,

$$\vec{e}(t,\vec{R}) = 0 \quad \text{for } t \leq 0 \quad \text{and} \quad \{\vec{R}:\ (x,y,z) \in \mathcal{M}_+\} \quad . \qquad (3.78)$$

Employing Equation (3.78) and using the fact that $\vec{e}(t,\vec{R})$ is a real function, it can then be shown (Papoulis, 1962) that the knowledge of either the real part of $\vec{E}(f,\vec{R})$ or its imaginary part is sufficient to determine $\vec{e}(t,\vec{R})$. Introducing the symbols "Im" and "Re" as the imaginary and real operators, respectively, $\vec{e}(t,\vec{R})$ may be written in the following alternate, but equivalent forms:

$$\vec{e}(t,\vec{R}) = 4\theta(t) \int_0^\infty \text{Re}\,[\vec{E}(f,\vec{R})] \cos(2\pi ft)\, df$$

$$= 2\theta(t) \int_{-\infty}^{\infty} \text{Re}\,[\vec{E}(f,\vec{R})]\, e^{j2\pi ft}\, df \qquad (3.79a)$$

and

$$\vec{e}(t,\vec{R}) = -4\theta(t) \int_0^\infty \text{Im}\,[\vec{E}(f,\vec{R})] \sin(2\pi ft)\, df$$

$$= -2\theta(t) \int_{-\infty}^{\infty} \text{Im}\,[\vec{E}(f,\vec{R})]\, e^{j2\pi ft}\, df \qquad (3.79b)$$

where $\theta(t)$ is the unit step function. In deriving the above equations the fact that $\vec{E}(-f,\vec{R}) = [\vec{E}(f,\vec{R})]^*$ was used ("*" denotes conjugate operator).

3.5.2 Numerical results and discussions

In this section, the time domain response of a single aperture will be determined by employing Equation (3.79). As a representative example, a double-exponential normally incident EMP illuminated on an aperture, with the dimensions 115 x 1.3 cm, will be considered.

The incident EMP may be represented as follows:

$$\vec{e}^{\,i}(t,\vec{R}) = \hat{y}E_0 \left\{ [e^{-\alpha(t-z/c)} - e^{-\beta(t-z/c)}]\, \theta(t - z/c) \right.$$
$$\left. - [e^{-\alpha(t-\tau-z/c)} - e^{-\beta(t-\tau-z/c)}]\, \theta(t - \tau - z/c) \right\} \qquad (3.80)$$

where

$$\alpha = 6.0 \times 10^6 \text{ sec}^{-1}$$

$$\beta = 2.0 \times 10^8 \text{ sec}^{-1}$$

$$\tau = 2.04189 \times 10^{-9} \text{ sec}$$

$$E_0 = 10^3 \text{ v/m} \quad .$$

The spectrum of $\vec{e}^{i}(t,\vec{R})$ can be readily determined by Fourier transforming (3.80), which yields

$$\vec{E}^{i}(f,\vec{R}) = \hat{y}E_0\left[\frac{1}{\alpha + j2\pi f} - \frac{1}{\beta + j2\pi f}\right](1 - e^{-j2\pi f\tau})\, e^{-jkz} \quad . \quad (3.81)$$

Figure 3.16 shows the behavior of $e_y^i(t,0)$ as a function of time and Figure 3.17 displays the behavior of $|E_y^i(f,0)|$ as a function of frequency.

To evaluate Equation (3.79), one must first compute $\vec{E}(f,\vec{R})$, the frequency spectrum of $\vec{e}(t,\vec{R})$, as described in the previous section. The aperture spectral response $\vec{E}(f,\vec{R})$ is computed at a set of discrete frequencies, seventy in this example. Rather than sampling $\vec{E}(f,\vec{R})$ uniformly in the frequency range $0 - 10^9$ Hz, it is more desirable to compute $\vec{E}(f,\vec{R})$ relatively densely in the neighborhood of the resonant frequencies of the aperture, where the response function $\vec{E}(f,\vec{R})$ varies rapidly, and less frequently for the frequencies, where the variation is relatively slow. Figures 3.18 and 3.19 display the behavior of $|\vec{E}(f,x = 0,\ y = 0,\ z = 2)|$ and Re $\{E(f,\ x = 0,\ y = 0,\ z = 2)\}$, respectively.

The time domain response $\vec{e}(t,\vec{R})$ may be computed from the knowledge of $\vec{E}(f,\vec{R})$ via Equation (3.79). The integrals that need to be evaluated in this process may be computed by the FFT algorithm (Brigham, 1974), which is known to be very efficient in handling these types of integrals. For an accurate evaluation of the integrals, $\vec{E}(f,\vec{R})$ must be adequately sampled in the frequency range of interest so that the criterion suggested by the sampling theorem (Ransom, 1972) is not violated. One finds that, according to this criterion, it is necessary to evaluate $\vec{E}(f,\vec{R})$ at least a total of 1000 points in the interval $0 - 10^9$ Hz where $|\vec{E}(f,\vec{R})|$ decreases to 60 dB below its maximum value. This, in turn,

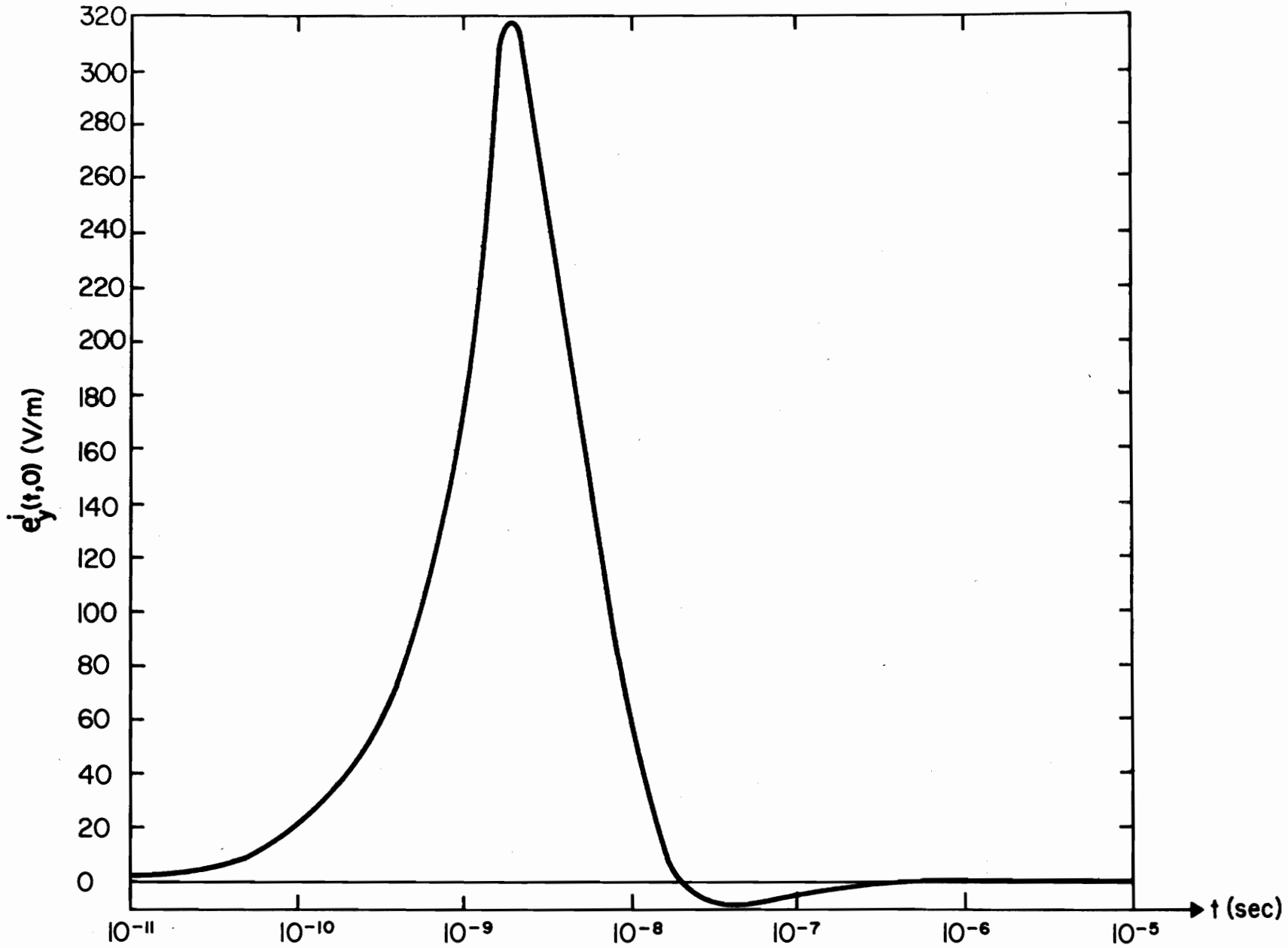

Figure 3.16. Time domain plot of the incident pulse.

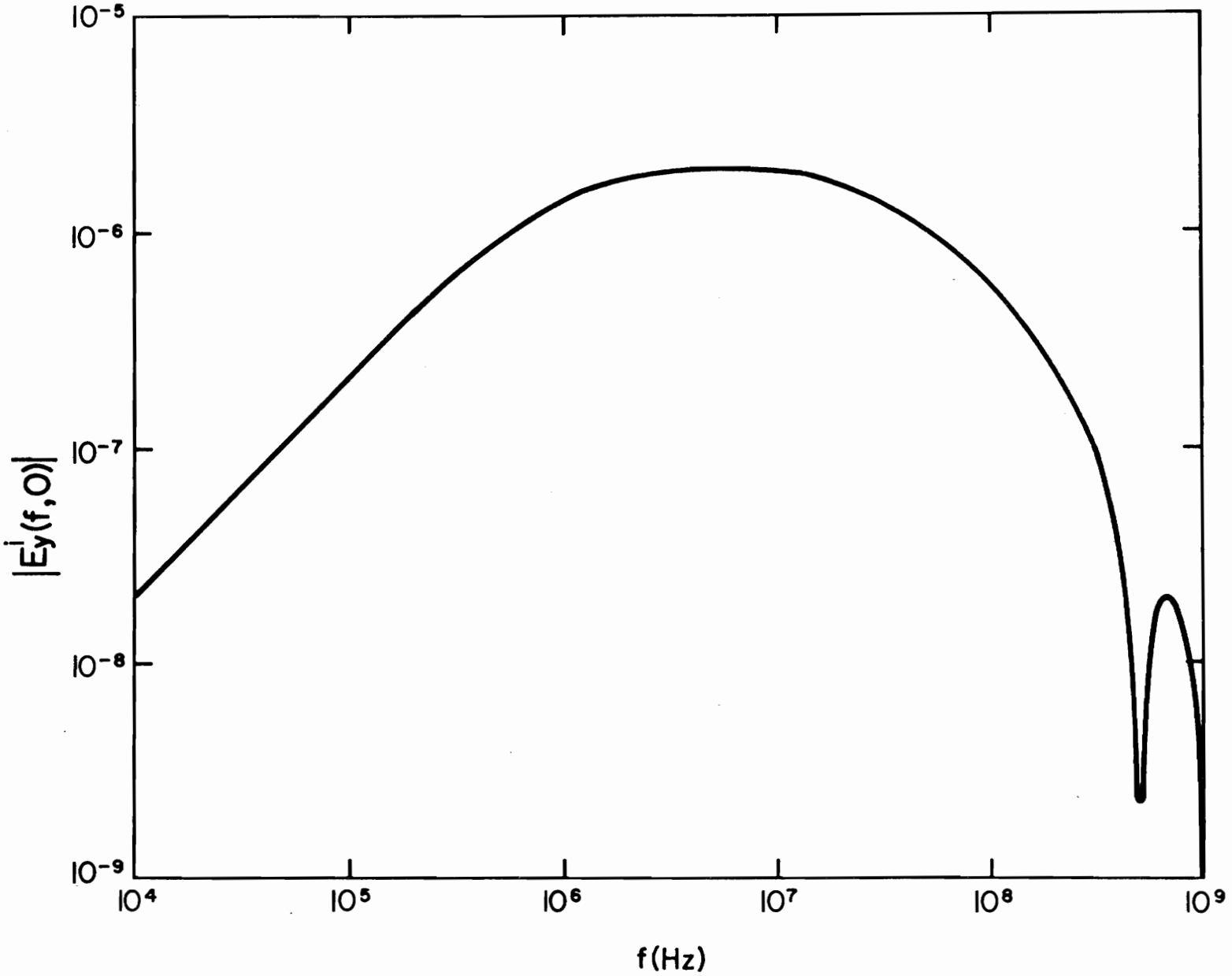

Figure 3.17. Frequency domain behavior of the incident pulse.

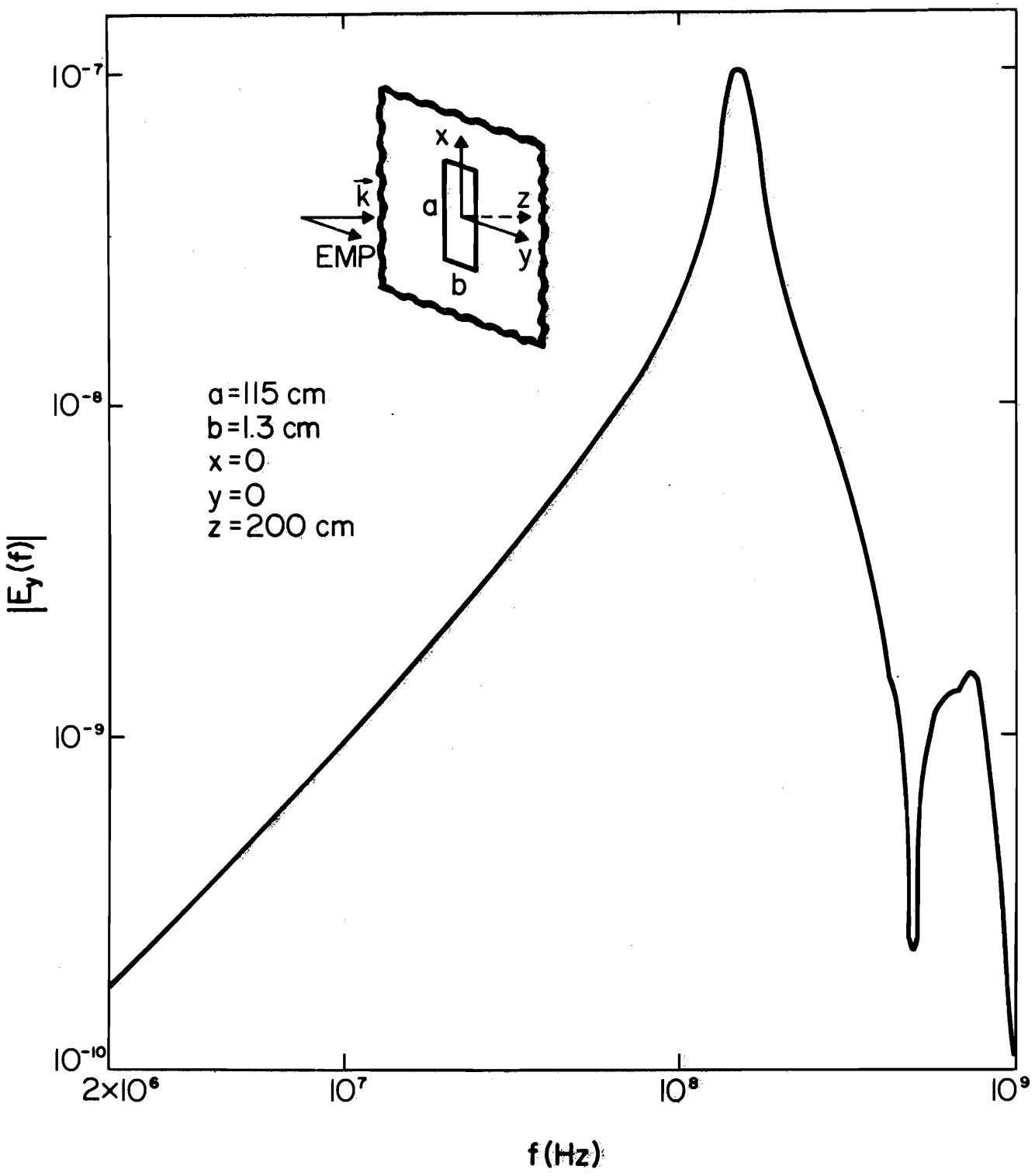

Figure 3.18. Frequency domain behavior of the amplitude of $E_y(f)$ field sampled at a point 2 meters behind the aperture on the z-axis.

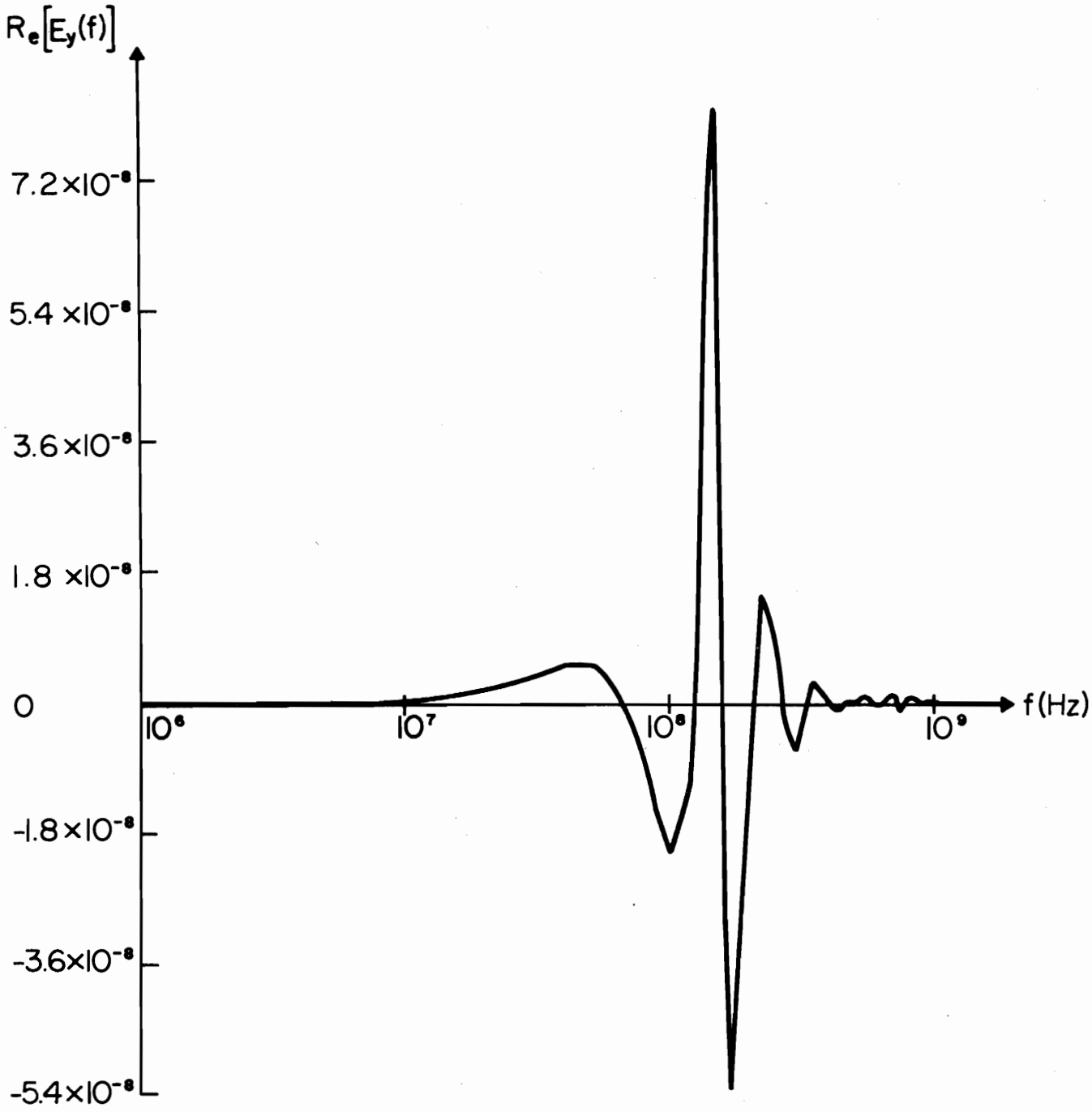

Figure 3.19. Frequency domain behavior of Re[$E_y(f)$] sampled at a point 2 meters behind the aperture as indicated in Figure 3.18.

would require that the function $\vec{E}(f,\vec{R})$ be evaluated at 1000 points also, which would clearly be extremely time consuming. However, one can employ an interpolation scheme to compute $\vec{E}(f,\vec{R})$ at the desired 1000 points by using its seventy samples that have been previously calculated. Extensive numerical experimentation has revealed that a linear interpolation scheme is adequate to determine the function with sufficient accuracy. The result of evaluating Equation (3.79a), using the scheme just outlined, is plotted in Figure 3.20. This figure displays the time domain behavior of the $e_y(t, x = 0, y = 0, z = 2)$ field sampled at a point located on the x-axis, 2 meters behind the aperture illuminated by the EMP (3.80).

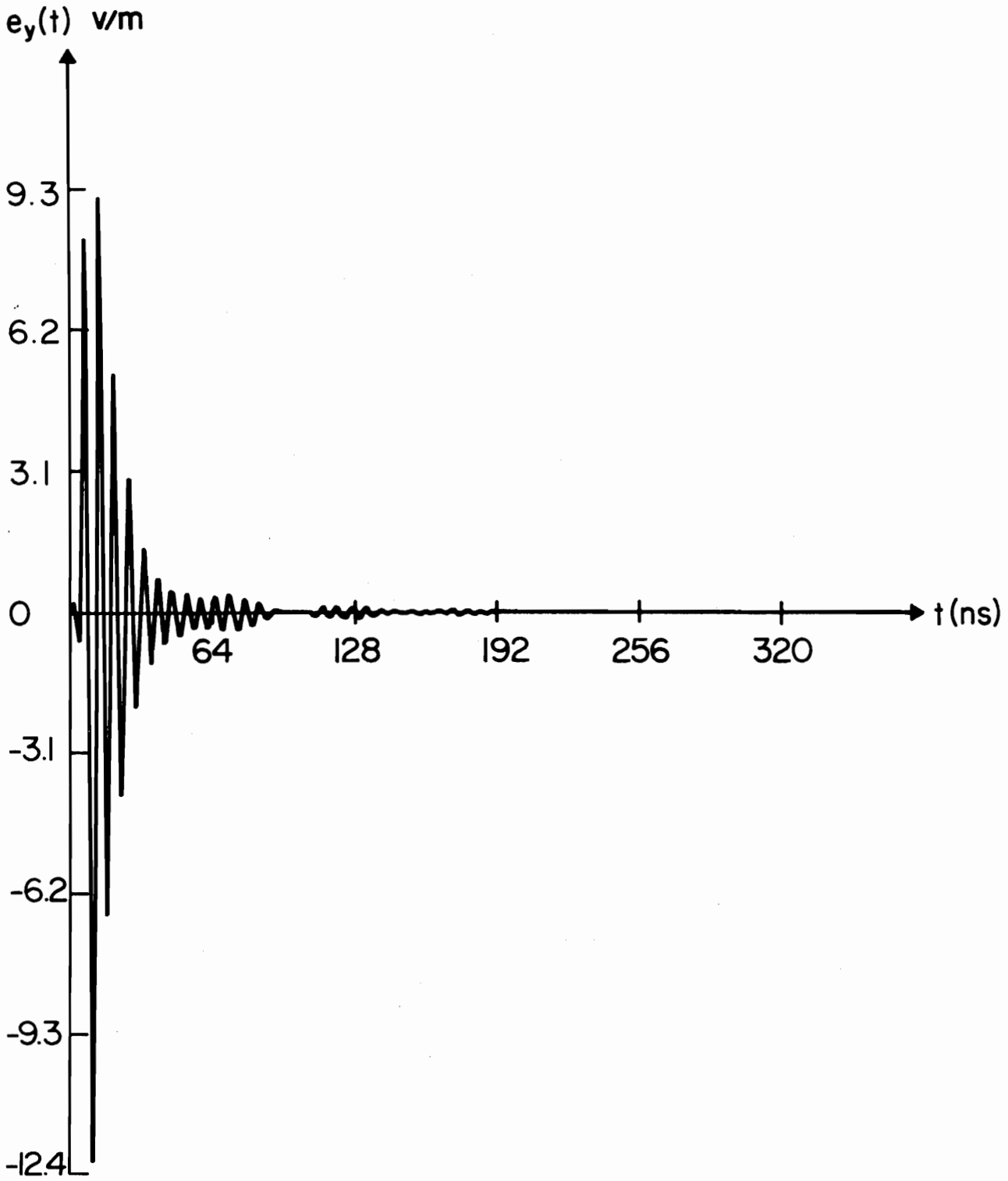

Figure 3.20. Time domain behavior of the $e_y(t)$ field sampled at a point 2 meters behind a single aperture as indicated in Figure 3.18.

4. ELECTROMAGNETIC WAVES DIFFRACTED BY SMALL APERTURES IN A PERFECTLY CONDUCTING SCREEN

4.1 Introduction

This chapter examines the behavior of the electromagnetic waves diffracted by small apertures. The method of analysis is based on the application of the formulas developed in the preceding chapter. These formulas have reduced the aperture diffraction problem to a solution of two decoupled, structurally simple integral equations, and the necessity for accounting for so-called edge conditions has been eliminated. As was previously shown, the edge conditions have been replaced by the obvious requirement on the edge that the field induced in the aperture must have no component tangential to the edge. In this chapter it is shown that for sufficiently small values of kD, where D is a certain length characterizing the dimensions of the aperture, the solution of the above-mentioned integral equations reduces to solving a sequence of successive electrostatic problems.

As an example, diffraction of an arbitrary, plane-wave incident field by circular and rectangular apertures is considered.

4.2 Rayleigh Series Analysis

The starting point is the application of the integral equation (3.33) given in the previous section. Using the fact that $J_{-n}(k\rho) = (-1)^n J_n(k\rho)$, Equation (3.33) may be rewritten as follows:

$$\iint_{\bar{A}} \begin{Bmatrix} E_x \\ E_y \end{Bmatrix} \frac{e^{-jk|\vec{\rho}-\vec{\rho}'|}}{2\pi|\vec{\rho}-\vec{\rho}'|}\, da' = \frac{1}{jk\gamma} \begin{Bmatrix} E^i_{0x} \\ E^i_{0y} \end{Bmatrix} e^{-jk(\alpha x+\beta y)}$$

$$+ \frac{\pi}{k} \begin{Bmatrix} -j \\ -1 \end{Bmatrix} \Bigg(\sum_{n=1}^{\infty} \Bigg\{ \Bigg[e^{j(n+1)\phi} C_n + \begin{Bmatrix} -1 \\ 1 \end{Bmatrix} e^{-j(n+1)\phi} C_{-n} \Bigg]$$

$$\cdot j^{n+1} J_{n+1}(k\rho) + \Bigg[\begin{Bmatrix} -1 \\ 1 \end{Bmatrix} e^{j(n-1)\phi} C_n + e^{-j(n-1)\phi} C_{-n} \Bigg]$$

$$\cdot j^{n-1} J_{n-1}(k\rho) \Bigg\} + \Bigg[e^{j\phi} + \begin{Bmatrix} -1 \\ 1 \end{Bmatrix} e^{-j\phi} \Bigg] jJ_1(k\rho)\, C_0 \Bigg) \quad . \tag{4.1}$$

Next the Rayleigh series expansion method is employed to convert Equation (4.1) into an integral equation valid for apertures whose dimensions are small relative to the wavelength. The procedure is based on a power series expansion in k and leads, in principle, to a sequence of simple integral equations like those occurring in potential theory. Rayleigh (1897) first proposed such a series expansion scheme for determining the approximate solution to diffraction and scattering problems using the application of the quasi-static analysis. Stevenson (1953) later discussed the application of the Rayleigh series in a rather rigorous mathematical fashion. He was able to show that the field scattered by a conducting body may be determined exactly in terms of the power series of k, if the Laplace equation separates for the geometry in question. Werner (1963) presented a rigorous mathematical justification for the application of the Rayleigh series. Kleinman (1967) employed the series approximation and completed Stevenson's work. The above-mentioned work, therefore, justifies the application of the Rayleigh series which can be written as follows

$$\vec{E} = \sum_{m=0}^{\infty} \vec{E}^{(m)} k^m \quad . \tag{4.2}$$

It is worthwhile here to quote the following statement given by Kleinman: "The validity of Rayleigh expansion has been established, thus this need no longer be an assumption but is a consequence of Maxwell's equations, the boundary conditions and radiation conditions."

A further assumption is that the coefficient C_n's appearing in Equation (4.1) can also be expanded in terms of the powers of k:

$$C_n = \sum_{m=0}^{\infty} C_n^{(m)} k^m \quad . \tag{4.3}$$

In order to expand the Bessel functions appearing in Equation (4.1), in terms of the power series of k, the following well-known expansion formula (Bowman, 1958) is used:

$$J_n(k\rho) = \frac{(k\rho)^n}{2^n n!} \left[1 - \frac{(k\rho)^2}{2(2n+2)} + \frac{(k\rho)^4}{2 \cdot 4 \cdot (2n+2)(2n+4)} \cdots\right] . \tag{4.4}$$

After substituting (4.4), (4.3) and (4.2) into (4.1), and making use of the expansion series for the kernel and the incident field, the following relation is finally established

$$\iint_{\bar{A}} \sum_{m=0}^{\infty} \sum_{n=0}^{\infty} \frac{1}{2\pi} \begin{Bmatrix} E_x^{(m)} \\ E_y^{(m)} \end{Bmatrix} \frac{j^n}{n!} |\vec{\rho} - \vec{\rho}'|^{n-1} k^{m+n} \, da' = \frac{1}{jk\gamma} \begin{Bmatrix} E_{0x}^{i} \\ E_{0y}^{i} \end{Bmatrix} \sum_{m=0}^{\infty} \frac{(-jk)^m}{m!} (\alpha x + \beta y)^m$$

$$+ \frac{\pi}{k} \begin{Bmatrix} -j \\ -1 \end{Bmatrix} \Bigg(\sum_{m=0}^{\infty} k^m \Bigg[\sum_{n=1}^{\infty} \Bigg\{ \Bigg[e^{j(n+1)\phi} \, C_n^{(m)} + \begin{Bmatrix} -1 \\ 1 \end{Bmatrix} e^{-j(n+1)\phi} \, C_{-n}^{(m)} \Bigg]$$

$$\cdot \frac{j^{n+1}}{2^{n+1}(n+1)!} (k\rho)^{n+1} \left(1 - \frac{(k\rho)^2}{2(2n+4)} + \cdots \right)$$

$$+ \Bigg[\begin{Bmatrix} -1 \\ 1 \end{Bmatrix} e^{j(n-1)\phi} \, C_n^{(m)} + e^{-j(n-1)\phi} \, C_{-n}^{(m)} \Bigg]$$

$$\cdot \frac{j^{n-1}}{2^{n-1}(n-1)!} (k\rho)^{n-1} \left(1 - \frac{(k\rho)^2}{2(2n)} + \cdots \right) \Bigg\} + C_0^{(m)} \Bigg[e^{j\phi} + \begin{Bmatrix} -1 \\ 1 \end{Bmatrix} e^{-j\phi} \Bigg] \frac{j}{2}$$

$$\cdot k\rho \left(1 - \frac{(k\rho)^2}{2 \cdot 2} + \cdots \right) \Bigg] \Bigg) \qquad . \tag{4.5}$$

Since the above relation must hold for all values of k, one can then conclude that the following equations must govern the behavior of the induced field in the aperture in terms of the powers of k, i.e.,

(i) From the coefficient of k^{-1}

$$0 = \frac{1}{j\gamma} \begin{Bmatrix} E_{0x}^{i} \\ E_{0y}^{i} \end{Bmatrix} + \pi \begin{Bmatrix} jC_1^{(0)} - jC_{-1}^{(0)} \\ -C_1^{(0)} - C_{-1}^{(0)} \end{Bmatrix} \tag{4.6}$$

(ii) From the coefficient of k^0

$$\iint_{\bar{A}} \begin{Bmatrix} E_x^{(0)} \\ E_y^{(0)} \end{Bmatrix} \frac{1}{2\pi|\vec{\rho} - \vec{\rho}'|}\, da' = \frac{-1}{\gamma} \begin{Bmatrix} E_{0x}^{i} \\ E_{0y}^{i} \end{Bmatrix} (\alpha x + \beta y)$$

$$+ \frac{\pi}{2} \begin{Bmatrix} \left(-C_2^{(0)} + C_0^{(0)}\right) e^{j\phi} + \left(C_{-2}^{(0)} - C_0^{(0)}\right) e^{-j\phi} \\ -j\left(C_2^{(0)} + C_0^{(0)}\right) e^{j\phi} - j\left(C_{-2}^{(0)} + C_0^{(0)}\right) e^{-j\phi} \end{Bmatrix} \rho$$

$$+ \pi \begin{Bmatrix} jC_1^{(1)} - jC_{-1}^{(1)} \\ -C_1^{(1)} - C_{-1}^{(1)} \end{Bmatrix} \qquad (4.7)$$

(iii) From the coefficient of k^1

$$\iint_{\bar{A}} \begin{Bmatrix} E_x^{(1)} \\ E_y^{(1)} \end{Bmatrix} \frac{1}{2\pi|\vec{\rho} - \vec{\rho}'|}\, da' + \frac{j}{2\pi} \iint_{\bar{A}} \begin{Bmatrix} E_x^{(0)} \\ E_y^{(0)} \end{Bmatrix} da' = \frac{-1}{2j\gamma} \begin{Bmatrix} E_{0x}^{i} \\ E_{0y}^{i} \end{Bmatrix} (\alpha x + \beta y)^2$$

$$+ \frac{\pi}{8} \begin{Bmatrix} j\left(C_1^{(0)} - C_3^{(0)}\right) e^{2j\phi} + j\left(-C_{-1}^{(0)} + C_{-3}^{(0)}\right) e^{-2j\phi} + 2j\left(-C_1^{(0)} + C_{-1}^{(0)}\right) \\ \left(C_1^{(0)} + C_3^{(0)}\right) e^{2j\phi} + \left(C_{-1}^{(0)} + C_3^{(0)}\right) e^{-2j\phi} + 2\left(C_1^{(0)} + C_{-1}^{(0)}\right) \end{Bmatrix} \rho^2$$

$$+ \frac{\pi}{2} \begin{Bmatrix} \left(-C_2^{(1)} + C_0^{(1)}\right) e^{j\phi} + \left(C_{-2}^{(1)} - C_0^{(1)}\right) e^{-j\phi} \\ -j\left(C_2^{(1)} + C_0^{(1)}\right) e^{j\phi} + j\left(C_{-2}^{(1)} + C_0^{(1)}\right) e^{-j\phi} \end{Bmatrix} \rho + \pi \begin{Bmatrix} jC_1^{(2)} - jC_{-1}^{(2)} \\ -C_1^{(2)} - C_{-1}^{(2)} \end{Bmatrix}$$

(4.8)

(iv) From the coefficient of k^2

$$\iint_{\bar{A}} \begin{Bmatrix} E_x^{(2)} \\ E_y^{(2)} \end{Bmatrix} \frac{1}{2\pi|\vec{\rho} - \vec{\rho}'|}\, da' + \frac{j}{2\pi} \iint_{\bar{A}} \begin{Bmatrix} E_x^{(1)} \\ E_y^{(1)} \end{Bmatrix} da' - \frac{1}{4\pi} \iint_{\bar{A}} \begin{Bmatrix} E_x^{(0)} \\ E_y^{(0)} \end{Bmatrix} |\vec{\rho} - \vec{\rho}'|\, da'$$

$$= \frac{1}{6\gamma} \begin{Bmatrix} E_{0x}^{i} \\ E_{0y}^{i} \end{Bmatrix} (\alpha x + \beta y)^3$$

$$+ \frac{\pi}{48} \left\{ \begin{array}{l} \left(-C_2^{(0)} + C_4^{(0)}\right) e^{3j\phi} + \left(C_{-2}^{(0)} - C_{-4}^{(0)}\right) e^{-3j\phi} \\ j\left(C_2^{(0)} + C_4^{(0)}\right) e^{3j\phi} + j\left(C_{-2}^{(0)} + C_{-4}^{(0)}\right) e^{-3j\phi} \\ \quad + \left(3C_2^{(0)} - 6C_0^{(0)}\right) e^{j\phi} + \left(3C_{-2}^{(0)} + 6C_0^{(0)}\right) e^{-j\phi} \\ \quad + j\left(3C_2^{(0)} + 6C_0^{(0)}\right) e^{j\phi} + j\left(3C_{-2}^{(0)} + 6C_0^{(0)}\right) e^{-j\phi} \end{array} \right\} \rho^3$$

$$+ \frac{\pi}{8} \left\{ \begin{array}{l} j\left(C_1^{(1)} - C_3^{(1)}\right) e^{2j\phi} + j\left(C_{-1}^{1} + C_{-3}^{1}\right) e^{-2j\phi} + 2j\left(-C_1^{(1)} + C_{-1}^{(1)}\right) \\ \left(C_1^{(1)} + C_3^{(1)}\right) e^{2j\phi} + \left(C_{-1}^{(1)} + C_{-3}^{(1)}\right) e^{-2j\phi} + 2\left(C_1^{(1)} + C_{-1}^{(1)}\right) \end{array} \right\} \rho^2$$

$$+ \frac{\pi}{2} \left\{ \begin{array}{l} \left(-C_2^{(2)} + C_0^{(2)}\right) e^{j\phi} + \left(C_{-2}^{(2)} - C_0^{(2)}\right) e^{-j\phi} \\ -j\left(C_2^{(2)} + C_0^{(2)}\right) e^{j\phi} - j\left(C_{-2}^{(2)} + C_0^{(2)}\right) e^{-j\phi} \end{array} \right\} \rho + \pi \begin{Bmatrix} j\left(C_1^{(3)} - C_{-1}^{(3)}\right) \\ -C_1^{(3)} - C_{-1}^{(3)} \end{Bmatrix}. \tag{4.9}$$

The above procedure may be similarly continued for higher-order powers of k.

The most significant feature of the integral equations appearing in (4.7), (4.8) and (4.9) is their resemblance to the integral equation with the electrostatic-type kernel, i.e., $\frac{1}{|\vec{\rho} - \vec{\rho}'|}$. This resemblance allows one to construct an analytical solution for the geometries for

which the corresponding electrostatic-type integral equation is solvable. For instance, the circular aperture will be discussed in the next section and the analytical solution of Equations (4.7), (4.8) and (4.9) will be presented.

Another important feature of the above equations is their coupling characteristic which demonstrates itself in a successive manner. The coupling that occurs among the equations is carried out by the constants $C_n^{(m)}$'s and the fields $E_x^{(m)}$'s and $E_y^{(m)}$'s from Equation (4.6) through Equation (4.9) successively. Therefore, it is necessary to be able to determine the constants $C_n^{(m)}$'s in each previous step. This is actually done by enforcing the condition (3.30), which is read as follows

$$\vec{E}^{(m)} \cdot \hat{\tau} = 0 \qquad m = 0,1,2, \ldots \qquad (4.10)$$

As will be shown in the next section, the above condition will be sufficient to construct the unique solution of the problem and thus the so-called edge condition need not be implemented.

4.3 Diffraction by an Electrically Small Circular Aperture

The problem of diffraction of electromagnetic waves by a circular aperture and its complementary companion, a circular disk, has been considered by many great scientists. Bethe (1944), who employed the scalar potential function approach, was able to construct the first two terms of the Rayleigh expansion series. Bouwkamp (1953) later developed a set of integro-differential equations and discovered the errors in the Bethe's solution. Following this line of thought, Grinberg and Pimenov (1957) were able to develop a new integral equation determining the series expansion solution for a circular disk due to a normal incident plane wave. Later on, Kuritsyn (1961) used Grinberg's

formulation and obtained the series expansion solution for an arbitrary incident plane wave on a circular disk. Finally, Eggiman (1961) implemented Bouwkamp's formulation and derived a set of recurrence relations for determining the series terms due to an arbitrary incident field for a circular disk. All of the above investigators followed the line of thought originally developed by Lord Rayleigh, namely, using Equation (4.2). Some of the researchers interested in this investigation tried to solve the problem exactly. Meixner and Andrejewski (1950) utilized the spheroidal wave functions and solved the problem. Later, Flammer (1955) employed the vector wave function technique in the oblate spheroidal coordinate system and presented the solution in terms of an infinite series. Nomura and Katsura (1955) were able to apply the method of expansion in the hypergeometric polynomial and to construct the solution of the problem for an incident plane wave. Jones (1956) employed a Fredholm-type integral equation and analyzed the scalar diffraction problem for a circular disc. Most of the above techniques are highly complex, and therefore difficult to use.

The formulation developed in the previous section will be employed in the next section to determine the solution for the first few terms of the Rayleigh expansion. The method is simple and the formulation is quite straightforward.

4.3.1 Solution of an integral equation with electrostatic-type kernel for a circular structure

The first step in determining the analytical solution of Equations (4.7), (4.8) and (4.9) for a circular structure is the determination of the solution of the following class of integral equations:

$$\iint_{\bar{A}} \frac{\sigma(\vec{\rho}')}{2\pi|\vec{\rho} - \vec{\rho}'|} da' = a_{00} + a_{11}e^{j\phi}\rho + \left(a_{02} + a_{22}e^{2j\phi}\right)\rho^2 + \left(a_{13}e^{j\phi} + a_{33}e^{3j\phi}\right)\rho^3$$

$$0 \leq \phi \leq 2\pi \quad , \quad 0 \leq \rho \leq a \tag{4.11}$$

where $\bar{A}$ represents the interior domain of a circular structure with radius a. Two different techniques for solving the above integral equation are discussed in Appendix D. The techniques are developed for more general cases than for that written in (4.11).

Using the result outlined in Appendix D, one derives the solution of Equation (4.11) as follows:

$$\begin{aligned}
\sigma(\rho) = {} & \frac{2}{\pi}\left(a^2 - \rho^2\right)^{-1/2} a_{00} + \frac{4}{\pi}\left(a^2 - \rho^2\right)^{-1/2} a_{11}e^{j\phi}\rho \\
& + \left[\frac{4a^2}{\pi}\left(a^2 - \rho^2\right)^{-1/2} - \frac{8}{\pi}\left(a^2 - \rho^2\right)^{1/2}\right] a_{02} \\
& + \frac{16}{3\pi}\left(a^2 - \rho^2\right)^{-1/2} a_{22}e^{2j\phi}\rho^2 \\
& + \frac{16}{3\pi}\left[3\left(a^2 - \rho^2\right)^{1/2} - \rho^2\left(a^2 - \rho^2\right)^{-1/2}\right] a_{13}e^{j\phi}\rho \\
& + \frac{32}{5\pi}\left(a^2 - \rho^2\right)^{-1/2} a_{33}e^{3j\phi}\rho^3 \\
& \qquad 0 \leq \rho \leq a \quad .
\end{aligned} \tag{4.12}$$

The above result clearly exhibits a square root-type singular behavior at the rim of the circular structure.

4.3.2 Zero-order solution of the field distribution in a circular aperture

In this section, the task is to solve Equation (4.7) with the application of Equation (4.12), which was developed in the previous section. It is easily observed that Equation (4.7) is independent of

its previous equation, namely, Equation (4.6). Therefore, all of the five unknown coefficients $C_0^{(0)}$, $C_2^{(0)}$, $C_{-2}^{(0)}$, $C_1^{(1)}$, and $C_{-1}^{(1)}$, and the two field components $E_x^{(0)}$ and $E_y^{(0)}$ must be determined by solving Equation (4.7), subject to the condition (4.10). This condition takes the following form for this case of interest

$$E_\phi^{(0)}(\vec{\rho}) = 0 \qquad \forall\phi: \; 0 \leq \phi \leq 2\pi \text{ and } |\vec{\rho}| = a \quad . \tag{4.13}$$

Using (4.12), a solution to the integral equation (4.7) may be written as

$$\begin{Bmatrix} E_x^{(0)} \\ E_y^{(0)} \end{Bmatrix} = -\frac{1}{\gamma} \begin{Bmatrix} \alpha E_{0x}^i \cos\phi + \beta E_{0x}^i \sin\phi \\ \alpha E_{0y}^i \cos\phi + \beta E_{0y}^i \sin\phi \end{Bmatrix} \frac{4\rho}{\pi(a^2 - \rho^2)^{1/2}}$$

$$+ \frac{j\pi}{2} \begin{Bmatrix} \left(jC_2^{(0)} - jC_{-2}^{(0)}\right) \cos\phi + \left(-C_2^{(0)} - C_{-2}^{(0)} + 2C_0^{(0)}\right) \sin\phi \\ \left(-C_2^{(0)} - C_{-2}^{(0)} - 2C_0^{(0)}\right) \cos\phi + \left(-jC_2^{(0)} + jC_{-2}^{(0)}\right) \sin\phi \end{Bmatrix}$$

$$\cdot \frac{4\rho}{\pi(a^2 - \rho^2)^{1/2}} + \frac{j\pi}{2} \begin{Bmatrix} 2C_1^{(1)} - 2C_{-1}^{(1)} \\ j2C_1^{(1)} - j2C_{-1}^{(1)} \end{Bmatrix} \frac{2}{\pi(a^2 - \rho^2)^{1/2}} \quad . \tag{4.14}$$

Now by expressing $E_\phi^{(0)}$ as $-E_x^{(0)} \sin\phi + E_y^{(0)} \cos\phi$ and by enforcing the condition (4.13), one derives the following set of equations:

$$
\begin{cases}
\dfrac{\alpha E^i_{0x}}{\gamma} - \dfrac{j\pi}{2}\left(jC_2^{(0)} - jC_{-2}^{(0)}\right) - \dfrac{\beta E^i_{0y}}{\gamma} + \dfrac{j\pi}{2}\left(-jC_2^{(0)} + jC_{-2}^{(0)}\right) = 0 \\
\dfrac{-\beta E^i_{0x}}{\gamma} + \dfrac{j\pi}{2}\left(-C_2^{(0)} - C_{-2}^{(0)} + 2C_0^{(0)}\right) - \dfrac{\alpha E^i_{0y}}{\gamma} + \dfrac{j\pi}{2}\left(-C_2^{(0)} - C_{-2}^{(0)} - 2C_0^{(0)}\right) = 0 \\
\dfrac{\beta E^i_{0x}}{\gamma} - \dfrac{j\pi}{2}\left(-C_2^{(0)} - C_{-2}^{(0)} + 2C_0^{(0)}\right) - \dfrac{\alpha E^i_{0y}}{\gamma} + \dfrac{j\pi}{2}\left(-C_2^{(0)} - C_2^{(0)} - 2C_0^{(0)}\right) = 0 \\
C_1^{(1)} - C_{-1}^{(1)} = 0 \\
C_1^{(1)} + C_{-1}^{(1)} = 0 \quad .
\end{cases}
\tag{4.15}
$$

The unique solution of the above set is easily determined as:

$$C_0^{(0)} = \frac{-j}{2\pi\gamma}\left(\beta E^i_{0x} - \alpha E^i_{0y}\right) \tag{4.16a}$$

$$C_2^{(0)} = \frac{1}{2\pi\gamma}\left[(-\alpha + j\beta)\, E^i_{0x} + (\beta + j\alpha)\, E^i_{0y}\right] \tag{4.16b}$$

$$C_{-2}^{(0)} = \frac{1}{2\pi\gamma}\left[(\alpha + j\beta)\, E^i_{0x} + (-\beta + j\alpha)\, E^i_{0y}\right] \tag{4.16c}$$

$$C_1^{(1)} = 0 \tag{4.16d}$$

$$C_{-1}^{(1)} = 0 \quad . \tag{4.16e}$$

Substituting the above results in expression (4.14) and using the facts that

$$\nabla \cdot \vec{E}^i = \alpha E^i_{0x} + \beta E^i_{0y} + \gamma E^i_{0z} = 0 \tag{4.17}$$

and

$$\begin{Bmatrix} E_\phi \\ E_\rho \end{Bmatrix} = \begin{pmatrix} -\sin\phi & \cos\phi \\ \cos\phi & \sin\phi \end{pmatrix} \begin{Bmatrix} E_x \\ E_y \end{Bmatrix} \tag{4.18}$$

one obtains

$$E_{\phi}^{(0)} = 0 \tag{4.19a}$$

$$E_{\rho}^{(0)} = \frac{2\rho}{\pi(a^2 - \rho^2)^{1/2}} E_{0z}^{i} \tag{4.19b}$$

which complete the computation of the zero-order solution of the field distribution in the circular aperture. Equations (4.19a) and (4.19b) agree exactly with those of Bouwkamp (1953), Copson (1946), and Bethe (1944), although they followed different lines of approach. Equation (4.19) clearly manifests the fact that the $E_{\phi}^{(0)}$ component of the field is zero in the entire aperture and the $E_{\rho}^{(0)}$ component is not zero only if $E_{0z}^{i} \neq 0$. That is, for the normal incidence case, no zero-order term will be induced in the aperture.

4.3.3 First-order solution of the field distribution in a circular aperture

Having determined the zero-order solution of the field distribution, the first-order solution will now be found by solving the integral equation (4.8) subject to the condition

$$E_{\phi}^{(1)}(\vec{\rho}) = 0 \quad \forall\phi: \ 0 \leq \phi \leq 2\pi \ \text{ and } \ |\vec{\rho}| = a \quad . \tag{4.20}$$

The method of solution is similar to the one presented in the previous section. One notes that Equation (4.8) is coupled by $E_{x}^{(0)}$ and $E_{y}^{(0)}$ to Equation (4.7) and by $C_{1}^{(0)}$ and $C_{-1}^{(0)}$ to Equation (4.6).

Using Equations (4.19) and (4.18), it is then easily seen that the following is true:

$$\iint_{\bar{A}} \begin{Bmatrix} E_x^{(0)} \\ E_y^{(0)} \end{Bmatrix} da' = \int_0^{2\pi} \int_0^{a} \begin{Bmatrix} E_\rho^{(0)} \cos\phi' - E_\phi^{(0)} \sin\phi' \\ E_\rho^{(0)} \sin\phi' + E_\phi^{(0)} \cos\phi' \end{Bmatrix} \rho' \, d\rho' \, d\phi' = 0 \quad . \tag{4.21}$$

The above result exposes the fact that the first-order solution and the zero-order solution are independent of each other. This, of course, is not true for higher-order terms.

In solving Equation (4.6), one readily derives $C_1^{(0)}$ and $C_{-1}^{(0)}$

$$C_{-1}^{(0)} = \frac{-1}{2\pi\gamma}\left(E_{0x}^i + jE_{0y}^i\right) \tag{4.22a}$$

$$C_1^{(0)} = \frac{1}{2\pi\gamma}\left(E_{0x}^i - jE_{0y}^i\right) \quad , \tag{4.22b}$$

and employing (4.12), a solution to the integral equation (4.8) may be written as

$$\begin{Bmatrix} E_x^{(1)} \\ E_y^{(1)} \end{Bmatrix} = \frac{1}{j\gamma\pi}\left\{\frac{4}{3}\left[(-\alpha^2+\beta^2)\cos 2\phi - 2\alpha\beta \sin 2\phi\right]\frac{\rho^2}{(a^2-\rho^2)^{1/2}}\right.$$

$$\left. - (\alpha^2+\beta^2)\frac{a^2}{(a^2-\rho^2)^{1/2}} + 2(\alpha^2+\beta^2)(a^2-\rho^2)^{1/2}\right\}\begin{Bmatrix} E_{0x}^i \\ E_{0y}^i \end{Bmatrix}$$

$$+ \frac{2}{3}\begin{Bmatrix} j\left[C_1^{(0)}-C_{-1}^{(0)}-C_3^{(0)}+C_{-3}^{(0)}\right]\cos 2\phi + \left[-C_1^{(0)}-C_{-1}^{(0)}+C_3^{(0)}+C_{-3}^{(0)}\right]\sin 2\phi \\ \left[C_1^{(0)}+C_{-1}^{(0)}+C_3^{(0)}+C_{-3}^{(0)}\right]\cos\phi + j\left[C_1^{(0)}-C_{-1}^{(0)}+C_3^{(0)}-C_{-3}^{(0)}\right]\sin 2\phi \end{Bmatrix}$$

$$\cdot \frac{\rho^2}{(a^2-\rho^2)^{1/2}} + 2\begin{Bmatrix} \left[-C_2^{(1)}+C_{-2}^{(1)}\right]\cos\phi + j\left[-C_2^{(1)}-C_{-2}^{(1)}+2C_0^{(1)}\right]\sin\phi \\ j\left[-C_2^{(1)}-C_{-2}^{(1)}-2C_0^{(1)}\right]\cos\phi + \left[C_2^{(1)}-C_{-2}^{(1)}\right]\sin\phi \end{Bmatrix}$$

$$\cdot \frac{\rho}{(a^2-\rho^2)^{1/2}} + \begin{Bmatrix} j\left[-C_1^{(0)}+C_{-1}^{(0)}\right]a^2 + 2j\left[C_1^{(2)}-C_{-1}^{(2)}\right] \\ \left[C_1^{(0)}+C_{-1}^{(0)}\right]a^2 - 2\left[C_1^{(2)}+C_{-1}^{(2)}\right] \end{Bmatrix}\frac{1}{(a^2-\rho^2)^{1/2}}$$

$$+ 2\begin{Bmatrix} j\left[C_1^{(0)}-C_{-1}^{(0)}\right] \\ -C_1^{(0)}+C_{-1}^{(0)} \end{Bmatrix}(a^2-\rho^2)^{1/2} \quad . \tag{4.23}$$

In order to determine the unknown coefficients $C_3^{(0)}$, $C_{-3}^{(0)}$, $C_2^{(1)}$, $C_{-2}^{(1)}$, $C_0^{(1)}$, $C_1^{(2)}$ and $C_{-1}^{(2)}$, Equation (4.22) is first substituted into (4.18) to obtain $E_\phi^{(1)}$ and then condition (4.20) is enforced. After performing some straightforward manipulations, the following results are obtained:

$$C_3^{(0)} = \frac{1}{2\pi\gamma}\,(\alpha^2 - \beta^2 - 2j\alpha\beta)\left(E_{0x}^i - jE_{0y}^i\right) \tag{4.24a}$$

$$C_{-3}^{(0)} = \frac{-1}{2\pi\gamma}\,(\alpha^2 - \beta^2 + 2j\alpha\beta)\left(E_{0x}^i + jE_{0y}^i\right) \tag{4.24b}$$

$$C_2^{(1)} = C_{-2}^{(1)} = C_0^{(1)} = 0 \tag{4.24c}$$

$$C_1^{(2)} = \frac{a^2}{12\pi\gamma}\left[(-\alpha^2 - 5\beta^2 - 4j\alpha\beta + 5)\,E_{0x}^i + (\beta^2 + 5\alpha^2 - 4j\alpha\beta - 5)\,jE_{0y}^i\right] \tag{4.24d}$$

$$C_{-1}^{(2)} = \frac{-a^2}{12\pi\gamma}\left[(-\alpha^2 - 5\beta^2 + 4j\alpha\beta + 5)\,E_{0x}^i - (\beta^2 + 5\alpha^2 + 4j\alpha\beta - 5)\,jE_{0y}^i\right]. \tag{4.24e}$$

By substituting the above results into Equation (4.23) and making use of Equations (4.17) and (4.18), one obtains:

$$E_\phi^{(1)} = \frac{8j}{3\pi}\,\gamma\left(E_{0y}^i\cos\phi - E_{0x}^i\sin\phi\right)(a^2 - \rho^2)^{1/2} + \frac{4j}{3\pi}\,(\alpha\sin\phi - \beta\cos\phi)(a^2 - \rho^2)^{1/2}\,E_{0z}^i \tag{4.25a}$$

and

$$E_\rho^{(1)} = \frac{2j}{3\pi}\,\gamma\left(E_{0x}^i\cos\phi + E_{0y}^i\sin\phi\right)\left[4(a^2 - \rho^2)^{1/2} + \frac{2\rho^2}{(a^2 - \rho^2)^{1/2}}\right] - \frac{4j}{3\pi}\left(\alpha\cos\phi + \beta\sin\phi\right)\frac{\rho^2 + a^2}{(a^2 - \rho^2)^{1/2}}\,E_{0z}^i \tag{4.25b}$$

which completes the determination of the first-order solution of the field distribution in the circular aperture. Solution (4.25) agrees with Bouwkamp's result (Van Bladel, 1964) completely. This solution also indicates the incompleteness of the result obtained by Bethe (1944), Copson (1946) and that given by Jackson (1962). It is noted that both $E_\rho^{(1)}$ and $E_\phi^{(1)}$ components are induced in the aperture for all possible incident angles.

For the cases where the wave vector of the incident plane wave lies in the plane of the aperture, Equations (4.25a) and (4.25b) take the following form:

$$E_\phi^{(1)} = \frac{4j}{3\pi} (\alpha \sin \phi - \beta \cos \phi)(a^2 - \rho^2)^{1/2} E_{0z}^i \qquad (4.26a)$$

$$E_\rho^{(1)} = \frac{-4j}{3\pi} (\alpha \cos \phi + \beta \sin \phi) \frac{\rho^2 + a^2}{(a^2 - \rho^2)^{1/2}} E_{0z}^i \, . \qquad (4.26b)$$

The above results demonstrate the fact that Equation (4.1) is valid even as $\gamma \to 0$.

4.3.4 Second-order solution of the field distribution in a circular aperture

Having determined the first-order solution of the field distribution in Section 4.3.3, it is the goal of this section to find the second-order solution by solving the integral equation (4.9) subject to the condition

$$E_\phi^{(2)}(\vec{\rho}) = 0 \qquad \forall \phi: \; 0 \leq \phi \leq 2 \quad \text{and} \quad |\vec{\rho}| = a \, . \qquad (4.27)$$

The method of analysis follows the same steps as applied in the previous sections. Here, Equation (4.9) is coupled by $C_{-1}^{(0)}$ and $C_1^{(0)}$ to Equation (4.6) by $C_0^{(0)}$, $C_2^{(0)}$, $C_{-2}^{(0)}$, $C_1^{(1)}$, $C_{-1}^{(1)}$, $E_x^{(0)}$ and $E_y^{(0)}$ to Equation (4.7), and by $C_2^{(1)}$, $C_{-2}^{(1)}$, $C_0^{(1)}$, $C_3^{(0)}$, $C_{-3}^{(0)}$, $C_1^{(2)}$, $C_{-1}^{(2)}$, $E_x^{(1)}$ and $E_y^{(1)}$ to Equation (4.8).

Using Equations (4.19) and (4.25), one can, after some manipulations, verify that the following relations are true:

$$-\frac{1}{4\pi}\iint_{\bar{A}}\begin{Bmatrix}E_x^{(0)}\\ \\ E_y^{(0)}\end{Bmatrix}\left|\vec{\rho}-\vec{\rho}'\right|\,da' = \frac{1}{16}\begin{Bmatrix}\cos\phi\\ \\ \sin\phi\end{Bmatrix}(2a^2\rho+\rho^3)\,E_{0z}^{i} \qquad (4.28)$$

and

$$\frac{j}{2\pi}\iint_{\bar{A}}\begin{Bmatrix}E_x^{(1)}\\ \\ E_y^{(1)}\end{Bmatrix}da' = \frac{4a^3}{3\pi}\begin{Bmatrix}-\gamma E_{0x}^{i}+\alpha E_{0z}^{i}\\ \\ -\gamma E_{0y}^{i}+\beta E_{0z}^{i}\end{Bmatrix}. \qquad (4.29)$$

Substituting (4.28) and (4.29) into (4.9), and employing (4.12), the following expression may be derived as a solution to the integral equation (4.9):

$$\begin{Bmatrix} E_x^{(2)} \\ E_y^{(2)} \end{Bmatrix} = -\frac{E_{0z}^i}{16}\begin{Bmatrix} \cos\phi \\ \sin\phi \end{Bmatrix}\left[\frac{8a^2}{\pi}(a^2-\rho^2)^{-1/2}\rho + \frac{16}{\pi}(a^2-\rho^2)^{1/2}\rho - \frac{16}{3\pi}(a^2-\rho^2)^{-1/2}\rho^3\right]$$

$$-\frac{4a^3}{3\pi}\begin{Bmatrix} -\gamma E_{0x}^i + \alpha E_{0z}^i \\ -\gamma E_{0y}^i + \beta E_{0z}^i \end{Bmatrix}\frac{2}{\pi}(a^2-\rho^2)^{-1/2}$$

$$+\frac{1}{6\gamma}\left\{\left[\left(\frac{\alpha^3}{4}-\frac{3}{4}\alpha\beta^2\right)\frac{32}{5\pi}(a^2-\rho^2)^{-1/2}\rho^3\cos 3\phi\right.\right.$$

$$+\left(\frac{3}{4}\alpha^3+\frac{3}{4}\alpha\beta^2\right)\left[\frac{16}{\pi}(a^2-\rho^2)^{1/2}\rho-\frac{16}{3\pi}(a^2-\rho^2)^{-1/2}\rho^3\right]\cos\phi$$

$$+\left(\frac{3}{4}\alpha^2\beta-\frac{1}{4}\beta^3\right)\frac{32}{5\pi}(a^2-\rho^2)^{-1/2}\rho^3\sin 3\phi$$

$$\left.+\left(\frac{3}{4}\beta^3+\frac{3}{4}\alpha^2\beta\right)\left[\frac{16}{\pi}(a^2-\rho^2)^{1/2}\rho-\frac{16}{3\pi}(a^2-\rho^2)^{-1/2}\rho^3\right]\sin\phi\right\}\begin{Bmatrix} E_{0x}^i \\ E_{0y}^i \end{Bmatrix}$$

$$+\frac{\pi}{48}\begin{Bmatrix} \left(-C_2^{(0)}+C_4^{(0)}\right)e^{j3\phi}+\left(C_{-2}^{(0)}-C_{-4}^{(0)}\right)e^{-j3\phi} \\ j\left(C_2^{(0)}+C_4^{(0)}\right)e^{j3\phi}+j\left(C_{-2}^{(0)}+C_{-4}^{(0)}\right)e^{-j3\phi} \end{Bmatrix}\frac{32}{5\pi}(a^2-\rho^2)^{-1/2}\rho^3$$

$$+\frac{\pi}{16}\begin{Bmatrix} \left(C_2^{(0)}-2C_0^{(0)}\right)e^{j\phi}+\left(-C_{-2}^{(0)}+2C_0^{(0)}\right)e^{-j\phi} \\ j\left(C_2^{(0)}+2C_0^{(0)}\right)e^{j\phi}+j\left(C_{-2}^{(0)}+2C_0^{(0)}\right)e^{-j\phi} \end{Bmatrix}\left[\frac{16}{\pi}(a^2-\rho^2)^{1/2}\rho\right.$$

$$\left.-\frac{16}{3\pi}(a^2-\rho^2)^{-1/2}\rho^3\right]+\frac{\pi}{8}\begin{Bmatrix} -jC_3^{(1)}e^{j2\phi}+jC_{-3}^{(1)}e^{-j2\phi} \\ C_3^{(1)}e^{j2\phi}+C_{-3}^{(1)}e^{-j2\phi} \end{Bmatrix}\frac{16}{3\pi}(a^2-\rho^2)^{-1/2}\rho^2$$

$$+\frac{\pi}{2}\begin{Bmatrix} \left(-C_2^{(2)}+C_0^{(2)}\right)e^{j\phi}+\left(C_{-2}^{(2)}-C_0^{(2)}\right)e^{-j\phi} \\ j\left(-C_2^{(2)}-C_0^{(2)}\right)e^{j\phi}+j\left(-C_{-2}^{(2)}-C_0^{(2)}\right)e^{-j\phi} \end{Bmatrix}\frac{4}{\pi}(a^2-\rho^2)^{-1/2}\rho$$

$$+\pi\begin{Bmatrix} jC_1^{(3)}-jC_{-1}^{(3)} \\ -C_1^{(3)}-C_{-1}^{(3)} \end{Bmatrix}\frac{2}{\pi}(a^2-\rho^2)^{-1/2} \qquad (4.30)$$

Although the above equation is valid for any angle of incidence, the computation of the field distribution will be performed only for the case of normal incidence, i.e., $\alpha = \beta = E^i_{0z} = 0$. Using (4.18) and (4.30) and enforcing the condition (4.27), one arrives at

$$C_4^{(0)} = C_{-4}^{(0)} = C_3^{(1)} = C_{-3}^{(1)} = C_2^{(2)} = C_0^{(2)} = C_{-2}^{(2)} = 0 \ , \tag{4.31a}$$

$$C_1^{(3)} = \frac{2ja^3}{3\pi^2}\left(E^i_{0x} + E^i_{0y}\right) \tag{4.31b}$$

and

$$C_{-1}^{(3)} = \frac{2ja^3}{3\pi^2}\left(-E^i_{0x} + E^i_{0y}\right) \ . \tag{4.31c}$$

It can be noted that the above results are only true for the case of normally incident electromagnetic plane waves.

Substituting (4.31), (4.24), (4.22) and (4.16) into (4.30), one obtains

$$E_\phi^{(2)} = 0 \tag{4.32a}$$

$$E_\rho^{(2)} = 0 \tag{4.32b}$$

which completes the computation of the second-order solution of the field distribution for the normally incident plane waves. The calculation of the higher-order terms of Expansion (4.2) may proceed in a similar manner discussed above.

In conclusion, the field distribution in the circular aperture takes the following form for the case of a normal incidence wave:

$$E_\phi = \frac{8j}{3\pi}\left(E^i_{0y}\cos\phi - E^i_{0x}\sin\phi\right)(a^2 - \rho^2)^{1/2}\, k + O(k^3) \tag{4.33a}$$

$$E_\rho = \frac{2j}{3\pi}\left(E^i_{0x}\cos\phi + E^i_{0y}\sin\phi\right)\left[4(a^2 - \rho^2)^{1/2} + \frac{2\rho^2}{(a^2 - \rho^2)^{1/2}}\right] k + O(k^3) \ . \tag{4.33b}$$

The above equations will be used in Section 4.4 where a comparison is made of the field distribution of a small square aperture with the field distribution of a small circular aperture.

4.3.5 Induced electric-dipole and magnetic-dipole moments

A technique based on the application of the equivalent electric and magnetic dipoles has been used extensively in low frequency analysis. Bethe (1944), Bouwkamp (1953), Grinberg and Pimenov (1957), Eggiman (1961) and others computed the dipole moments for different orders of k. Later Chen (1970), Taylor (1973), Chen and Baum (1974) and others used the concept of dipole moment and investigated the problem of excitations of cavities with small openings. In this section, in order to complete our analysis for the problem of diffraction by circular apertures in the low frequency regime, the equivalent dipole moments will be determined by employing the formulas developed before. The results obtained here will be compared with those for the rectangular aperture in the next section.

Knowing the E-field in the aperture, the magnetic current can be defined as

$$\vec{K}(\vec{\rho}) = 2\hat{z} \times \vec{E}(\vec{\rho}) \quad . \tag{4.34}$$

Then the magnetic charge distribution takes the following form:

$$m(\vec{\rho}) = \frac{j}{\omega} \nabla \cdot \vec{K} \quad . \tag{4.35}$$

Using the above formulas, the induced electric-dipole and magnetic-dipole moments are defined by

$$\vec{P} = \frac{\varepsilon}{2} \iint_{\bar{A}} \vec{\rho}' \times \vec{K} \, da' \tag{4.36}$$

and

$$\vec{M} = \frac{1}{\mu} \iint_{\bar{A}} \vec{\rho}' \, m \, da' \quad , \tag{4.37}$$

respectively.

Substituting (4.19) and (4.25) into (4.34) and simplifying the result one arrives at

$$\vec{K} = -\left(E_{\phi}^{(0)} + E_{\phi}^{(1)}k\right)\hat{\rho} + \left(E_{\rho}^{(0)} + E_{\rho}^{(1)}k\right)\hat{\phi} + O(k^2) \quad . \tag{4.38}$$

By substituting (4.38) into (4.35), the magnetic charge distribution is readily determined to be

$$m = \frac{-8}{\pi\omega}\left[\left(-\gamma E_{0x}^{i} + \alpha E_{0z}^{i}\right)\sin\phi + \left(\gamma E_{0y}^{i} - \beta E_{0z}^{i}\right)\cos\phi\right]\frac{\rho}{(a^2 - \rho^2)^{1/2}}k \quad . \tag{4.39}$$

Upon using the fact

$$\nabla \times \vec{E}^{i} = -j\omega\mu H^{i} \quad , \tag{4.40}$$

it can be readily shown that Equation (4.39) may further be simplified as

$$m = \frac{8\mu}{\pi}\left[H_{0y}^{i}\sin\phi + H_{0x}^{i}\cos\phi\right]\frac{\rho}{(a^2 - \rho^2)^{1/2}} \quad . \tag{4.41}$$

Inserting (4.41) into (4.37) and performing the integration, one finally obtains the following expression for the magnetic-dipole moment

$$\vec{M} = \frac{16a^3}{3}\left(H_{0x}^{i}\hat{x} + H_{0y}^{i}\hat{y}\right) + O(k^2) \quad . \tag{4.42}$$

After substituting (4.38) into (4.36) and performing the integration, the electric-dipole moment P is determined to be

$$\vec{P} = \frac{8}{3}a^3\varepsilon E_{0z}^{i}\hat{z} + O(k^2) \quad . \tag{4.43}$$

Equations (4.42) and (4.43) represent the well-known first-order solution calculated by Bethe (1944). Although Bethe's formula for the magnetic vector $\vec{K}$ was not complete, his result for the dipole moments as shown here is correct. This conclusion was first verified by Bouwkamp (1953) using a different approach.

Having determined the electric and magnetic dipoles, the radiated field may then be computed by applying the following equation (Jones, 1964)

$$\vec{E} = \frac{e^{-jkR}}{4\pi\varepsilon}\left\{\left(\frac{1}{R^3} + \frac{jk}{R^2}\right)\left[3\hat{R}(\hat{R}\cdot\vec{P}) - \vec{P}\right] - \frac{k^2}{R}\hat{R}\times(\hat{R}\times\vec{P})\right\}$$

$$+ \frac{\eta}{4\pi} e^{-jkR}\left(\frac{jk}{R^2} - \frac{k^2}{R}\right)\hat{R}\times\vec{M} \quad . \qquad (4.44)$$

4.4 Numerical Result for an Electrically Small Rectangular Aperture

In the previous section analytical results for the circular aperture problem were presented for the low frequency regime. The rectangular geometry, however, does not lend itself to analytical processing, so the associated integral equation for this problem must be solved numerically. As will be apparent from the discussion to be presented in this section, a comparison of the results for the circular and rectangular apertures provides considerable insight into the low frequency behavior of the aperture coupling problem. In particular, it will be shown that it is possible to extrapolate the results for a rectangular aperture over a sizeable range in the low frequency regime, with a minimal amount of numerical work.

4.4.1 Field distribution

Integral equation (4.1) is used to generate the solution of the field distribution in an electrically small rectangular aperture. The solid curves in Figure 4.1 show the behavior of the E-field sampled along the principal axes of a square aperture excited by a normally incident plane wave. Only the dominant component of the field, i.e., E_y, is shown in the figure. Presented here are the results for the aperture which was sectionalized into 5 x 5 square patches. Three different dimensions (D/λ = .1, .02, .05) have been considered.

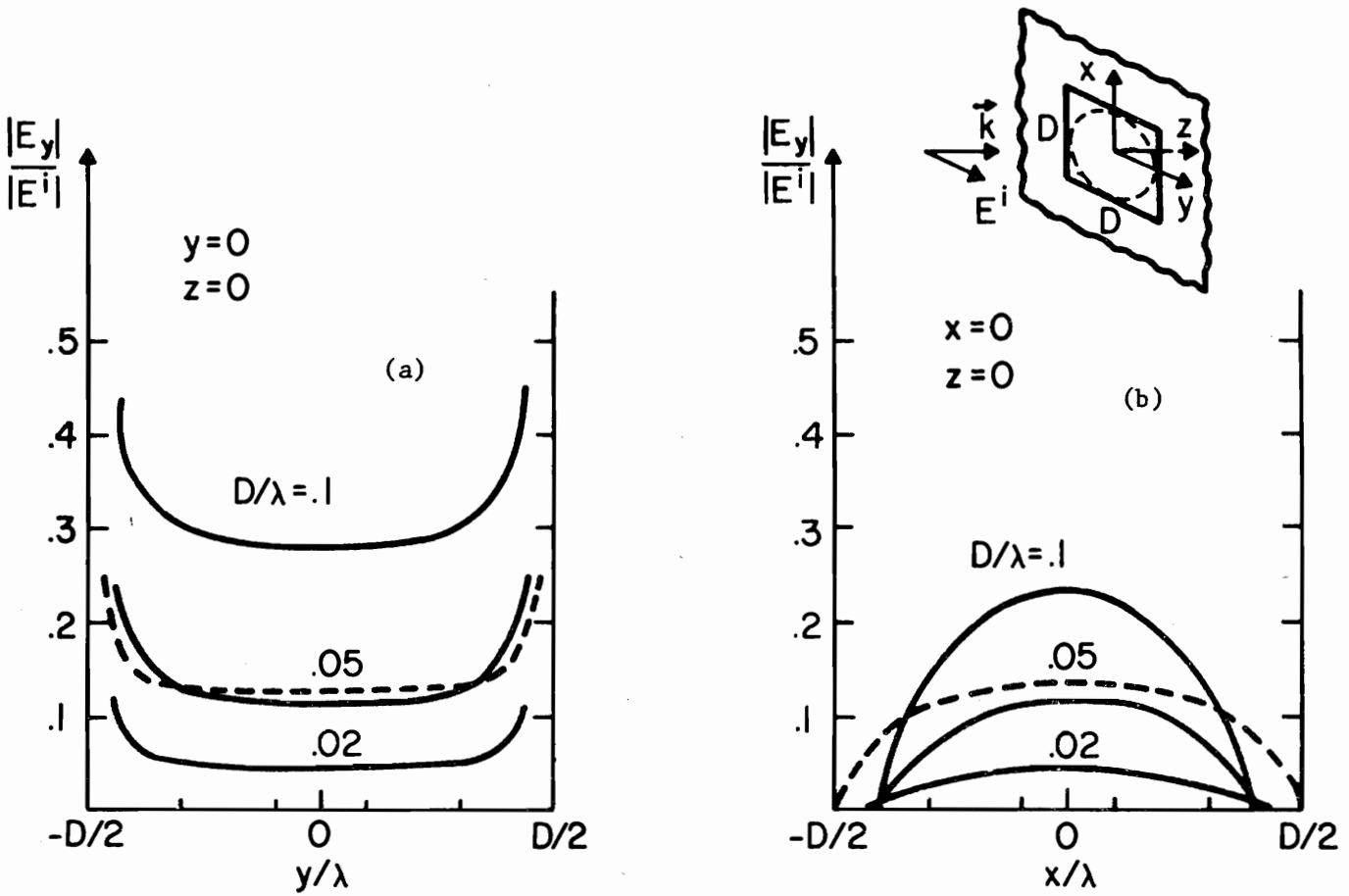

Figure 4.1. E-field distribution in electrically small square and circular apertures. (a) E_y-field sampled along y-axis. (b) E_y-field sampled along x-axis. Integral equation (——) solution for square aperture. First order (---), low frequency, analytical solution for the circular aperture ($D/\lambda = .05$).

The numerical results plotted in Figure 4.1 demonstrate that proper edge behavior has been achieved for all three cases. The same figure also shows that the induced field in the aperture decreases steadily by increasing the wavelength. For the limiting case $D/\lambda \to 0$, the induced field in the aperture is, of course, zero.

Next, the results for the square and circular apertures will be compared. To do this, one returns to Section 4.3.4 and employs Equations (4.33a) and (4.33b). Since the incident field being considered is normal to the plane of the aperture and polarized along the y-axis, (4.33a) and (4.33b) may be simplified to yield the following expressions for the E-field in the circular aperture:

$$\vec{E}_\phi \simeq \vec{E}_\phi^{(1)}{}_k = \frac{16j}{3\lambda}\left(\frac{D^2}{4} - \rho^2\right)^{1/2} E_{0y}^i \cos\phi\hat{\phi} \qquad (4.45a)$$

$$\vec{E}_\rho \simeq \vec{E}^{(1)}{}_k = \frac{4j}{3\lambda}\left\{4\left(\frac{D^2}{4} - \rho^2\right)^{1/2} + \frac{2\rho^2}{\left(\frac{D^2}{4} - \rho^2\right)^{1/2}}\right\} E_{0y}^i \sin\phi\hat{\rho} \quad . \qquad (4.45b)$$

The above equations are employed to generate the dashed curves which are also plotted in Figure 4.1 for convenience of comparison. These curves exhibit the behavior of the E-field along the x and y axis of a circle inscribed within the square aperture. Comparison between the dashed curve and the solid curve in Figure 4.1 reveals that for $D/\lambda \leq .1$, the first-order analytical solution for the circular aperture and numerical solution for the square aperture agree well along the x and y axes. For $D/\lambda \leq .1$, it becomes necessary to include higher-order terms in the expansion (4.33) in order to obtain an accurate solution for the circular aperture problem.

The solid curve in Figure 3.18 displays the variation of the E_y-field as a function of D/λ sampled at the center of a square aperture. This result is compared with that obtained using (4.33) for a circular aperture of diameter D/λ. Simplifying (4.33) for the particular incident field shown in Figure 4.2 results in

$$\vec{E}_y \simeq \vec{E}_y^{(1)}{}_k = \frac{8j}{3}\frac{D}{\lambda} E^i \hat{y} \quad . \tag{4.46}$$

The above equation verifies that the variation of the amplitude of E_y/E^i as a function of D/λ is linear and that its phase is always 90^o (see Figure 4.2). Thus, there is the important result that in the low frequency regime there is a great similarity between the field behaviors in square and circular apertures.

4.4.2 Diffracted field

In this section, the formulation given in Section 4.3.5 is used to compute the field radiated by the equivalent dipoles of a small circular aperture. This result is then compared with that obtained for the square aperture using the numerical technique.

The dipole moment representation is possible only for aperture geometries for which Laplace's equation is separable. This, of course, is true for the circular aperture, as discussed in Section 4.3.5. Equation (4.44) has been used here to generate the dashed curves in Figure 4.3. To make a comparison with the square aperture, equations (3.42) and (3.14) have been used to construct the solid curves shown in the same figure. The phase plot, represented by the solid curve, coincides entirely with the phase curve obtained for the circular aperture. Comparison of the amplitude curves in Figure 4.3 shows that the dipole moment results for the circular aperture and the integral equation

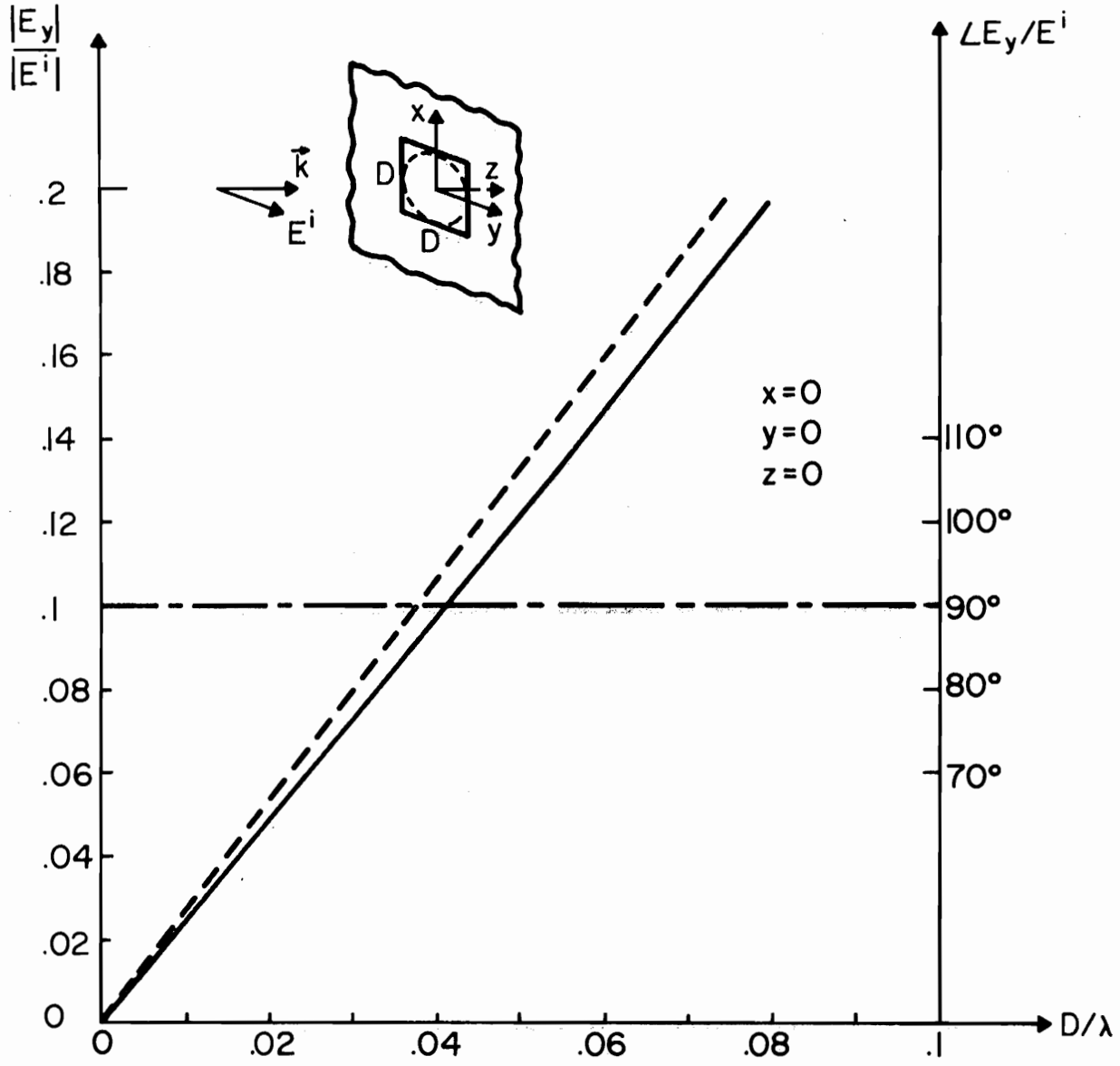

Figure 4.2. E_y-field at the center of square and circular apertures. Amplitude curves (——) obtained from integral equation solution for a square aperture. Amplitude curve (---) for the circular aperture. Phase curve (—— -) for square the circular apertures.

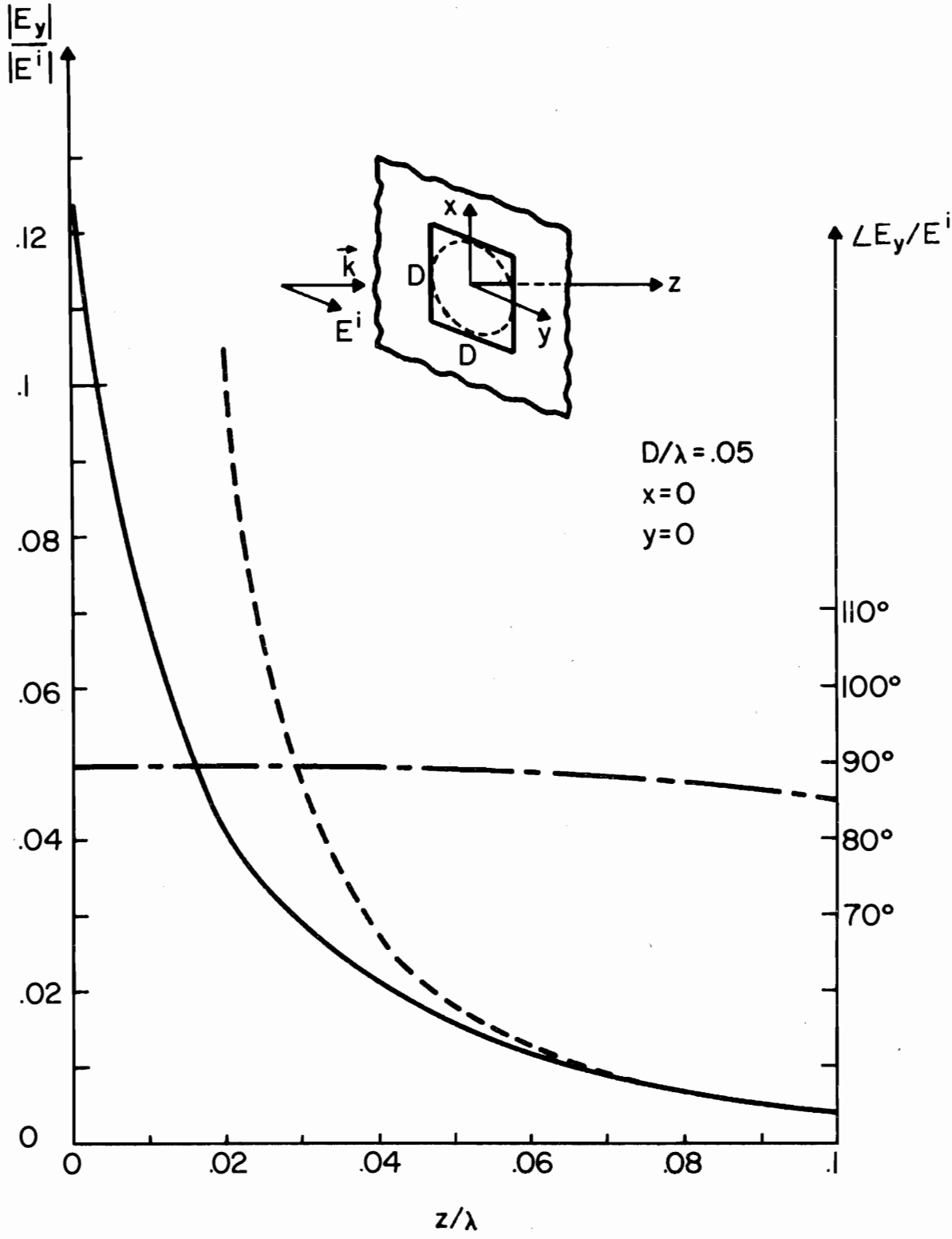

Figure 4.3. E_y-field distribution sampled along the z-axis. Integral equation solution (——) for square aperture. Dipole moment results (----) for circular aperture. Phase curves (—— -) obtained from integral equation and dipole moment techniques.

results for the square aperture exhibit very similar behavior for distances $z/\lambda > .08$ behind the aperture. However, for close distances, i.e., $0 \leq z/\lambda \leq .08$, the two curves deviate considerably from each other. The solid curve, which has been obtained numerically, shows a more correct behavior for distances close to the aperture in comparison with the dashed curve generated by the dipole moment approach. In fact, the solid curve monotonically approaches the correct value of the field at $z = 0$, whereas the dashed curve shows a singular behavior. These results show that one should be careful in using the dipole moment technique when computing the fields in the immediate vicinity of an aperture.

5. SCATTERING OF ELECTROMAGNETIC WAVES BY INFINITELY THIN PLANAR SCATTERERS

5.1 Introduction

In this chapter, the problem of scattering of electromagnetic waves by infinitely thin planar scatterers will be discussed. This problem has received considerable attention in recent years, because of its importance in modeling complex bodies. Many different techniques have been suggested to obtain a proper formulation of this scattering problem in different frequency ranges. Most of the available methods are mainly concerned either with smooth closed scatterers, or with thin structures which possess a continuous curvature at the edge (regular curve). In this work, a new set of integral equations is derived to determine the induced current distribution in a thin planar scatterer of any arbitrary shape.

A perfectly conducting, infinitely thin, planar scatterer is the complement, in the electromagnetic sense, of a perfectly conducting, infinitely thin screen from which an area having the shape of the scatterer has been removed. Therefore, one possibility for invoking the proper formulation of the thin planar scatterer problem is to apply Babinet's principle [see, for instance, Jones (1964)] to the formulation obtained for the aperture problem in Chapter 3. However, this approach is not taken in this chapter, but instead, a direct method based on the application of the vector potential technique (Harrington, 1961) will be presented. The results obtained here will then be compared with those in Chapter 3.

5.2 Integral Equations for Infinitely Thin Planar Surfaces

The necessity of applying a new set of integral equations originates from the fact that the conventional E- and H-integral equations (Poggio and Miller, 1973) do not exhibit good numerical behavior when they are used for infinitely thin structures. For instance, the question of the failure of the H-integral equation for infinitely thin structures, which has been examined by Mittra et al. (1973), shows that, for thin structures, the H-integral equation is not complete by itself and an additional condition must be added for completeness. The numerically ill-conditioned nature of the E-integral equation for thin cylindrical structures has been discussed by Davis (1974), who has shown that improper coupling between the current components results in unstable numerical solutions.

As an illustration, take the case of a plane electromagnetic wave with arbitrary polarization which is incident upon an infinitely thin, perfectly conducting plate. The geometry of the structure is shown in Figure 5.1. Assuming $e^{j\omega t}$ time convention, the incident wave may be written as

$$\vec{H}^i = \left(H^i_{0x}\, \hat{x} + H^i_{0y}\, \hat{y} + H^i_{0z}\, \hat{z} \right) e^{jk(\alpha x+\beta y+\gamma z)} \tag{5.1}$$

where $\alpha = \sin\theta^i \cos\phi^i$, $\beta = \sin\theta^i \sin\phi^i$, $\gamma = \cos\theta^i$, $k = 2\pi/\lambda$, and θ^i and ϕ^i are the elevation and azimuthal angles of incidence, respectively.

If the induced current in the structure is denoted by $\vec{J}\delta(z) = (J_x\, \hat{x} + J_y\, \hat{y})\, \delta(z)$, the vector potential $\vec{A}$ takes the following form:

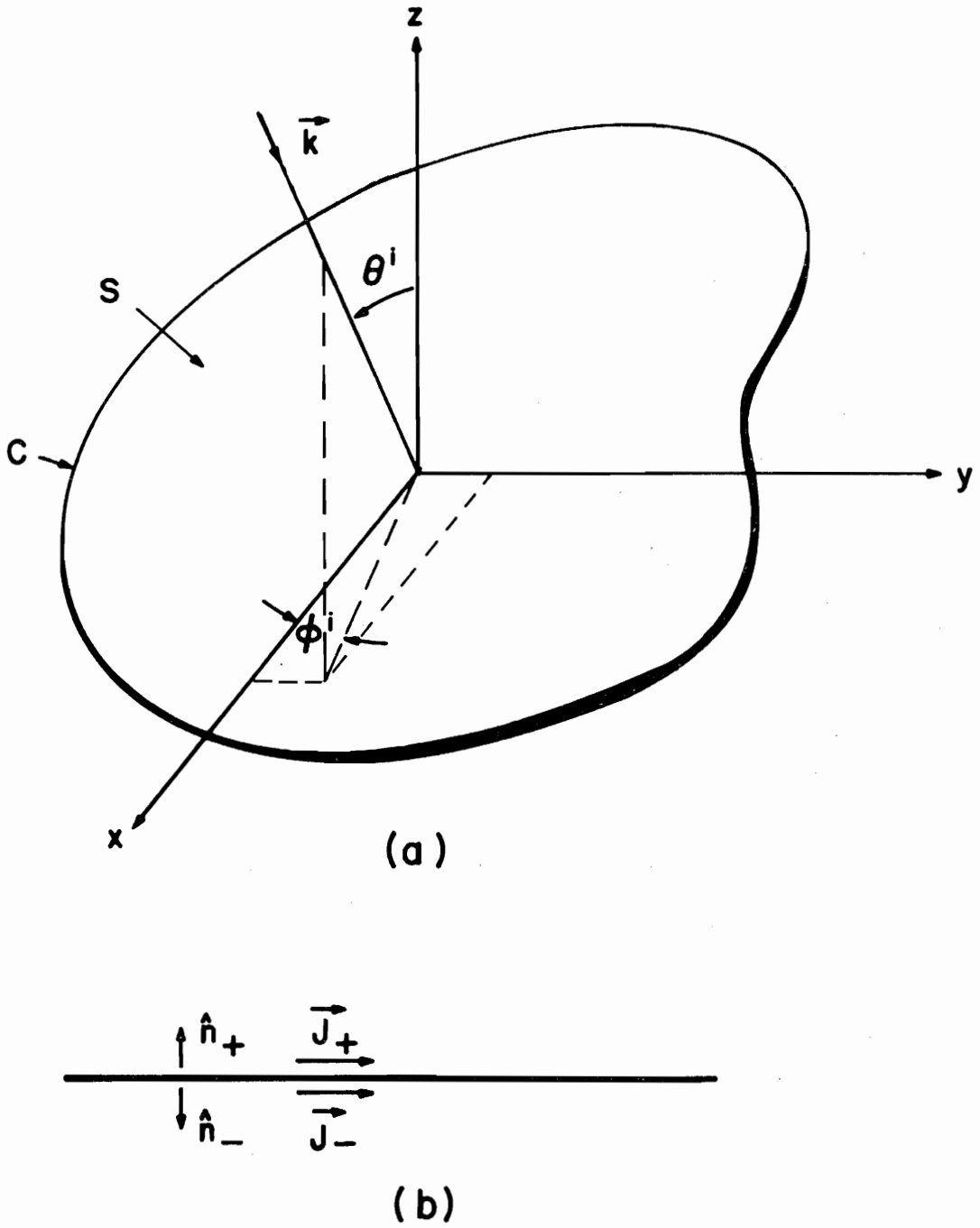

Figure 5.1. (a) An infinitely thin scatterer lying in the x,y plane. (b) Induced currents in top and bottom surfaces of (a).

$$\vec{A} = \iiint \vec{J}\delta(z')\, g_0(\vec{R}'|\vec{R})\, da' = \iint_{\bar{S}} \vec{J} g_0(\vec{\rho}'|\vec{R})\, da' \quad ; \qquad (5.2)$$

g_0 is defined in Equation (2.24). The interior region and the rim of the scatterer shown in Figure 5.1 are denoted by S and C, respectively. The symbol $\bar{S}$ is used to designate the union of S and C, i.e., $\bar{S} = S \cup C$. Clearly, in performing the surface integration in Equation (5.2), the distinction between S and $\bar{S}$ makes no difference.

Using the fact that the scattered H-field is

$$\vec{H}^s = \nabla \times \vec{A} \qquad (5.3)$$

and employing Maxwell's equations, the scattered E-field will then be

$$j\omega\epsilon\vec{E}^s = \nabla \times \nabla \times \vec{A} - \vec{J}\delta(z) \quad . \qquad (5.4)$$

Since the scatterer is perfectly conducting, the total tangential electric field on its surface must be zero, i.e.,

$$\hat{z} \times (\vec{E}^i + \vec{E}^s) = 0 \qquad \{\vec{R}: \ (x,y,z=0) \in \bar{S}\} \quad . \qquad (5.5)$$

By using Maxwell's equations the following statement can be verified (Javid and Brown, 1963): if the tangential E-field is zero on a surface $\bar{S}$ ($\bar{S}$ is a closed set including the rim), then the normal H-field would be zero on S (S is an open set constructed by excluding the rim from $\bar{S}$). Perhaps it is worthwhile to mention that the converse of the above statement is not generally true. Employing this fact, one concludes that

$$\hat{z} \cdot (\vec{H}^i + \vec{H}^s) = 0 \qquad \{\vec{R}: \ (x,y,z=0) \in S\} \quad . \qquad (5.6)$$

Substituting Equation (5.4) and Equation (5.3) into Equations (5.5) and (5.6), respectively, one arrives at

$$\hat{z} \times [\nabla \times \nabla \times \vec{A} - \vec{J}\delta(z)] = -\hat{z} \times \nabla \times \vec{H}^i \qquad \{\vec{R}: \ (x,y,z = 0) \in \bar{S}\} \tag{5.7}$$

and

$$\hat{z} \cdot \nabla \times \vec{A} = -\hat{z} \cdot \vec{H}^i \qquad \{\vec{R}: \ (x,y,z = 0) \in S\} \ . \tag{5.8}$$

As a first step toward obtaining the desired integral equation, the x and y derivatives of Equation (5.8) are substituted into Equation (5.7) to obtain

$$\frac{\partial^2}{\partial z^2} \vec{A} + \vec{J}\delta(z) = \hat{z} \times \frac{\partial \vec{H}^i}{\partial z} \qquad \{\vec{R}: \ (x,y,z = 0) \in S\} \ . \tag{5.9}$$

Utilizing the fact that

$$\left(\frac{\partial^2}{\partial x^2} + \frac{\partial^2}{\partial y^2} + \frac{\partial^2}{\partial z^2} + k^2\right) \vec{A} = -\vec{J}\delta(z) \ , \tag{5.10}$$

and comparing Equation (5.9) with Equation (5.10), one finally arrives at

$$\left(\frac{\partial^2}{\partial x^2} + \frac{\partial^2}{\partial y^2} + k^2\right) \iint_{\bar{S}} \vec{J} g_0(\vec{\rho}' | \vec{\rho}) \, da' = -\hat{z} \times \frac{\partial \vec{H}^i}{\partial z}\bigg|_{z=0} \qquad \{\vec{\rho}: \ (x,y) \in S\} \ . \tag{5.11}$$

The similarity between Equations (5.11) and (3.18) is now quite obvious. This result can be used as a basis to give a simple proof to Babinet's principle.

It should be noted that the range of validity of Equation (5.11) is strictly restricted to $\{\vec{\rho}: \ (x,y) \in S\}$. Specifically, this equation is not valid at the rim (edge) of the structure, i.e., $\{\vec{\rho}: \ (x,y) \in C\}$,

because Equation (5.8) was not defined at the rim. One further notices that if Equation (5.1) were to represent a complete description of the problem, it would have implied that the two current components J_x and J_y are indeed uncoupled with respect to the incident polarization. It is well known that this situation is true for an infinite planar structure only, and that two components of the current are always coupled in a finite structure. This coupling phenomenon becomes evident, however, when Equation (5.11) is transformed into an alternate form, shown below, and when appropriate boundary conditions are imposed on J_x and J_y at the rim of the structure.

By following the same analytical scheme as was developed in Section 3.2, one finally arrives at the desired integral equation

$$\iint_{\bar{S}} \begin{Bmatrix} J_x \\ J_y \end{Bmatrix} \frac{e^{-jk|\vec{\rho}-\vec{\rho}'|}}{4\pi|\vec{\rho}-\vec{\rho}'|}\, da' = \frac{+1}{jk\gamma} \begin{Bmatrix} H^i_{0y} \\ -H^i_{0x} \end{Bmatrix} e^{jk(\alpha x+\beta y)}$$

$$+ \frac{\pi}{k} \begin{Bmatrix} 1 \\ -j \end{Bmatrix} \sum_{n=-\infty}^{\infty} C_n \left[j^{n+1} e^{j(n+1)\phi} J_{n+1}(k\rho) + \begin{Bmatrix} 1 \\ -1 \end{Bmatrix} j^{n-1} e^{j(n-1)\phi} J_{n-1}(k\rho) \right]$$

$$\{\vec{\rho}: \quad (x,y) \in \bar{S}\} \quad . \tag{5.12}$$

In the above equation (ρ,ϕ) are the polar coordinates of the point (x,y). The reader is referred to the work of Rahmat-Samii and Mittra (1974) for the derivation of the above equation. The similarity between Equations (5.12) and (3.33) is indeed a clear manifestation of Babinet's principle. It should be noted that Equation (5.12) satisfies both Equation (5.8) and Equation (5.11).

The unknown currents J_x and J_y and unknown coefficients C_n's can be obtained by solving Equation (5.12) in conjunction with the condition

$$\vec{J} \cdot \hat{\nu} = 0 \qquad \{\vec{\rho}: \ (x,y) \in C\} \tag{5.13}$$

where $\hat{\nu}$ is a unit normal to the edge of the structure in its plane. Condition (5.13) is used to ensure the uniqueness of the solution. For more detailed discussion, Jones' paper (1952) on diffraction by an edge is recommended. The procedure of obtaining the solution of Equation (5.12) follows the same steps as described in Section (3.2). Note that in contrast to the conventional E-integral equation there are no differential operators in the kernel of Equation (5.12), making it rather convenient for numerical processing.

Often, it is desirable to compute the induced current distribution on planar scatterers due to a plane wave incident at a grazing angle. This computation then allows one to determine the scattered field and consequently the radar cross section at this angle. The grazing angle incidence (edge on incidence) occurs when the wave vector $\vec{k}$ lies in the plane of the scatterer. Obviously, for this case $\theta = 90°$ and $\gamma = 0$, and Equation (5.12) does not hold in its present form. In order to be able to extend the domain of validity for Equation (5.12) to the limiting situation $\gamma \to 0$, the two following cases will be discussed: (i) H^i - parallel polarized incident field, and (ii) E^i - parallel polarized incident field.

In case (i), the $\vec{H}^i$-field is parallel to the plane of the scatterer, i.e., $\hat{z} \cdot \vec{H}^i = 0$. One also obtains $-\hat{z} \times \nabla \times \vec{H}^i = 0$ for the edge incident case ($\theta = 90°$). Therefore, the right-hand sides of both Equations (5.7) and (5.8) are zero, indicating that the first term in the right-hand side of Equation (5.12) is zero, too, Imposing condition (5.13), it is then easily observed that C_n's = 0, and hence

$$\vec{J} = 0 \quad \text{for the } H^i\text{-parallel field and } \theta^i = 90^\circ \ . \qquad (5.14)$$

The above result is not totally unexpected, because for this special case, the incident wave cannot detect the existence of the scatterer and thus passes by without any alteration.

In case (ii), however, one expects that the induced current is not zero. In this case, the E^i-field is parallel to the plane of the scatterer, and hence the tangential E^i-field will not be zero on the scatterer. Since the E^i-field is parallel to the plane of the scatterer, the H^i-field takes the following form:

$$\vec{H}_0^i = (-\cos\theta^i \cos\phi^i \hat{x} - \cos\theta^i \sin\phi^i \hat{y} + \sin\theta^i \hat{z})H \ . \qquad (5.15)$$

The limit of the first term in the right-hand side of Equation (5.11) may now be determined as

$$\lim_{\theta^i \to 90^\circ} \left[\frac{-1}{jk \cos\theta^i} \begin{Bmatrix} H_{0y}^i \\ -H_{0x}^i \end{Bmatrix} e^{jk(x\sin\theta^i\cos\phi^i + y\sin\theta^i\sin\phi^i)} \right]$$

$$= \frac{1}{jk} \begin{Bmatrix} H \sin\phi^i \\ -H\cos\phi^i \end{Bmatrix} e^{jk(x\cos\phi^i + y\sin\phi^i)} \ . \qquad (5.16)$$

Substituting the above equation into Equation (5.12), one finally obtains the desired integral equation for the E^i-parallel polarized incident field propagating at a grazing angle.

The far field scattered by the obstacle may be readily computed, using Equation (5.4), once the current distribution on the obstacle has been determined from the solution of Equation (5.12). The scattering

cross section may then be evaluated by employing the following definition (Mentzer, 1955; Hollis et al., 1970):

$$\sigma(\theta^i,\phi^i;\theta^s,\phi^s) = \lim_{R\to\infty} 4\pi R^2 \frac{|E^s(\theta^s,\phi^s)|^2}{|E^i(\theta^i,\phi^i)|^2} = \lim_{R\to\infty} 4\pi R^2 \frac{|H^s(\theta^s,\phi^s)|^2}{|H^i(\theta^i,\phi^i)|^2} \quad (5.17)$$

where (θ^i,ϕ^i) and (θ^s,ϕ^s) are directions in spherical coordinates of the incident and scattered field, respectively. Furthermore,

$\sigma = \sigma_R$ [monostatic cross section or radar cross section (RCS)], if

$$\theta_i = \theta_s,\ \phi_i = \phi_s$$

σ_b (bistatic cross section), otherwise.

5.3 Integral Equation for Infinitely Long Strips

The geometry of an infinitely long strip is shown in Figure 5.2. The strip, which lies in the x-y plane, such that its edges are parallel to the y-axis, has a width designated as W. It is then assumed that the wave vector of the plane-wave incident field is normal to the y-axis.

Since the structure is infinite along the y-axis and since the $\vec{k}$ vector is normal to this axis, the solution of the problem will be independent of the y-coordinate and will be reduced to a two-dimensional problem. Using this fact, Equation (5.11) may be written as follows:

$$\left(\frac{\partial^2}{\partial x^2} + k^2\right) \int_{-W}^{0} \vec{J} dx \int_{-\infty}^{\infty} g_0(\vec{\rho}'|\vec{\rho})\, dy' = -\hat{z} \times \frac{\partial \vec{H}^i}{\partial z}\bigg|_{z=0} \qquad \{\vec{x}:\ x \in (-W,0)\} \quad . \quad (5.18)$$

The infinite integration can easily be evaluated to result in

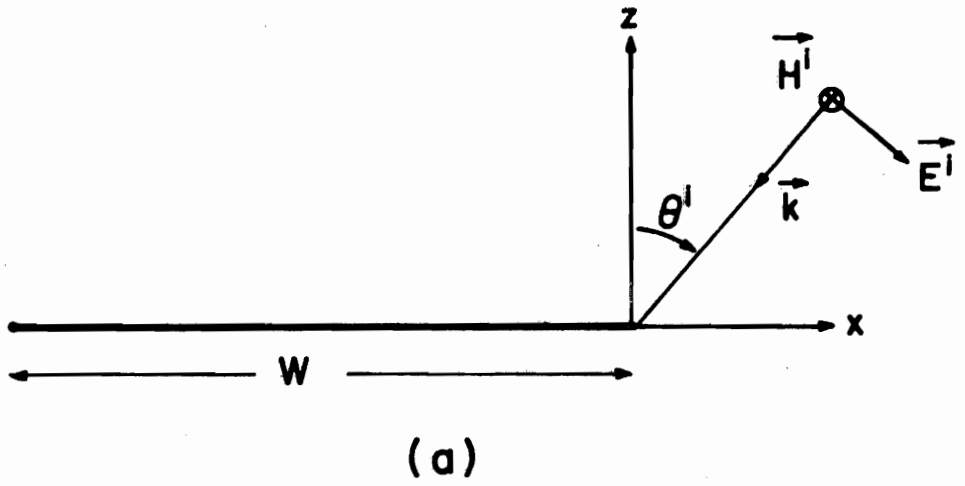

(a)

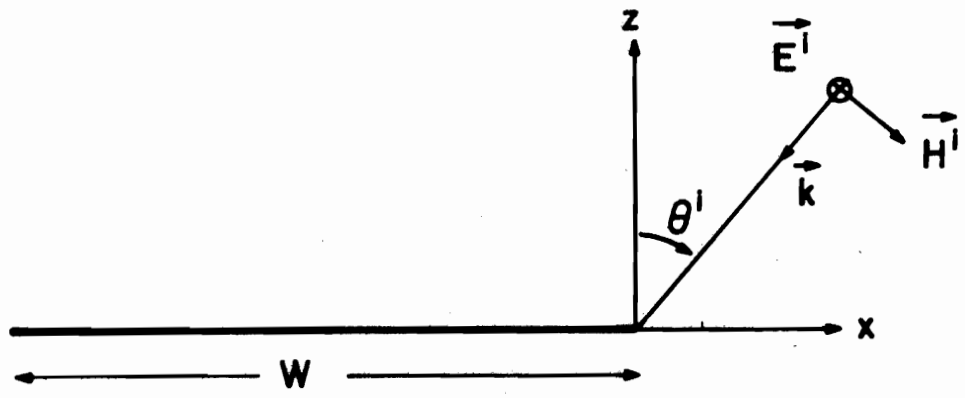

(b)

Figure 5.2. Geometry of an infinitely long strip. (a) $\vec{H}^i$-polarization. (b) $\vec{E}^i$-polarization.

$$\int_{-\infty}^{\infty} \frac{e^{-jk\sqrt{(x-x')^2+(y-y')^2}}}{4\pi\sqrt{(x-x')^2+(y-y')^2}}\,dy' = \frac{1}{4j}H_0^2(k|x-x'|) \quad (5.19)$$

where H_0^2 is the zero-order Hankel function of the second type.

In Appendix E, a simple technique has been introduced to show that the following well-known equation holds

$$\left(\frac{d^2}{dx^2}+k^2\right)\frac{e^{-jk|x-x'|}}{2jk} = -\delta(x-x') \quad . \quad (5.20)$$

Applying Green's function technique (Stakgold, 1967) to Equation (5.18) and using the above result, it can be demonstrated that the following equation is true:

$$\int_{-W}^{0} \vec{J}\,\frac{1}{4j}H_0^2(k|x-x'|)\,dx' = \int_{-W}^{0} -\hat{z}\times\frac{\partial\vec{H}^i}{\partial z}\bigg|_{z=0}\frac{1}{2jk}e^{-jk|x-x'|}\,dx'$$

$$+\vec{C}_1\cos kx + \vec{C}_2\sin kx \qquad \{\vec{x}:\ x\in[-W,0]\}\ . \quad (5.21)$$

In the above equation cos kx and sin kx are the homogeneous solutions of the operator $\left(\frac{d^2}{dx^2}+k^2\right)$, and $\vec{C}_1$ and $\vec{C}_2$ are two unknown constants yet to be determined.

The incident plane wave may be written as below

$$\vec{H}^i = \vec{H}_0^i\,e^{jk(\alpha x+\gamma z)} \quad (5.22)$$

where $\alpha = \sin\theta^i$, $\gamma = \cos\theta^i$ and $\vec{H}_0^i$ denotes either $H_{0y}^i\,\hat{y}$ or $H_{0x}^i\,\hat{x} + H_{0z}^i\,\hat{z}$ as shown in Figures 5.2a and 5.2b. Substituting Equation (5.22) into Equation (5.21) and performing the resulting integration in the right-hand side of Equation (5.21), one obtains

$$\int_{-W}^{0} -\hat{z} \times \left.\frac{\partial \vec{H}^i}{\partial z}\right|_{z=0} \frac{1}{2jk} e^{-jk|x-x'|} \, dx' = \frac{-1}{jk\gamma} \hat{z} \times \vec{H}_0^i e^{jk\alpha x}$$

$$+ \frac{\gamma}{2jk} \hat{z} \times \vec{H}_0^i \left[\frac{1}{1+\alpha} e^{-jk(1+\alpha)W} e^{-jkx} + \frac{1}{1-\alpha} e^{jkx} \right] . \tag{5.23}$$

In deriving the above equation, the fact that $\alpha^2 + \gamma^2 = 1$ was used.

To simplify Equation 5.21, two special cases will now be considered:

(i) The polarization of the incident field is such that the $\vec{H}^i$-field is parallel to the edge of the strip, as shown in Figure 5.2a. In this case, the induced current in the structure will only possess the J_x component. Using this result, Equation (5.21) may be written as

$$\int_{-W}^{0} J_x \frac{1}{4j} H_0^2(k|x - x'|) \, dx' = \frac{1}{jk\gamma} H_{0y}^i e^{jk\alpha x} + C_1 \cos kx + C_2 \sin kx . \tag{5.24}$$

To derive the right-hand side of the above equation, the second terms in the r.h.s. of Equations (5.21) and (5.23) were combined to give the second term in Equation (5.24). It can be readily seen that Equation (5.23) satisfies Equation (5.8), and hence Equation (5.24) is indeed the desired integral equation.

In order to be able to obtain the unique solution of Equation (5.24), one should first determine C_1 and C_2. This is done by imposing the condition (5.13), which reads

$$J_x(0) = J_x(-W) = 0 . \tag{5.25}$$

(ii) The polarization of the incident field is such that the E^i-field is parallel to the edge of the strip, as shown in Figure 5.2b. In this case, the induced current in the structure will only possess the

J_y component. Using this result, Equation (5.20) may be written as

$$\int_{-W}^{0} J_y \frac{1}{4j} H_2^0(k|x - x'|)\, dx' = \frac{-1}{jk\gamma} H_{0x}^i e^{jk\alpha x} \quad . \tag{5.26}$$

In contrast to Equation (5.24), there are no homogeneous terms in Equation (5.26), as the satisfaction of Equation (5.8) results in the following condition:

$$\frac{-\gamma}{2jk} H_{0x}^i \left[\frac{1}{1+\alpha} e^{-jk(1+\alpha)W} e^{-jkx} + \frac{1}{1-\alpha} e^{jkx}\right] + C_1 \cos kx + C_2 \sin kx = 0 \; . \tag{5.27}$$

Equation (5.26) is the desired integral equation, and it need not be subjected to any auxiliary condition as Equation (5.25).

5.4 Integral Equation Representation of Induced Shadow-Side Current for Infinitely Thin Obstacles

The induced current $\vec{J}$ of an infinitely thin obstacle may be decomposed into $\vec{J}_+$ and $\vec{J}_-$ components as follows:

$$\vec{J} = \vec{J}_+ + \vec{J}_- \quad , \tag{5.28}$$

where $\vec{J}_+$ and $\vec{J}_-$ designate the induced current in the upper surface and the lower surface of the obstacle, as shown in Figure 5.1, respectively. J_+ is called the lit-side induced current ($\hat{n}_+ \cdot \vec{k} < 0$), and J_- is named the shadow-side induced current ($\hat{n}_- \cdot \vec{k} > 0$). It can then be shown that the following is true (Mittra et al., 1973):

$$\vec{J}_+ - \vec{J}_- = 2\hat{z} \times \vec{H}^i \quad . \tag{5.29}$$

For the special case, where the obstacle is an infinite plane, one readily concludes that $\vec{J}_- = 0$, and hence $\vec{J}_+ = \vec{J} = 2\hat{z} \times \vec{H}^i$.

Substituting $\vec{J}_+$ from Equation (5.28) into Equation (5.27), the following equation results:

$$\vec{J} = 2\vec{J}_- + 2\hat{z} \times \vec{H}^i \quad . \tag{5.30}$$

The desired integral equation for the shadow-side current can now be constructed by simply substituting Equation (5.30) into Equation (5.12) to obtain

$$2 \iint_S \begin{Bmatrix} J_{-x} \\ J_{-y} \end{Bmatrix} \frac{e^{-jk|\vec{\rho}-\vec{\rho}'|}}{4\pi|\vec{\rho} - \vec{\rho}'|} da' + 2 \iint_S \begin{Bmatrix} -H_x^i \\ H_y^i \end{Bmatrix} \frac{e^{-jk|\vec{\rho}-\vec{\rho}'|}}{4\pi|\vec{\rho} - \vec{\rho}'|} da'$$

$$= \text{right-hand side of Equation (5.12)} \quad . \tag{5.31}$$

The above equation must be solved in conjunction with the condition

$$\hat{\nu} \cdot \vec{J}_- = -\hat{\nu} \cdot \hat{z} \times \vec{H}^i \qquad \{\vec{\rho}: \ (x,y) \in C\} \tag{5.32}$$

in order to obtain the unique solution.

Integral equation (5.31) has some special features when it is used for large obstacles (high-frequency regime). It is noted that $\vec{J}_-$ decays rapidly away from the rim of the obstacle (Li, 1972), and hence the first integral in the right-hand side of Equation (5.31) may be approximated by simply performing the integration over a narrow ribbon around the rim of the obstacle. One hopes that future numerical calculations will exhibit the use of integral equation (5.31).

5.5 Numerical Results and Discussions

In this section, the procedure for extracting the numerical solution of integral equation (5.12) will be outlined. Some numerical results will be presented for the induced current distribution in

rectangular scatterers. Numerical results will also be obtained for the radar cross section (RCS) of rectangular scatterers for different angles of incidence.

By following the same steps as developed in Section 3.3.1 and employing the moment method, a discretized version of Equation (5.12) can be constructed as follows:

$$\sum_{m=1}^{M}\sum_{n=1}^{N}\begin{Bmatrix} J_x(x'_m,y'_n) \\ J_y(x'_m,y'_n) \end{Bmatrix} g_0(x_\ell,y_p;x'_m,y'_n)\,\Delta x'\,\Delta y'$$

$$= \frac{1}{jk\gamma}\begin{Bmatrix} H^i_{0y} \\ -H^i_{0x} \end{Bmatrix} e^{jk(\alpha x_\ell+\beta y_p)}$$

$$+ \frac{\pi}{k}\begin{Bmatrix} 1 \\ -j \end{Bmatrix} \sum_{n=-L+1}^{L} C_n \left[j^{n+1} e^{j(n+1)\phi} \cdot J_{n+1}(k\rho) + \begin{Bmatrix} 1 \\ -1 \end{Bmatrix} j^{n-1} e^{j(n-1)\phi}\, J_{n-1}(k\rho) \right], \tag{5.33}$$

$$\ell = 1, \ldots, M;\ p = 1, \ldots, N$$

where $\rho = (x_\ell^2 + y_p^2)^{1/2}$, $\phi = \arctan(y_p/x_\ell)$, and 2L corresponds to the total number of matching points on the rim.

A general computer program has been written for the IBM 360/75 system that computes the current distribution and RCS for an arbitrary incident angle, arbitrary polarization, and arbitrary dimensions of the rectangular scatterer. Figures 5.3 and 5.4 show the distribution of the two components of the induced current sampled along the principal axes, for an obliquely incident plane wave with E_y polarization. Note that the two components of the current exhibit correct behaviors at the edge of the scatterer, and that they are significantly different from the results given by the physical optics approximation, i.e.,

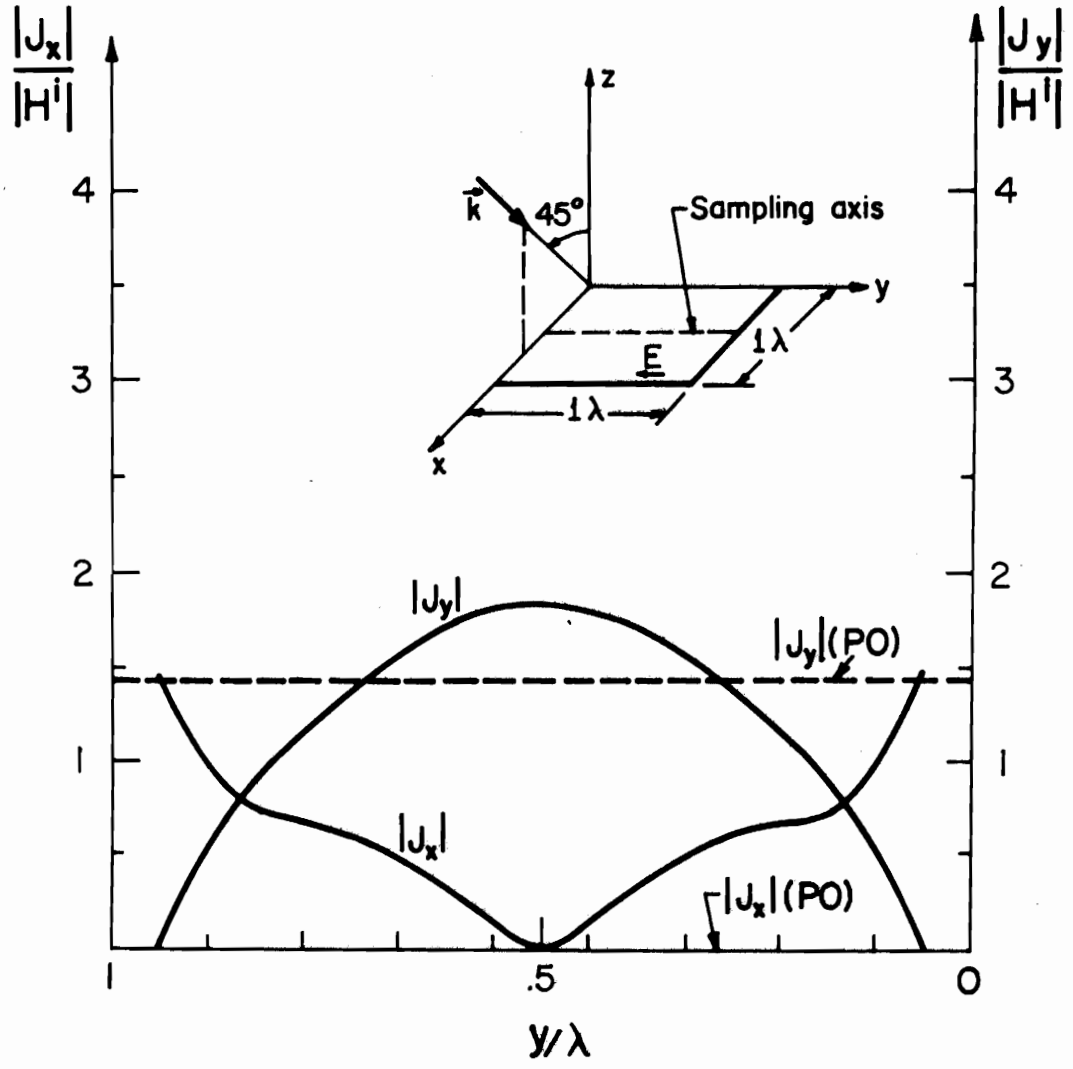

Figure 5.3. Amplitude of current distribution on 1λ x 1λ plate. x = λ/2 and y is a variable.

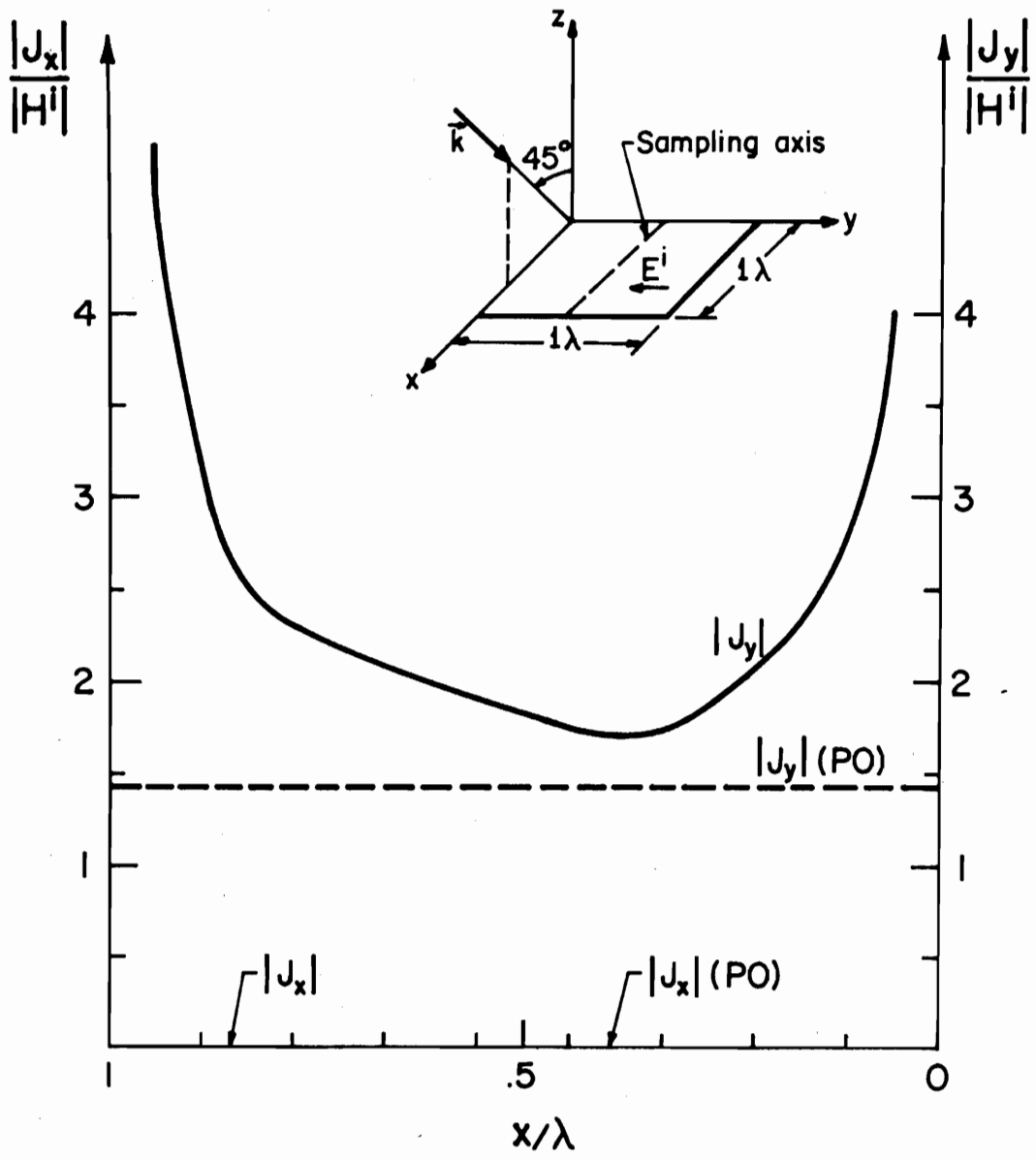

Figure 5.4. Amplitude of current distribution on 1λ x 1λ plate. y = λ/2 and x is a variable.

$$\vec{J}^{PO} = 2\hat{z} \times \vec{H}^{i} \quad . \tag{5.34}$$

In the process of analyzing the numerical behavior of Equation (5.33), it has been noticed that even when the condition $\vec{J} \cdot \hat{\nu} = 0$ is applied to only a fraction of the subsections around the rim, this condition is satisfied at the in-between point as long as the separation between the match points is not too large. The behavior of the solution is shown pictorially in the three-dimensional plots of Figures 5.5 and 5.6. Figure 5.5 shows the J_y component of the current distribution due to a normal incident field only prior to the incorporation of the contributions of the homogeneous terms in Equation (5.33). It is obvious that by itself this current distribution does not have the correct behavior at the rim, since it exhibits a singular behavior all around the rim. This was to be expected, however, because the solution of Equation (5.13) is not complete without the homogeneous terms. Using the homogeneous terms and requiring that the normal component of the current must be zero at the center of the dashed regions as indicated in Figure 5.6, one obtains the current distribution as shown in the same figure. The current distribution now has the correct behavior around the entire rim, even though the condition $\vec{J} \cdot \hat{\nu} = 0$ has been imposed at only a third of the subsections around the rim. It may be of interest to mention that the above numerical results have been obtained with a matrix size of 81 x 81 for the 1λ square scatterer.

In solving Equation (5.33), similar processes described in Equations (3.50), (3.51) and (3.52) are followed. More precisely, one first enforces the condition $\vec{J} \cdot \hat{\nu} = 0$ at the edge patches to determine c_n's, and then uses these c_n's to evaluate the current distribution $\vec{J}$

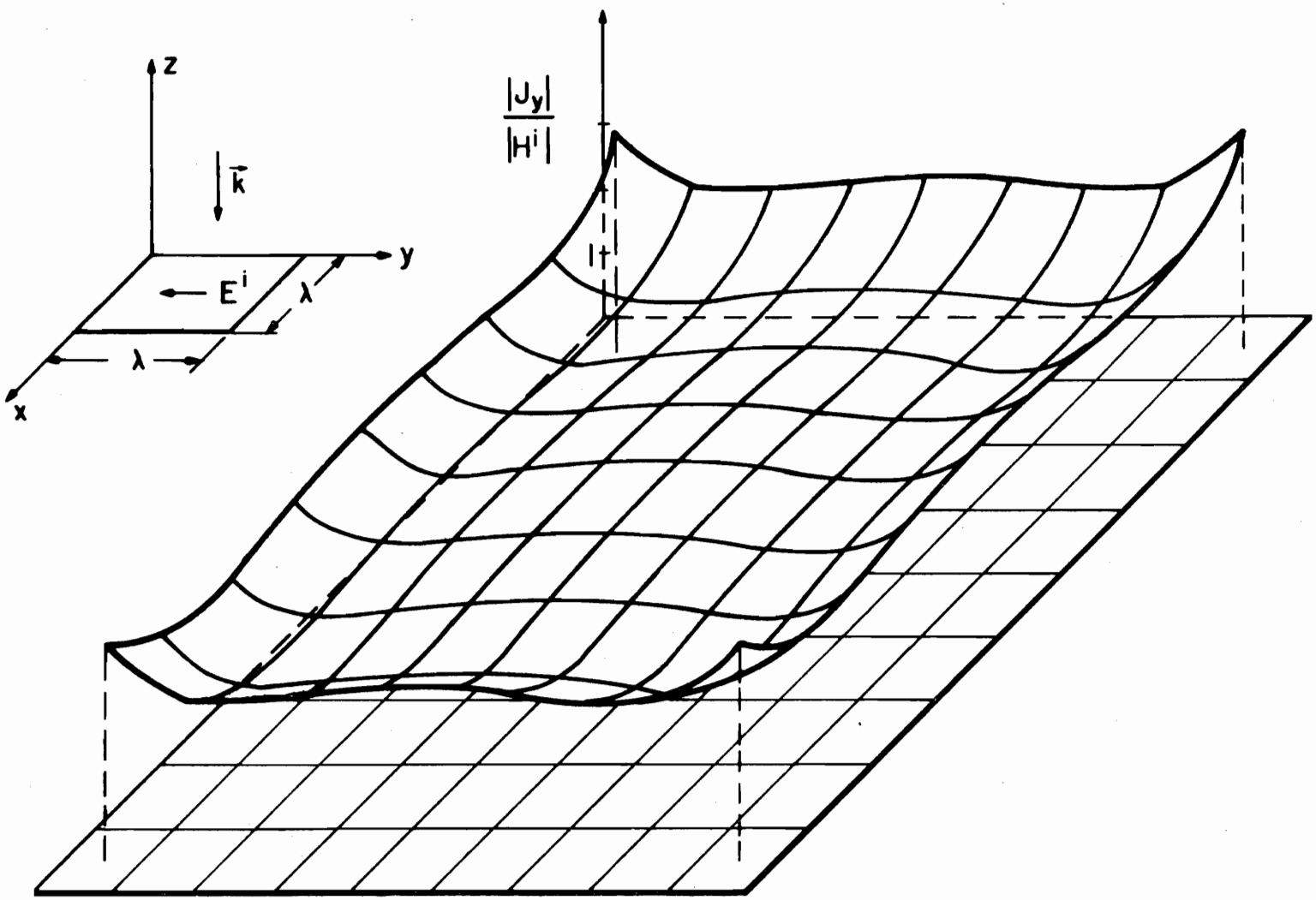

Figure 5.5. Amplitude of J_y component of current distribution computed from Equation (5.33) prior to incorporating contribution of homogeneous terms.

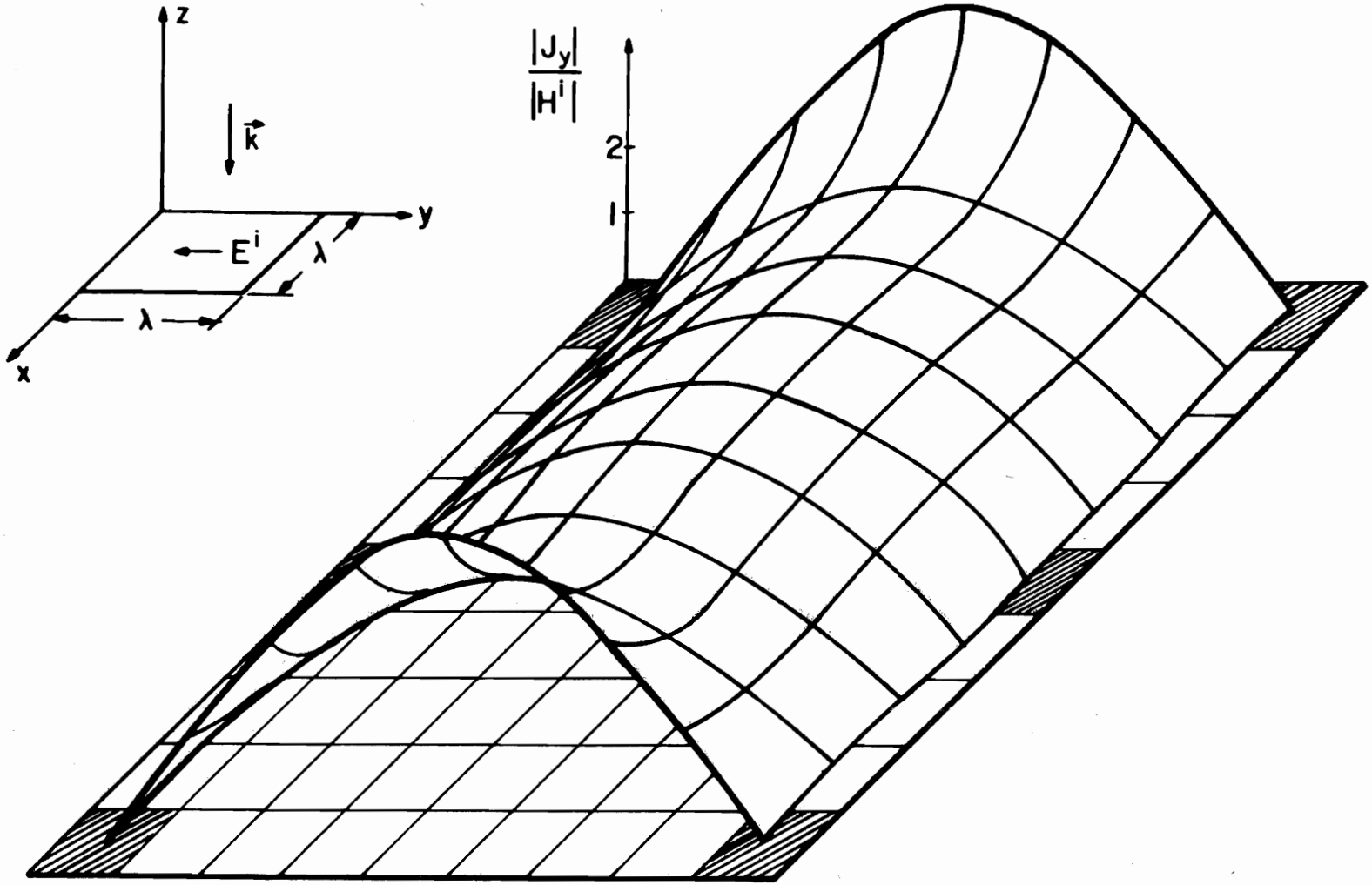

Figure 5.6. Amplitude of J_y component of current distribution obtained from Equation (5.33) after adding homogeneous term contributions.

on the entire structure. Therefore, it would be of interest to check how well the enforced condition $\vec{J} \cdot \hat{\nu} = 0$ will be recovered at the end of the process. This is done by displaying some numerical results for the two components of the current distribution on a square plate for a normally incident plane wave with the E^i-field polarized along the y-axis. The plate is one wavelength square and is subsectionalized into 81 subsections. A general computer program, which was written for handling arbitrary incident angles, is used to derive the solution and no advantage is taken of the symmetry of the problem, although the matrix could be reduced considerably for this special case. The numerical results for the real and imaginary parts of the two current components are displayed in Tables 5.1 and 5.2. It is readily noticed that the condition $\vec{J} \cdot \hat{\nu} = 0$ has been recovered perfectly, as the normal components of the current distribution at the edge patches are of the order 10^{-16}, which is practically zero. One further notices that the current components exhibit the desired symmetrical and asymmetrical behaviors completely. These results indicate that the numerical stability in deriving the final result, current distribution is fairly good.

Figure 5.7 shows the RCS versus the angle of incidence for a $1\lambda \times 1\lambda$ scatterer illuminated with an E_y^i-polarized plane wave. This result has been compared with those derived by using the physical optics approximation (PO) and the geometrical theory of diffraction (GTD). For this comparison the formulations given by Ross (1966) have been used, and the results of computations obtained employing his formulas have also been plotted in Figure 5.7. For angles of incidence less than 20° from the normal, all three methods are in good agreement. Even better

TABLE 5.1

REAL AND IMAGINARY PARTS OF THE J_y-CURRENT ON THE 1.λ x 1.λ PLATE

FOR A NORMAL E^i_y-POLARIZED INCIDENT FIELD

J_y

x \ y								
	10(-16)	1.2462	2.6700	3.7203	4.1247	3.7203	2.6700	1.2462	10(-16)
	-j10(-16)	-j.3562	-j1.4611	-j2.5249	-j2.9419	-j2.5249	-j1.4611	-j.3562	-j10(-16)
	10(-16)	1.0400	1.8900	2.5274	2.7637	2.5274	1.8900	1.0400	10(-16)
	-j10(-16)	+j.4368	+j.0100	-j.4473	-j.6371	-j.4473	+j.0100	+j.4368	-j10(-16)
	10(-16)	1.1047	1.9491	2.5687	2.7966	2.5687	1.9491	1.1047	10(-16)
	-j10(-16)	+j.6151	+j.3394	-j.0055	-j.1534	-j.0055	+j.3394	+j.6151	-j10(-16)
	10(-16)	1.1493	2.0078	2.6309	2.8591	2.6309	2.0078	1.1493	10(-16)
	-j10(-16)	+j.7001	+j.4974	+j.2070	+j.07939	+j.2070	+j.4974	+j.7001	-j10(-16)
	10(-16)	1.1654	2.0312	2.6577	2.8868	2.6577	2.0312	1.1654	10(-16)
	-j10(-16)	+j.7252	+j.5441	+j.2699	+j.1482	+j.2699	+j.5441	+j.7252	-j10(-16)
	10(-16)	1.1493	2.0078	2.6309	2.8591	2.6309	2.0078	1.1493	10(-16)
	-j10(-16)	+j.7001	+j.4974	+j.2070	+j.0793	+j.2070	+j.4974	+j.7001	-j10(-16)
	10(-16)	1.1047	1.9491	2.5687	2.7966	2.5687	1.9491	1.1047	10(-16)
	-j10(-16)	+j.6151	+j.3394	-j.0055	-j.1534	-j.0055	+j.3394	+j.6151	-j10(-16)
	10(-16)	1.0400	1.8900	2.5274	2.7637	2.5274	1.8900	1.0400	10(-16)
	-j10(-16)	+j.4368	+j.0100	-j.4473	-j.6371	-j.4473	+j.0100	+j.4368	-j10(-16)
	10(-16)	1.2462	2.6700	3.7203	4.1247	3.7203	2.6700	1.2462	10(-16)
	-j10(-16)	-j.3562	-j1.4611	-j2.5249	-j2.9419	-j2.5249	-j1.4611	-j.3562	-j10(-16)

TABLE 5.2

REAL AND IMAGINARY PARTS OF THE J_x-CURRENT ON THE 1.λ x 1.λ PLATE

FOR A NORMAL E_y^i-POLARIZED INCIDENT FIELD

J_x

x \ y								
-10(-16) +j10(-16)	-10(-16) +j10(-16)	-10(-16) +j10(-16)	10(-16) -j10(-16)	-10(-16) -j10(-16)	10(-16) -j10(-16)	10(-16) -j10(-16)	10(-16) +j10(-16)	-10(-16) -j10(-16)
.6037 -j.1708	.1736 -j.1043	.0936 -j.0726	.0416 -j.0377	10(-11) -j10(-10)	-.0416 +j.0377	-.0936 +j.0726	-.1736 +j.1043	-.6037 +j.1708
.6228 -j.2915	.2019 -j.1214	.1089 -j.0795	.0484 -j.0401	10(-11) -j10(-11)	-.0484 +j.0401	-.1089 +j.0795	-.2019 +j.1214	-.6228 +j.2915
.3912 -j.2035	.1309 -j.0803	.0712 -j.0509	.0317 -j.0253	10(-11) -j10(-12)	-.0317 +j.0253	-.0712 +j.0509	-.1309 +j.0803	-.3912 +j.2035
-10(-10) -j10(-10)	10(-11) -j10(-11)	10(-11) -j10(-11)	10(-12) +j10(-11)	10(-12) +j10(-11)	10(-12) +j10(-11)	-10(-11) +j10(-11)	-10(-11) +j10(-10)	-10(-11) +j10(10)
-.3912 +j.2035	-.1309 +j.0803	-.0712 +j.0509	-.0317 +j.0253	10(-11) +j10(-12)	.0317 -j.0253	.0712 -j.0509	.1309 -j.0803	.3912 -j.2035
-.6228 +j.2915	-.2019 +j.1214	-.1089 +j.0795	-.0484 +j.0401	10(-11) +j10(-12)	.0484 -j.0401	.1089 -j.0795	.2019 -j.1214	.6228 -j.2915
-.6037 +j.1708	-.1736 +j.1043	-.0936 +j.0726	-.0416 +j.0377	10(-11) +j10(-12)	.0416 -j.0377	.0936 -j.0726	.1736 -j.1043	.6037 -j.1708
-10(-16) +j10(-16)	10(-16) -j10(-16)	10(-16) -j10(-16)	-10(-16) -j10(-16)	10(-16) -j10(-16)	-10(-16) -j10(-16)	-10(-16) +j10(-16)	-10(-16) -j10(-16)	-10(-16) +j10(-16)

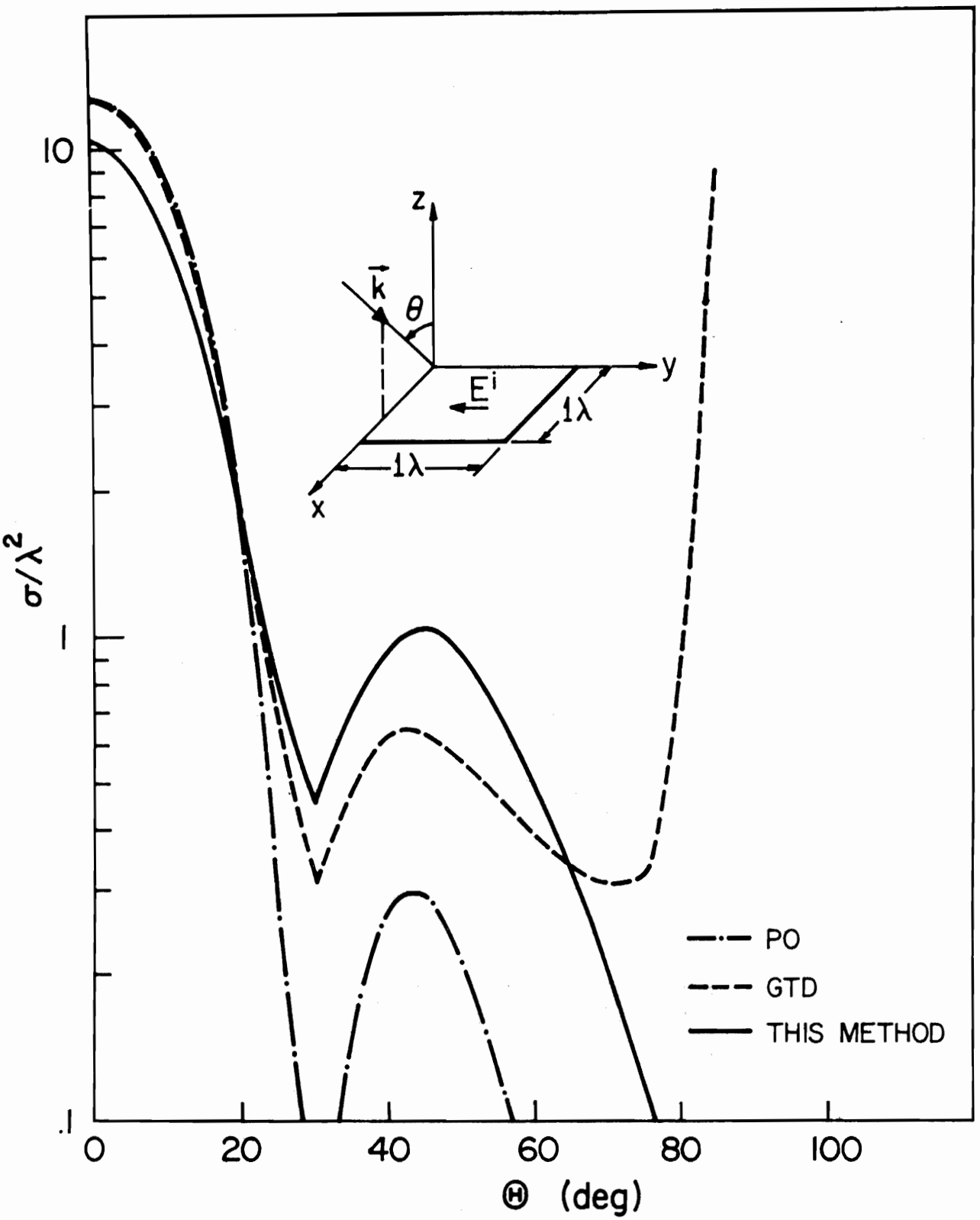

Figure 5.7. RCS of 1λ x 1λ plate versus aspect angle. PO and GTD curves have been obtained by employing the formulations given by Ross (1966).

agreement might have been obtained by imposing the boundary condition $\vec{J} \cdot \hat{\nu} = 0$ at precisely the physical edge of the plate rather than at the center of the edge sections. For angles of incidence between 20° and 65°, one observes that the result obtained in this work shows better agreement with the GTD than with that obtained by using the physical optics approach. For angles greater than 80°, the results computed from the GTD formula given by Ross (1966) appear to become increasingly inaccurate; however, the results obtained via the present approach appear to be good for the entire angular range.

Figure 5.8 displays the plot of RCS computations of a square scatterer for normal incidence and different scatterer sizes and a comparison of these curves with the corresponding ones reported in the Radar Cross Section Handbook (Ruck, 1970). In this figure, the solid curve has been computed via the present formulation; circles indicate the experimentally measured data (Ruck, 1970); and the dashed curve has been obtained by applying the variational technique (Ruck, 1970). It is evident that the result obtained in this work exhibits a closer agreement with experimental data than those computed via the variational approach.

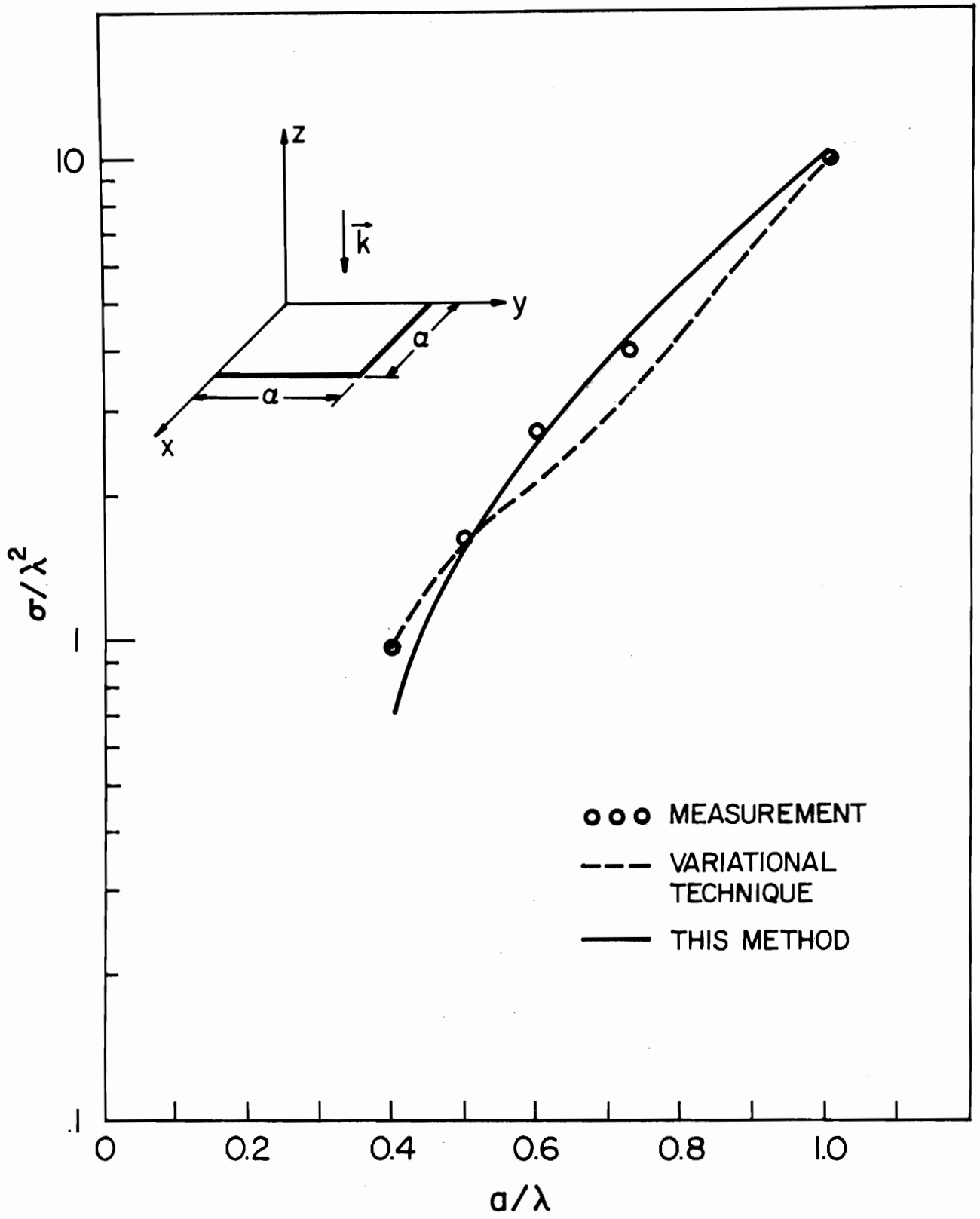

Figure 5.8. RCS of square plate for normally incident plane wave. Measurement and variational technique curves are given in the Radar Cross Section Handbook (Ruck, 1970).

6. ELECTROMAGNETIC COUPLING THROUGH AN APERTURE INTO A TWO-PARALLEL-PLATE REGION

6.1 Introduction

Recently, the problem of electromagnetic compatibility of electronic systems, subject to EMP, has revived researchers' interest in analyzing the coupling phenomenon through apertures into cavities. The use of this study is vitally important in solving many typical problems. For instance, apertures may occur because of a shielded door being improperly seated, defects in weld, etc., all of which may provide points of entry via the aperture coupling.

Though the problem of electromagnetic coupling through small apertures into a cavity has received considerable attention, little is known about this problem when the aperture size is approximately that of the wavelength. The reader is referred to the works of Muller (1961), Liu (1969), Chen (1970), Sancer and Varvatsis (1970), Van Bladel (1972), Taylor (1973), Chen and Baum (1974) and others who have investigated small aperture coupling problems. The basic idea behind their approaches was that the aperture field could be approximated as though the aperture were perforated in a single infinite screen, using Bethe's approximation. This approach, however, fails when the cavity is at resonance, or when the size of the aperture is of the order of the wavelength.

In this chapter, by using the results obtained in Chapters 2 and 3, an integral equation will be constructed to determine the induced field in an aperture perforated in a structure with two-parallel-plate geometry. This problem is an example which is analytically tractable and its numerical solution provides some insights into the coupling problems.

6.2 Derivation of an Integral Equation

The geometry of the structure under consideration in this section is displayed in Figure 6.1. This structure consists of two perfectly conducting, infinitely thin plates located at distance w parallel to each other. In order to orient the space, a Cartesian coordinate system, with its z-axis normal to the plates and its x-y plane parallel to the plates, is erected as shown in the figure. The plates are labeled I and II to denote the z = 0 and z = w boundaries, respectively. Plate I is perforated by an arbitrarily shaped aperture, as shown in the figure. The notations introduced in Chapter 2 are assumed here with no changes. It is further assumed that a monochromatic wave $\vec{E}^i$, $\vec{H}^i$, originating from a source situated in the half space $\mathcal{M}_-$, is incident upon the structure. In this section, by exactly following the steps developed in Section 3.2, an integral equation will be constructed for determination of the tangential E-field in the aperture.

The starting point is to split up the electromagnetic field $\vec{E}$, $\vec{H}$ at any point in space, into an incident field $\vec{E}^i$, $\vec{H}^i$, a reflected field $\vec{E}^r$, $\vec{H}^r$ (associated with the reflected wave that exists when the aperture is closed), and diffracted field $\vec{E}^d$, $\vec{H}^d$, due to the aperture alone. It is then found that in $\mathcal{M}_-$

$$\vec{E}_- = \vec{E}^i_- + \vec{E}^r_- + \vec{E}^d_- \tag{6.1}$$

and in $\mathcal{M}_+$

$$\vec{E}_+ = \vec{E}^d_+ \quad . \tag{6.2}$$

In the above equation, $\vec{E}$ may be replaced by $\vec{H}$ to determine the proper equation for $\vec{H}_-$ and $\vec{H}_+$ fields (Equations 3.2 and 3.4). The reflected field can, in general, be constructed from the knowledge of the incident field and the knowledge of the parameters which describe the reflecting surface.

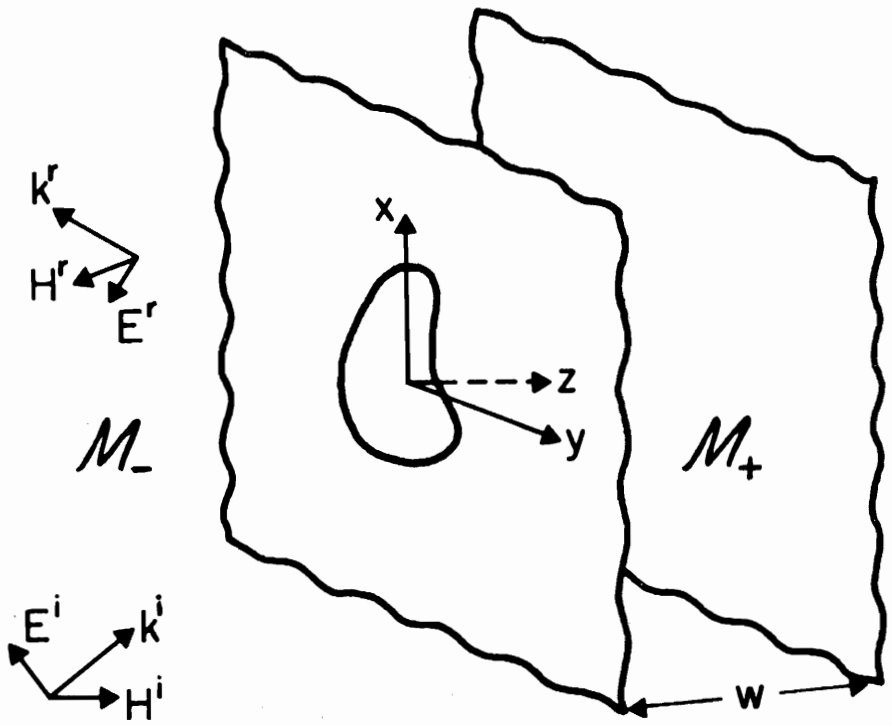

Figure 6.1. Aperture in a perfectly conducting screen with a back plate illuminated by a plane wave.

To determine $\vec{E}_-$ and $\vec{E}_+$ in Equations (6.1) and (6.2), diffracted fields $\vec{E}_-^d$ and $\vec{E}_+^d$ remain to be evaluated. This is done by employing Equations (2.10) and (2.17), which read as follows:

$$\vec{E}_{\pm}^{d} = -\iint_A \hat{n}_{\mp} \times \vec{E}^d(\vec{R}') \cdot \nabla' \times \bar{\bar{G}}_{\pm}(\vec{R}'|\vec{R})da'$$

$$\{\vec{R}:(x,y,z) \in \mathcal{M}_{\pm}\} \tag{6.3}$$

where $\bar{\bar{G}}_+(\vec{R}'|\vec{R})$ and $\bar{\bar{G}}_-(\vec{R}'|\vec{R})$ have already been defined in Equations (2.37) and (3.6), and may be rewritten as follows

$$\bar{\bar{G}}_{\pm}(\vec{R}'|\vec{R}) = \left(\bar{\bar{I}} - \frac{1}{k^2}\nabla'\nabla\right)\begin{Bmatrix} G_+ - G_- \\ g_- - g_+ \end{Bmatrix} + 2\hat{z}\hat{z}\begin{Bmatrix} G_- \\ g_- \end{Bmatrix}. \tag{6.4}$$

In Equation (6.4), the scalar functions G_+, G_-, g_-, and g_+, are those introduced in Equations (2.27), (2.28), (2.40), respectively.

As was discussed in Chapter 3, the next step requires that both the tangential E-field and the tangential H-field must be continuous in passing through the aperture. Continuity of the tangential E-field at the aperture is automatically guaranteed once Equation (6.3) is used. The continuity of the tangential H-field may be enforced by employing Equation (3.13) and noticing that the following is true

$$\lim_{z\to+0} \hat{n} \times \vec{H}_+ = \lim_{z\to-0} \hat{n} \times \vec{H}_- \iff \lim_{z\to+0} \hat{n} \cdot \vec{E}_+ = \lim_{z\to-0} \hat{n} \cdot \vec{E}_-$$

and

$$\lim_{z\to+0} \frac{\partial}{\partial z} \hat{n} \times \vec{E}_+ = \lim_{z\to-0} \frac{\partial}{\partial z} \hat{n} \times \vec{E}_- \qquad \{\vec{R}:(x,y,z) \in A\} \tag{6.5}$$

where $\hat{n}$ may be considered either as $\hat{n}_+ = \hat{z}$ or as $\hat{n}_- = -\hat{z}$. Equation (6.5) exposes the following fact, namely, continuity of the normal component of the E-field, along with continuity of the normal derivative of

the tangential E-field in the aperture, enforces continuity of the tangential H-field in the aperture A.

The desired integral equation can be constructed by substituting Equations (6.1) and (6.2) into Equation (6.5). Prior to the substitution, one first simplifies Equation (6.3) by applying the identities given in Appendix 2-A. It is then found that

$$\nabla' \times \bar{\bar{G}}_{\pm}(\vec{R}'|\vec{R}) = \nabla' \begin{Bmatrix} G_+ - G_- \\ g_- - g_+ \end{Bmatrix} \times \bar{\bar{I}} + 2\nabla' \begin{Bmatrix} G_- \\ g_- \end{Bmatrix} \times \hat{z}\hat{z}. \qquad (6.6)$$

By substituting Equation (6.6) into Equation (6.3) and using the fact that

$$G_+\Big|_{z'=0} = G_-\Big|_{z'=0}, \quad \left(\frac{\partial}{\partial z'}G_{\pm}\right)\Big|_{z'=0} = \pm\frac{\partial}{\partial z}\left(G_{\pm}\Big|_{z'=0}\right),$$

and

$$\sqrt{(x-x')^2 + (y-y')^2 + (z+2nw)^2} = |\vec{\rho} - \vec{\rho}' + (z+2nw)\hat{z}|, \qquad (6.7)$$

one finally obtains the simplified form of Equation (6.3):

$$\vec{E}^d_{\pm} = \pm 2\frac{\partial}{\partial z}\iint_A (E_x\hat{x} + E_y\hat{y})\, g_{n_0}(\vec{\rho}'|\vec{R})da'$$

$$\pm 2\hat{z}\left(\frac{\partial}{\partial x}\iint_A E_x\, g_{n_0}(\vec{\rho}|\vec{R})da' + \frac{\partial}{\partial y}\iint_A E_y\, g_{n_0}(\rho'|\vec{R})da'\right) \qquad (6.8)$$

where

$$g_n(\vec{\rho}'|\vec{R}) = G_+\Big|_{z'=0} = G_-\Big|_{z'=0} = \sum_{n\in Z}\frac{e^{-jk|\vec{\rho}-\vec{\rho}'+(z+2nw)\hat{z}|}}{4\pi|\vec{\rho}-\vec{\rho}'+(z+2nw)\hat{z}|} \qquad (6.9)$$

in which Z is the set of all positive and negative integers, including zero. Equation (6.8) is quite similar to Equation (3.14) and, in fact, E^d_- is the same in both equations. Later, Equation (6.8) will be used to compute the diffracted field in the cavity region $\mathcal{M}_+$.

Enforcing the continuity of the normal component of the E-field by simply substituting Equation (6.8) into Equation (6.5), one readily derives the equation

$$2\left\{\frac{\partial}{\partial x}\iint_{\bar{A}} E_x[g_0(\vec{\rho}'|\vec{R}) + g_n(\vec{\rho}'|\vec{R})]da' + \frac{\partial}{\partial y}\iint_{\bar{A}} E_y[g_0(\vec{\rho}'|\vec{R}) + g_n(\vec{\rho}'|\vec{R})]da'\right\}\Bigg|_{z=0} = \hat{n}_- \cdot (\vec{E}^i_- + \vec{E}^r_-)\Big|_{z=0}$$

$$\{\vec{R}:(x,y,z) \in A\} \quad . \tag{6.10}$$

Similarly, the continuity of the normal derivative of the tangential E-field results in

$$2\left\{\frac{\partial^2}{\partial z^2}\left[\iint_{\bar{A}} (E_x\hat{x} + E_y\hat{y})(g_0(\vec{\rho}'|\vec{R}) + g_n(\vec{\rho}'|\vec{R}))da'\right]\right\}\Bigg|_{z=0}$$

$$= \left\{\frac{\partial}{\partial z}[(E^i_{-x} + E^r_{-x})\hat{x} + (E^i_{-y} + E^r_{-y})\hat{y}]\right\}\Bigg|_{z=0}$$

$$\{\vec{R}:(x,y,z) \in A\} \quad . \tag{6.11}$$

Employing Equations (6.10) and (6.11), and following the steps developed in Equations (3.17)-(3.33), one finally determines the desired integral equation:

$$\iint_{\bar{A}} \begin{Bmatrix} E_x \\ E_y \end{Bmatrix} \sum_{n\in Z_+} \frac{e^{-jk|\vec{\rho}-\vec{\rho}'+(2nw)\hat{z}|}}{2\pi|\vec{\rho}-\vec{\rho}'+(2nw)\hat{z}|}\,da' = \text{Right-hand side of Equation (3.33).}$$

$$\{\vec{\rho}:(x,y) \in \bar{A}\} \tag{6.12}$$

where Z_+ denotes the set of all positive integers including zero. In deriving Equation (6.12) the following formula was used

$$[g_0(\vec{\rho}'|\vec{R}) + g_n(\vec{\rho}'|\vec{R})]\Big|_{z=0} = \sum_{n\epsilon Z_+} \frac{e^{-jk|\vec{\rho}-\vec{\rho}'+(2nw)\hat{z}|}}{2\pi|\vec{\rho}-\vec{\rho}'+(2nw)\hat{z}|} \quad . \quad (6.13)$$

As described previously, Equation (6.12) must be solved in conjunction with the condition (3.30) to provide the proper solution.

6.3 Numerical Results and Discussions

6.3.1 Matrix equation and kernel evaluation

This section will be concerned with extracting the numerical solution of the integral Equation (6.12) by applying the moment method. Because of the almost identical structure of Equations (6.12) and (3.33), the numerical procedure developed in Section 3.3 can be readily employed to determine the solution. Therefore, Equation (6.12) may be discretized in the manner demonstrated in Equation (3.42).

Since the kernel of integral equation (6.12) is more complicated than that of Equation (3.33), it should be analyzed in more detail. An analysis of the kernel shows that the singular term arises when $n = 0$ in the summation appearing in the kernel. This, as a result, allows the self-patch integration as obtained in Equation (3.43) for the singular term to be used. Since an infinite summation cannot be handled directly by the computer, it must be truncated in a manner that provides an acceptable numerical approximation to the summation (Hamming, 1973). For the infinite summation given in Equation (6.13), one first truncates the summation and then approximates the residual terms.

Truncating Equation (6.13) results in the following equation:

$$\sum_{n\epsilon Z_+} \frac{e^{-jk|\vec{\rho}-\vec{\rho}'+(2nw)\hat{z}|}}{2\pi|\vec{\rho}-\vec{\rho}'+(2nw)\hat{z}|} = \sum_{n=0}^{L} \frac{e^{-jk|\vec{\rho}-\vec{\rho}'+(2nw)\hat{z}|}}{2\pi|\vec{\rho}-\vec{\rho}'+(2nw)\hat{z}|} + R_L \quad (6.14)$$

where R_L denotes the residual term. For the index L such that

$$\frac{|\vec{\rho}-\vec{\rho}'|}{2Lw} << 1 \quad , \tag{6.15}$$

the residual term R_L may be approximated as follows

$$R_L = \sum_{n=L+1}^{\infty} \frac{e^{-jk|\vec{\rho}-\vec{\rho}'+(2nw)\hat{z}|}}{2\pi|\vec{\rho}-\vec{\rho}'+(2nw)\hat{z}|} \approx \left[\sum_{n=1}^{\infty} \frac{e^{-jk(2nw)}}{2\pi(2nw)} - \sum_{n=1}^{L} \frac{e^{-jk(2nw)}}{2\pi(2nw)}\right] . \tag{6.16}$$

Upon using the following formula (Collin, 1960)

$$\sum_{n=1}^{\infty} \frac{e^{-jnx}}{n} = -\ell n(1-e^{-jx}) = -\ell n(2 \sin \frac{x}{2}) + j \frac{\pi-x}{2} \quad , \tag{6.17}$$

$$0 < x < 2\pi$$

Equation (6.14) may finally be approximated in the following form

$$\sum_{n\varepsilon Z_+} \frac{e^{-jk|\vec{\rho}-\vec{\rho}'+(2nw)\hat{z}|}}{2\pi|\vec{\rho}-\vec{\rho}'+(2nw)\hat{z}|} \approx \sum_{n=0}^{L} \frac{e^{-jk|\vec{\rho}-\vec{\rho}'+(2nw)\hat{z}|}}{2\pi|\vec{\rho}-\vec{\rho}'+(2nw)\hat{z}|} -$$

$$\left[\sum_{n=1}^{L} \frac{e^{-jk(2nw)}}{4\pi nw} + \frac{1}{4\pi w} \ell n(1-e^{-j2kw})\right] . \tag{6.18}$$

The terms appearing in the bracket on the right-hand side of Equation (6.18) are independent of the location of observation points ($\vec{\rho}$) and source points ($\vec{\rho}'$); hence, they can be evaluated once for all the points. This approximation introduces only a small loss of accuracy but produces a substantial saving in computing time. It is further noticed that the aforementioned infinite series is not uniformly convergent and, in fact, it is divergent for the values of $w = \lambda/2, \lambda, 3\lambda/2, \ldots$. These values are related to the resonances of the two-parallel-plate structures. Numerical results have revealed that for values of $|\vec{\rho}-\vec{\rho}'|/\lambda \leq \sqrt{2}$, $w/\lambda > 2$, and slightly away from the resonant separations, L = 20 would provide an adequate approximation in Equation (6.18). The validity of using Equation (6.18) is studied in detail in Appendix F, and the interested reader is referred to this appendix.

6.3.2 Resonance solutions

Since only for the resonant values of $w = \lambda/2, \lambda, 3\lambda/2, \ldots$, does the kernel of integral equation (6.12) fail to converge, this integral equation cannot be used to determine the E-field in the aperture for the resonant values of w. Furthermore, one expects that the aperture tangential E-field must be zero at the resonant separations, because only for zero value of a tangential E-field could both the r.h.s. and l.h.s. of Equation (6.12) match.

To study the behavior of the integral equation (6.12) at resonant situations, one starts by assuming that an incident plane wave originating from $\mathcal{M}_-$ impinges on the structure as shown in Fig. 6.1. This incident field may take the following form:

$$\vec{E}^i = (\vec{E}^i_{0t} + E^i_{0z}\,\hat{z})e^{-jk(\vec{k}_t\cdot\vec{\rho}+\gamma z)} \qquad (6.19)$$

$$\{\vec{R}:(x,y,z) \in \mathcal{M}_-\}$$

where $\vec{E}^i_{0t} = \hat{x}E^i_{0x} + \hat{y}E^i_{0t}$, $\vec{k}_t = \alpha\hat{x} + \beta\hat{y}$, and α, β and γ have already been defined for Equation (3.19). Using Maxwell's equations, it is readily found that the H^i-field is

$$\vec{H}^i = \frac{1}{\eta}(\vec{k}_t + \gamma\hat{z}) \times \vec{E}^i \qquad (6.20)$$

$$\{\vec{R}:(x,y,z) \in \mathcal{M}_-\}$$

where $\eta = \sqrt{\mu/\epsilon}$ is the intrinsic impedance of the medium. The field reflected from plate I when the aperture is closed may be written as:

$$\vec{E}^r = (-\vec{E}^i_{0t} + \hat{z}E^i_{0z})e^{-jk(\vec{k}_t\cdot\vec{\rho}-\gamma z)} \qquad (6.21)$$

$$\{\vec{R}:(x,y,z) \in \mathcal{M}_-\}$$

Similarly, the reflected H^r-field takes the following form:

$$\vec{H}^r = \frac{1}{\eta} (\vec{k}_t - \gamma\hat{z}) \times \vec{E}^r \quad . \tag{6.22}$$

$$\{\vec{R}: (x,y,z) \in \mathcal{M}_-\}$$

The total field in the region $\mathcal{M}_-$ is obtained by simply adding the incident and reflected fields, namely,

$$\vec{E} = \vec{E}^i + \vec{E}^r = \left[-2j\vec{E}^i_{0t} \sin(k\gamma z) + 2E^i_{0z}\,\hat{z}\cos(k\gamma z)\right] e^{-jk|\vec{k}_t\cdot\vec{\rho}|} \quad ,$$

$$\{\vec{R}: (x,y,z) \in \mathcal{M}_-\} \tag{6.23}$$

and similarly

$$\vec{H} = \vec{H}^i + \vec{H}^r \quad . \tag{6.24}$$

It is now desirable to determine under what conditions E and H, defined in Equations (6.23) and (6.24), can be extended to the region $\mathcal{M}_+$ to provide the complete solution of the problem, both in the $\mathcal{M}_-$ and $\mathcal{M}_+$ regions. To investigate this, three different cases will be examined:

i) $kw \neq n\pi/\gamma$ where $n \in Z_+$. Extending $\vec{E}$ and $\vec{H}$ to the region $\mathcal{M}_+$, it is easily seen that Maxwell's equations and the continuity conditions will be satisfied, but the solution fails to satisfy the boundary condition (2.8) on the plate II. Therefore, Equation (6.23) does not provide the complete solution and, as indicated before, the integral Equation (6.21) must be solved to construct the complete solution of the problem.

ii) $kw = n\pi/\gamma$ where $n \in Z_+$ and $\gamma \neq 1$. Extending $\vec{E}$ and $\vec{H}$ to the region $\mathcal{M}_+$, one readily observes that Maxwell's equations, the continuity conditions and the boundary conditions are satisfied. One may first believe that this is the complete solution of this particular problem. However, careful examination reveals that this solution does not satisfy the radiation condition (2.12) in the region $\mathcal{M}_+$

along a direction parallel to the plates; hence, this construction (6.23) cannot provide the proper solution for this case. The proper solution is obtained by solving the integral equation (6.21). It is noted that for the values of $kw = n\pi/\gamma$, the kernel of the integral equation is convergent.

iii) $kw = n\pi$ where $n \in Z_+$ and $\gamma = 1$. Extending $\vec{E}$ and $\vec{H}$ to the region $\mathcal{M}_+$, one readily finds that all the Maxwell's equations, the continuity conditions, the boundary conditions and the radiation condition are satisfied in both the $\mathcal{M}_-$ and $\mathcal{M}_+$ regions. Therefore, by employing the uniqueness theorem, this will be the only possible solution of the problem, and it takes the following form:

$$\vec{E} = -2jE^i_{0t} \sin(kz) \qquad (6.25)$$

$$\{\vec{R}: (x,y,z) \in \mathcal{M}_- \cup \mathcal{M}_+\} .$$

It is further noticed that for the values of $kw = n\pi$, the kernel of the integral equation (6.21) diverges, indicating that this integral equation cannot be used to provide the solution.

In conclusion, it has been found that the complete solution of the problem could be constructed analytically (Equation 6.25) for the case of normal incidence ($\gamma = 1$) and resonant separations ($kw = n\pi$). Determination of the solution for the case $kw = n\pi$ and $\gamma \neq 1$ deserves special treatment, which has not been completed in this work.

in this work.

6.3.3 The numerical result of the E-field distribution in the aperture and in the cavity region $\mathcal{M}_+$

In this section some numerical results will be presented for the two parallel-plate structure. The numerical results for the aperture field are obtained by solving integral equation (6.2) in the manner

discussed in the previous sections. The E_+^d-field is then evaluated by performing the integration given in Equation (6.8). As an example, rectangular apertures are considered here, although the method of solution is almost the same for any aperture configuration. The basic difference is the description of a proper algorithm for enforcing the condition $\vec{E} \cdot \tau = 0$ at the rim, which is done very easily for rectangular apertures.

Figures 6.2 and 6.3 show the amplitude distribution of the E_y-field, dominant component of the induced field, along the principal axes of $.3\lambda \times .3\lambda$ and $.5\lambda \times .5\lambda$ apertures, respectively. As shown in these figures, the incident field is normal to the plates and polarized along the y-axis. These results, which have been compared with those of a single aperture (no back plate), show that away from the resonant separations - in this case, for example, $w = 2.8\lambda$ - the aperture fields are almost the same and no substantial changes could be observed. Figure 6.4 displays the behavior of the E_y-field in a rectangular aperture sampled at two different points as a function of the separation distance w/λ. Except around the resonant separation, this field varies very slowly as a function of w/λ, and does not show substantial change when compared with the case $w/\lambda = \infty$(no back plate). At resonant separation, however, the field tends very sharply towards zero, as described by Equation (6.25) (this is not shown in Figure 6.4).

After determining the aperture field, the diffracted E-field in the cavity region $\mathcal{M}_-$ may be readily computed using Equation (6.8). The results derived in this manner are plotted as curves shown in Figures 6.4 and 6.5. Figure 6.4 displays the behavior of the amplitude

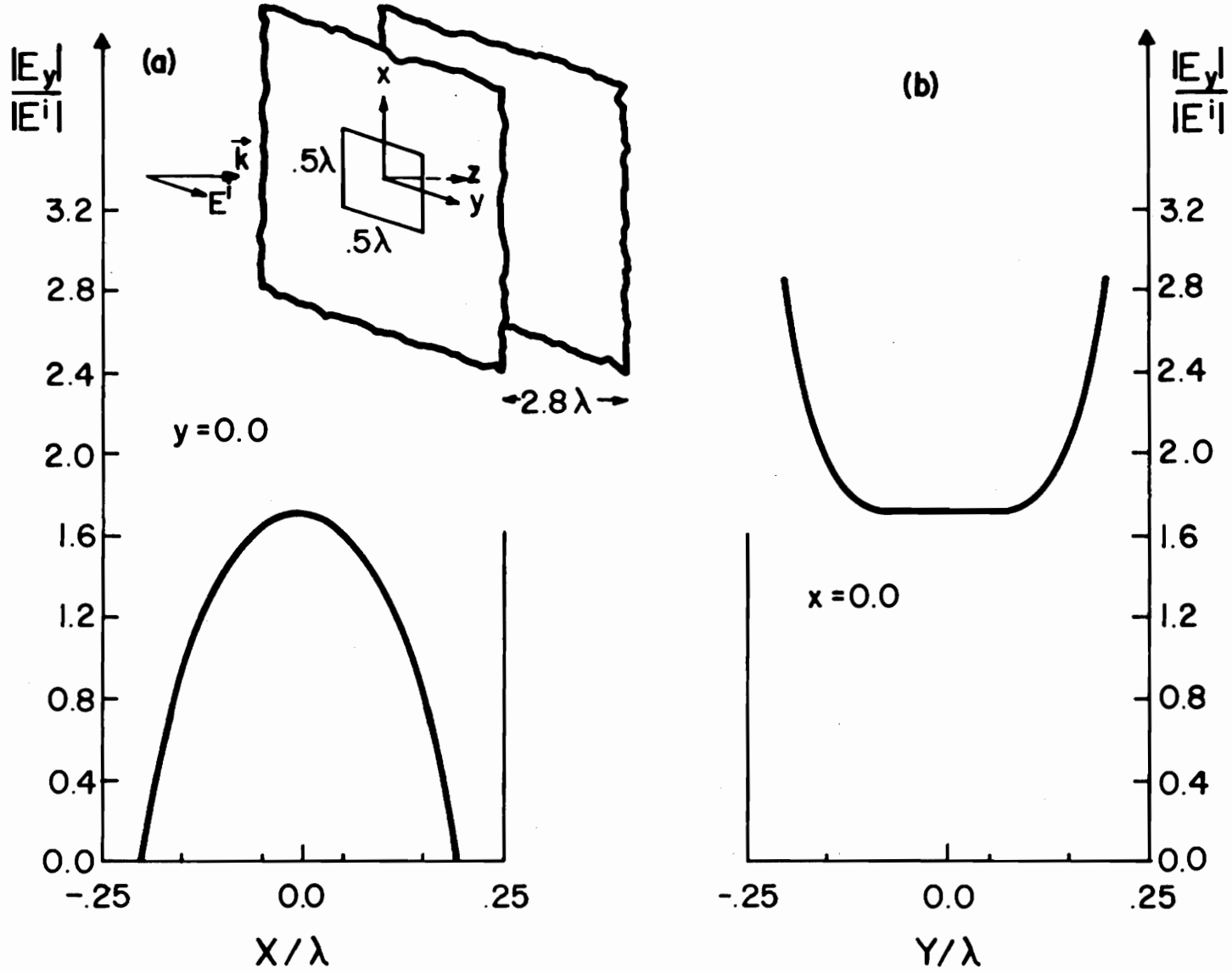

Figure 6.2. Amplitude distribution of the E_y-field in a .5λ x .5λ square aperture with back plate due to a normally incident plane wave. (a) E_y-field sampled along the x-axis. (b) E_y-field sampled along y-axis.

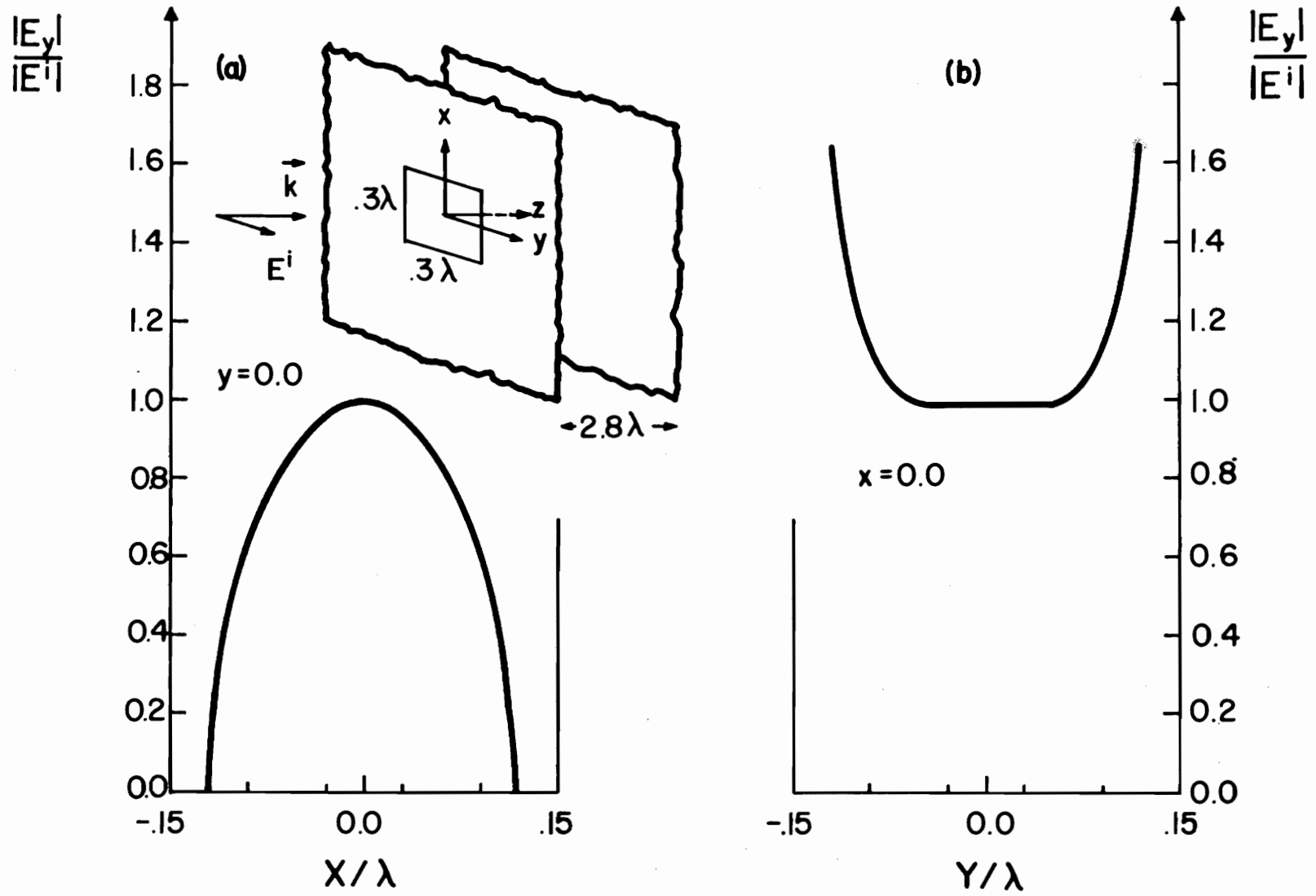

Figure 6.3. Amplitude distribution of the E_y-field in a .3λ x .3λ square aperture with back plate due to a normally incident plane wave. (a) E_y-field sampled along the x-axis. (b) E_y-field sampled along the y-axis.

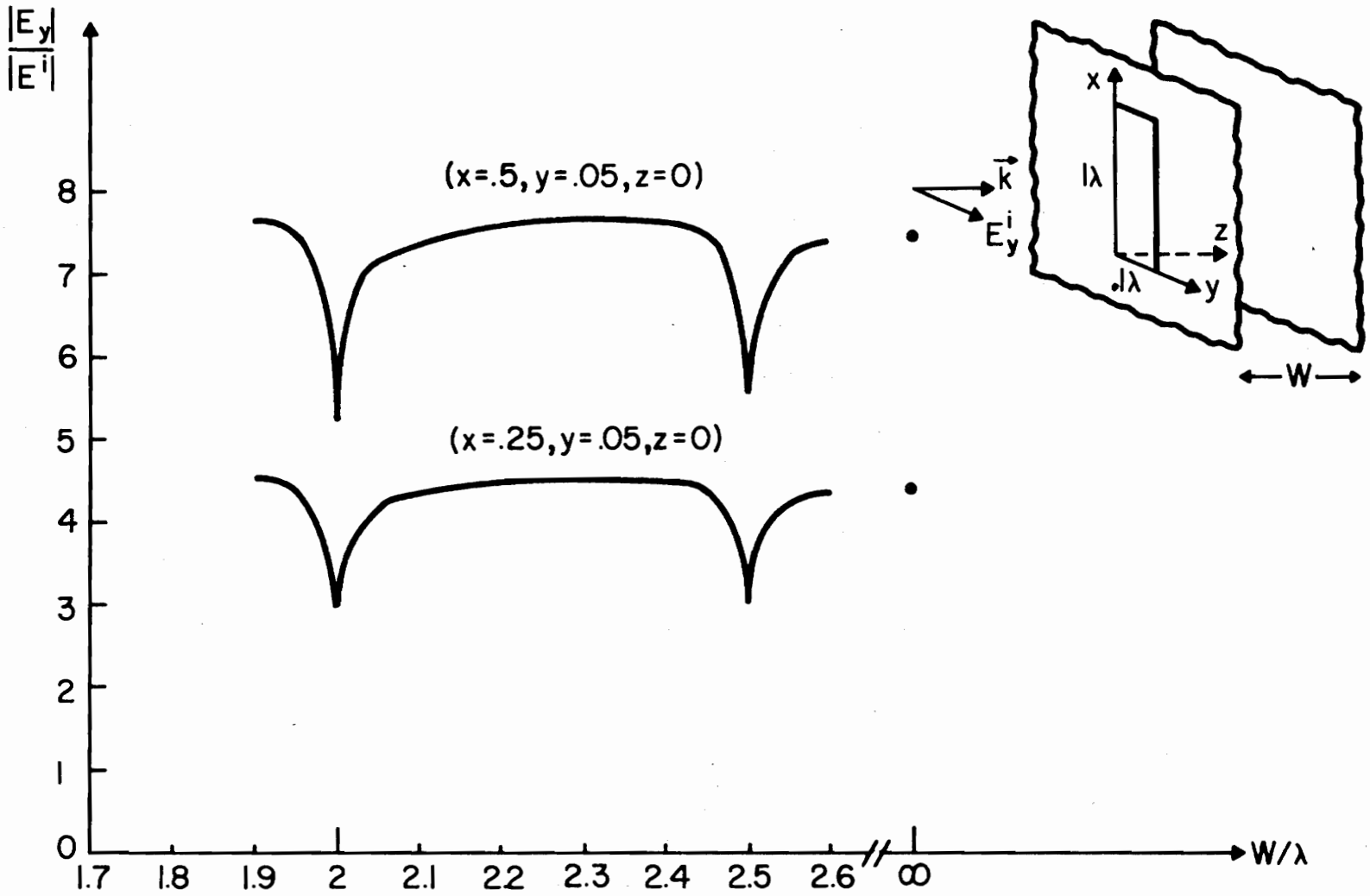

Figure 6.4. E_y-field sampled at two different points in the aperture as a function of W/λ.

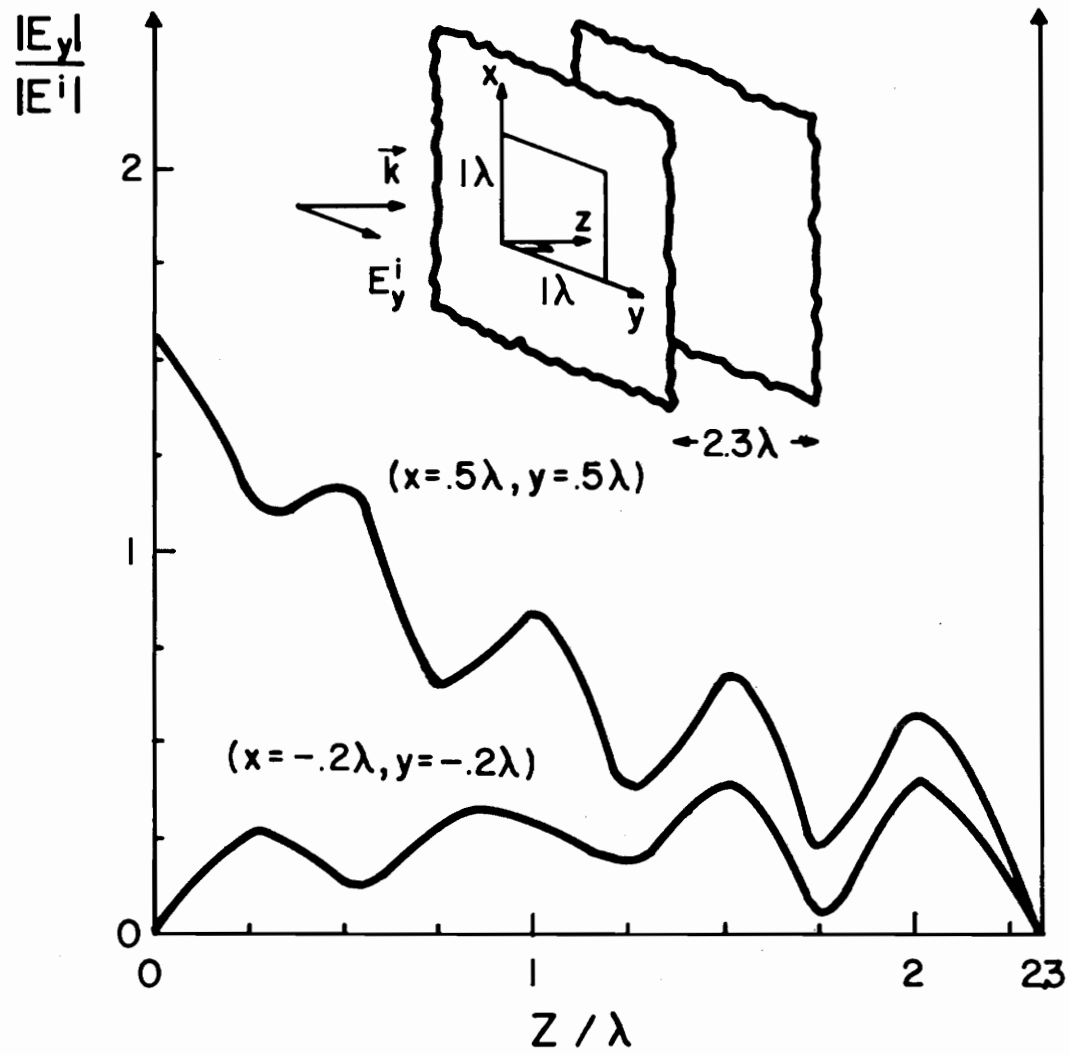

Figure 6.5. E_y-field distribution sampled along the two lines parallel to the z-axis in the two-parallel-plate region.

of the dominant component of the E-field sampled along two different lines parallel to the z-axis and Figure 6.6 shows the field coupled into the parallel-plate region via a rectangular aperture of dimension $1\lambda \times .1\lambda$ illuminated by a normally incident plane wave.

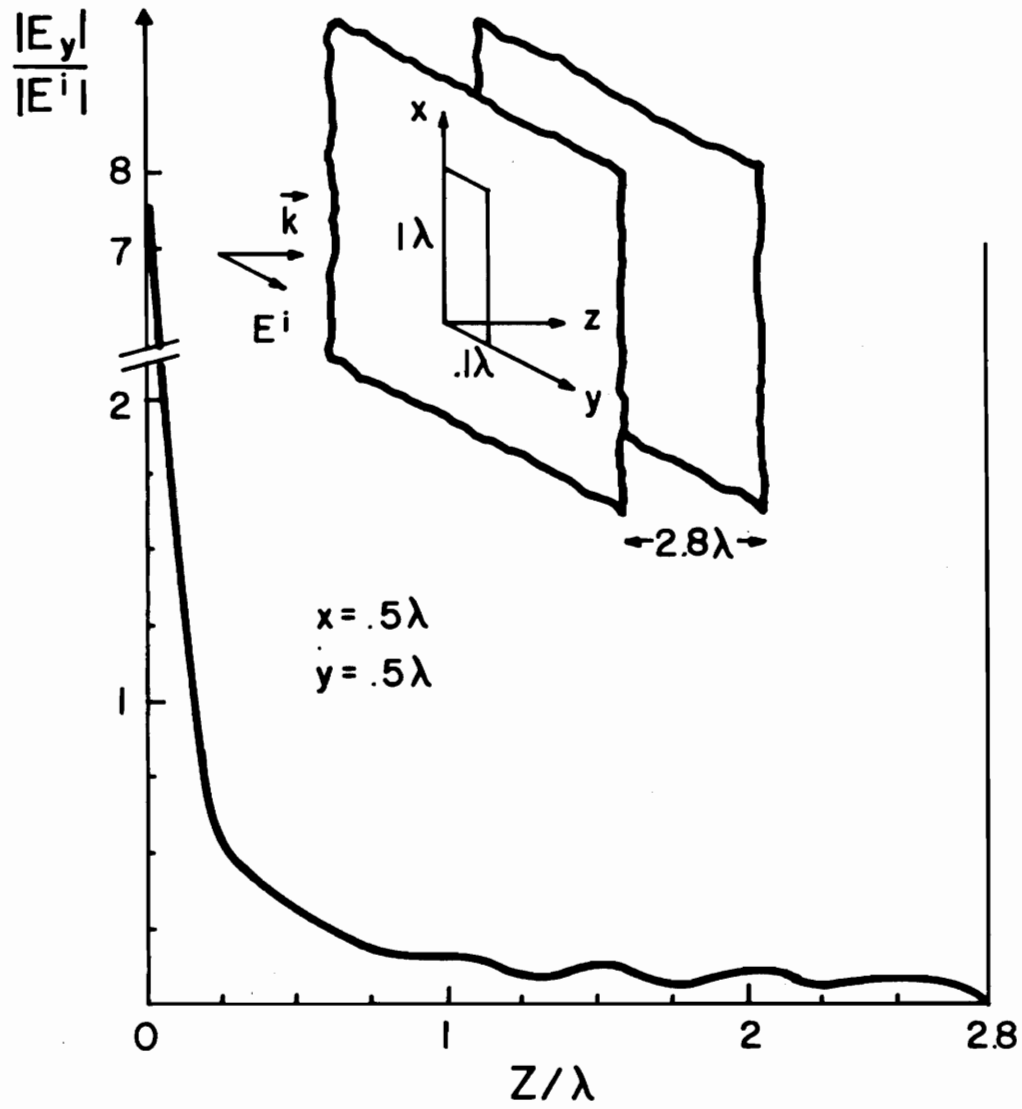

Figure 6.6. E_y-field sampled along a line parallel to the z-axis and passing through the center of the aperture in the two-parallel-plate region.

7. CONCLUSIONS AND RECOMMENDATIONS

In this investigation the problems of aperture diffraction in an infinite screen, aperture coupling into a two-parallel-plate region, and scattering by infinitely thin planar structures in intermediate and low frequency regions were investigated in a unified fashion. Based on the application of the dyadic and vector potential formalisms, a new set of integral equations was constructed to formulate the problem. These integral equations, which are structurally simple, were found suitable for numerical analysis.

The knowledge of the tangential E-field in apertures was shown to be sufficient for calculating the diffracted field in a cavity region, if the proper dyadic Green's function had been constructed. The dyadic Green's function was determined for a two-parallel-plate region and a semi-infinite space by employing the theory of images.

Considering diffraction by apertures in a perfectly conducting screen, a new set of integral equations was obtained, determining the tangential E-field in the aperture. This integral equation was constructed in a novel way by simply enforcing the continuity of the tangential derivative of the normal E-field and the normal derivative of the tangential E-field. The aforementioned continuity conditions were shown to automatically satisfy the necessary continuity condition for both tangential E- and H- fields in crossing the aperture. The structurally simple nature of the new integral equations was compared with the conventional ones. The tangential components of the aperture E-field were decoupled in new equations, making them numerically attractive. Furthermore, their kernels did not possess any differential

operator which made them less singular than conventional integral equations. The interaction of the aperture rim with the incident field was accounted for in the integral equations by introducing a set of particular homogeneous terms in the formulation. The necessity of applying the so-called edge condition was eliminated and, instead, the unique solution of the problem was determined by imposing the obvious condition that the tangential component of the E-field at the rim was zero. Numerical results were presented, supporting the validity of the formulation. Rectangular aperture results were calculated for the induced tangential E-field and diffracted field due to various incident fields and aperture dimensions. The time domain behavior of the diffracted field by a narrow aperture was also calculated using FFT algorithms. Results were compared with those obtained through application of other techniques and experimental data.

The low frequency analysis of the aperture diffraction problem was presented in a systematic fashion, employing the integral equation constructed in this thesis. These equations were found quite suitable, considering the low frequency regions, and the problem was reduced to solving a sequence of successive integral equations which possess an electrostatic-type kernel. The first few terms of the Rayleigh series expansion were determined analytically for a circular aperture illuminated by an obliquely incident plane wave. The incompleteness of Bethe's and Copson's solutions were pointed out. Results were compared with those obtained by others and perfect agreement was observed. Furthermore, the low frequency results of rectangular apertures were computed and their similarities with those of circular apertures were shown.

The problems of scattering of electromagnetic waves by infinitely

thin and perfectly conducting planar scatterers were investigated in great detail. Using the vector potential formulation, a new set of integral equations was constructed determining the induced current in the structure. The expected similarity, due to Babinet's principle, among these integral equations and those obtained for the aperture problem was discussed. The integral equations were further simplified to compute the induced current in an infinitely long strip, and their similarities with that of the well-known Hallen's integral equation were demonstrated. The method of moments was used as a basic technique of digitizing the integral equations for numerical solution. Results were presented for the induced current distribution and RCS computation of rectangular scatterers. These results were finally compared with those obtained using GTO, PO, and variational methods.

The problem of electromagnetic coupling by an aperture into a two-parallel-plate region was investigated. To obtain a complete set of integral equations for determining the tangential E-field in the aperture, the dyadic formulations were used. It was found that these integral equations could have been considered as a generalized version of those obtained for apertures in an infinite screen. The complex nature of the kernel of the integral equation around the resonant separation of the two plates was analyzed. It was found that, for some special cases, an analytical solution could be constructed for determining the induced field inside the two-parallel-plate region. Numerical results were presented for the induced field in the aperture and inside the parallel-plate region as functions of aperture dimensions and parallel-plate separations.

Some comments about the possible future investigations branching from this study would be of interest. In this thesis the numerical calculation

has been merely done by applying the step function as the basis function and determining the numerical solution of the integral equations for rectangular-shaped structures. It would be of interest to use higher-order basis functions particularly to investigate their effect in computing the field or current components at the rim of the structure. Application of the integral equations obtained in this thesis for analyzing more complicated shape structures would be worthwhile. Furthermore, an investigation on the numerical stability of the integral equations for large structures (with characteristic dimensions larger than one wavelength) would be significant.

APPENDIX A

DYADIC GREEN'S THEOREM

In this appendix a proof is given for the construction of the dyadic Green's theorem. Some identities which are used very often in the dyadic operational analysis are also listed in this appendix.

The starting point for the construction of the dyadic Green's theorem is to employ the Gauss theorem. This theorem states that for any vector function $\vec{F}$ with continuous first derivatives throughout a volume V and over the enclosing surface ∂V, the following relation holds

$$\iiint_V \nabla \cdot \vec{F} \, d\nu \quad \iint_{\partial V} \vec{F} \cdot \hat{n} \, da \tag{A.1}$$

where n is the outward unit normal. By letting

$$\vec{F} = \vec{Q} \times \nabla \times \vec{P} - \vec{P} \times \nabla \times \vec{Q} \quad , \tag{A.2}$$

and substituting it into relation (A.1), one easily obtains the following equation which is known as vector Green's theorem

$$\iiint_V (\vec{P} \cdot \nabla \times \nabla \times \vec{Q} - \vec{Q} \cdot \nabla \times \nabla \times \vec{P}) \, d\nu = \iint_{\partial V} (\vec{Q} \times \nabla \times \vec{P} - \vec{P} \times \nabla \times \vec{Q}) \cdot \hat{n} \, da. \tag{A.3}$$

Let $\bar{\bar{Q}}$ by a dyadic function with a necessary differentiability property, and let $\vec{a}$ be an arbitrary constant vector. One can then define the vector $\vec{Q}$ to be

$$\vec{Q} = \bar{\bar{Q}} \cdot \vec{a} \, . \tag{A.4}$$

Substituting (A.4) into (A.3) and using the identities listed at the end of this appendix, one arrives at

$$\iiint_V (\vec{P} \cdot \nabla \times \nabla \times \bar{\bar{Q}} \cdot \vec{a} - \nabla \times \nabla \times \vec{P} \cdot \bar{\bar{Q}} \cdot \vec{a}) \, d\nu$$

$$= -\iint_{\partial V} [(\hat{n} \times \nabla \times \vec{P}) \cdot \bar{\bar{Q}} \cdot \vec{a} + (\vec{n} \times \vec{P}) \cdot \nabla \times \bar{\bar{Q}} \cdot \vec{a}] \, da \, . \tag{A.5}$$

Since the above relation holds for any vector $\vec{a}$, one concludes that

$$\iiint_V (\vec{P} \cdot \nabla \times \nabla \times \bar{\bar{Q}} - \nabla \times \nabla \times \vec{P} \cdot \bar{\bar{Q}}) \, dv$$

$$= -\iint_{\partial V} [(\hat{n} \times \nabla \times \vec{P}) \cdot \bar{\bar{Q}} + (\hat{n} \times \vec{P}) \cdot \nabla \times \bar{\bar{Q}}] \, da$$

$$= -\iint_{\partial V} \hat{n} \cdot [\nabla \times \vec{P} \times \bar{\bar{Q}} - \vec{P} \times \nabla \times \bar{\bar{Q}}] \, da \, . \qquad (A.6)$$

The above equation is known as the dyadic Green's theorem (Tai, 1971).

Some useful relations in dyadic analysis are listed below (Van Bladel, 1964):

(1) $(\vec{a} \cdot \bar{\bar{Q}}) \cdot \vec{b} = \vec{a} \cdot (\bar{\bar{Q}} \cdot \vec{b}) = \vec{a} \cdot \bar{\bar{Q}} \cdot \vec{b}$

(2) $(\vec{a} \times \vec{b}) \cdot \bar{\bar{Q}} = \vec{a} \cdot (\vec{b} \times \bar{\bar{Q}}) = -\vec{b} \cdot (\vec{a} \times \bar{\bar{Q}})$

(3) $(\vec{a} \cdot Q) \times \vec{b} = \vec{a} \cdot (\bar{\bar{Q}} \times \vec{b}) = \vec{a} \cdot \bar{\bar{Q}} \times \vec{b}$

(4) $(\vec{a} \times \bar{\bar{Q}}) \times \vec{b} = \vec{a} \times (\bar{\bar{Q}} \times \vec{b}) = \vec{a} \times \bar{\bar{Q}} \times \vec{b}$

(5) $\vec{a} \cdot \bar{\bar{Q}} \cdot \vec{b} = \vec{b} \cdot \bar{\bar{Q}}^T \cdot \vec{a}$

(6) $\nabla(\vec{a} \cdot \vec{b}) = (\vec{A} \cdot \nabla) \vec{b} + (\vec{b} \cdot \nabla) \vec{a} + \vec{a} \times \nabla \times \vec{b} + \vec{b} \times \nabla \times \vec{a}$

(7) $\nabla \cdot \nabla \times \bar{\bar{Q}} = 0$

(8) $\nabla \times \nabla \vec{a} = 0$

(9) $\nabla \cdot (\phi \bar{\bar{Q}}) = \nabla\phi \cdot \bar{\bar{Q}} + \phi \nabla \cdot \bar{\bar{Q}}$

(10) $\nabla \times (\phi \bar{\bar{Q}}) = \nabla\phi \times \bar{\bar{Q}} + \phi \nabla \times \bar{\bar{Q}}$

where in the above equations ϕ , $\vec{a}$ and $\bar{\bar{Q}}$ are differentiable scalar function, differentiable vector function, and differentiable dyadic function, respectively.

APPENDIX B

LIMITING PROCEDURE FOR INTEGRALS

In this appendix, the limit of a singular integral, which was presented in Chapter 3, is discussed. It is shown that the limit must be defined with great care if the correct answer is to result.

The singular integral to be considered in this appendix has the following form

$$\vec{S}(\vec{R}) = 2\,\hat{z} \times \nabla \times \iint_{\bar{A}} (\vec{E}(\vec{\rho}') \times \hat{z})\, g_0\,(\vec{\rho}'|\vec{R})\, da' \quad . \tag{B.1}$$

Clearly, this integral has a singular behavior at point $\vec{\rho}' = \vec{R}$. It is expected that the limit of $\vec{S}$ as $z \to 0$ approaches $-\hat{z} \times \vec{E}(\vec{\rho})$. To show this, one needs only consider the x-component, which reads

$$S_x(\vec{R}) = -2 \frac{\partial}{\partial z} \iint_{\bar{A}} E_y(\vec{\rho}')\, g_0\,(\vec{\rho}'|\vec{R})\, da' \quad . \tag{B.2}$$

In order to exclude the region of singularity, $\bar{A}$ is decomposed into two regions as follows

$$\bar{A} = (\bar{A} - A_\Delta) \cup A_\Delta \tag{B.3}$$

where A_Δ is a circular region centered at $\vec{\rho}$ with radius Δ. Using (A.3), the limit of S_x may be expressed as

$$\lim_{z\to 0} S_x(\vec{R}) = S_x(\vec{\rho}) = -2 \iint_{\bar{A}-A_\Delta} E_y(\vec{\rho}') \frac{\partial}{\partial z}\, g\,(\vec{\rho}'|\vec{R})\Big|_{z=0} da'$$

$$- \lim_{z\to 0} 2 \frac{\partial}{\partial z} \iint_{A_\Delta} E_y(\vec{\rho}')\, g_0\,(\vec{\rho}'|\vec{R})\, da' \quad . \tag{B.4}$$

It can be readily verified that

$$\frac{\partial}{\partial z} g_0(\vec{\rho}'|\vec{R})\Big|_{z=0} = \frac{\partial}{\partial z} \frac{e^{-jk\sqrt{(x-x')+(y-y')^2+z^2}}}{4\pi\sqrt{(x-x')^2+(y-y')^2+z^2}}\Bigg|_{z=0} = 0, \quad \rho' \notin A_\Delta \quad . \tag{B.5}$$

Therefore, the determination of S_x will be completed if the second term in the right-hand side of (B.4) is determined. To simplify the computational procedure, the origin is shifted to the point $\vec{\rho}$ and S_x is written as

$$S_x(0) = -\lim_{\Delta\to 0}\lim_{z\to 0} 2\frac{\partial}{\partial z}\iint_{A_\Delta} E_y(\vec{\rho}')g_0(\vec{\rho}'|\vec{R})\,da' =$$

$$-\lim_{\Delta\to 0}\lim_{z\to 0} 2\frac{\partial}{\partial z}\int_0^\Delta\int_0^{2\pi} E_y(0)\frac{e^{-jk\sqrt{\rho'^2+z^2}}}{4\pi\sqrt{\rho'^2+z^2}}\,\rho'd\rho'd\phi' \quad . \tag{B.6}$$

In constructing the above equation, it is assumed that E_y is regular in region A. Further simplification of (B.6) provides the following desirable result:

$$S_x(0) = -E_y(0)\lim_{\Delta\to 0}\lim_{z\to 0}\frac{\partial}{\partial z}\int_0^\Delta \left[1-jk\sqrt{\rho'^2+z^2}+k^2(\rho'^2+z^2)+\right.$$

$$\left.\ldots\right]\frac{\rho'}{\sqrt{\rho'^2+z^2}}\,d\rho' = -E_y(0)\lim_{\Delta\to 0}\lim_{z\to 0}\frac{\partial}{\partial z}\int_0^\Delta \frac{\rho'}{\sqrt{\rho'^2+z^2}}\,d\rho'$$

$$= -E_y(0)\lim_{\Delta\to 0}\lim_{z\to 0}\frac{\partial}{\partial z}\sqrt{\Delta^2+z^2}-z = E_y(0) \quad . \tag{B.7}$$

An important consideration is that

$$\lim_{\Delta\to 0}\lim_{z\to 0}\frac{\partial}{\partial z}\int_0^\Delta \frac{\rho'}{\sqrt{\rho'^2+z^2}}\,d\rho' = \lim_{\Delta\to 0}\lim_{z\to 0}\int_0^\Delta \frac{\partial}{\partial z}\frac{\rho'}{\sqrt{\rho'^2+z^2}}\,d\rho'$$

$$\neq \lim_{\Delta\to 0}\int_0^\Delta \lim_{z\to 0}\frac{\partial}{\partial z}\frac{\rho'}{\sqrt{\rho'^2+z^2}}\,d\rho' = 0 \quad . \tag{B.8}$$

Therefore, it has been found that the "$\lim_{\Delta\to 0} \lim_{z\to 0} \int$" procedure must be followed to obtain the correct result. The reader is referred to the work of Mikhlin (1957) and Davis (1974), who have considered different types of singular integrals.

APPENDIX C

SELF-PATCH INTEGRATION

In this appendix the computational procedure of the self-patch integration is summarized. The self-patch integral has the following form:

$$I_S = k \int_{-\Delta x/2}^{\Delta x/2} \int_{-\Delta y/2}^{\Delta y/2} \frac{e^{-jk\sqrt{x'^2+y'^2}}}{2\pi\sqrt{x'^2+y'^2}}\, dx'dy' \qquad (C.1)$$

where x and y are the dimensions of the rectangular patch over which the integration is performed. Using the symmetry of the kernel with respect to the origin and performing the integration in polar coordinates, (C.1) may be written as:

$$I_S = 4k \left\{ \int_0^{\alpha} \int_0^{\Delta x/2\cos\phi'} \frac{e^{-jk\rho'}}{2\pi\rho'}\, \rho'\, d\rho'\, d\phi' + \int_{\alpha}^{\pi/2} \int_0^{\Delta y/2\sin\phi'} \frac{e^{-jk\rho'}}{2\pi\rho'}\, \rho'\, d\rho'\, d\phi' \right\} \qquad (C.2)$$

where $\alpha = \tan^{-1} \Delta y/\Delta x$.

To approximate the integration given in (C.2), one expands $e^{-jk\rho'}$ in terms of the Taylor series and integrates the result as shown below

$$I_S \approx \frac{2k}{\pi} \left\{ \int_0^{\alpha} \left[\frac{\Delta x}{2\cos\phi'} - \frac{jk}{2} \left(\frac{\Delta x}{2\cos\phi'}\right)^2 - \frac{k^2}{3} \left(\frac{\Delta x}{2\cos\phi'}\right)^3 + \ldots \right] d\phi' \right.$$

$$\left. + \int_{\alpha}^{\pi/2} \left[\frac{\Delta y}{2\sin\phi'} - \frac{jk}{2} \left(\frac{\Delta y}{2\sin\phi'}\right)^2 - \frac{k^2}{3} \left(\frac{\Delta y}{2\sin\phi'}\right)^3 + \ldots \right] d\phi' \right\}. \qquad (C.3)$$

Finally the above equation may be simplified (Dwight, 1965), resulting in the following equation:

$$I_S \approx \frac{1}{\pi}\left\{k\Delta x \ell n\left|\tan\left(\frac{\pi}{4}+\frac{1}{2}\tan^{-1}\frac{\Delta y}{\Delta x}\right)\right| + k\Delta y \ell n\left|\tan\left(\frac{\pi}{4}+\frac{1}{2}\tan^{-1}\frac{\Delta x}{\Delta y}\right)\right| - \frac{-jk^2\Delta x\Delta y}{2}\right\} - \frac{1}{\pi}\left\{\frac{k^3\Delta x^3}{12}\left[\frac{\Delta y\sqrt{\Delta x^2+\Delta y^2}}{2\Delta x^2} + \frac{1}{2}\ell n\left|\tan\left(\frac{\pi}{4}+\frac{1}{2}\tan^{-1}\frac{\Delta y}{\Delta x}\right)\right|\right] + \frac{k^3\Delta y^3}{12}\left[\frac{\Delta x\sqrt{\Delta x^2+\Delta y^2}}{2\Delta y^2} + \frac{1}{2}\ell n\left|\tan\left(\frac{\pi}{4}+\frac{1}{2}\tan^{-1}\frac{\Delta x}{\Delta y}\right)\right|\right]\right\} . \quad (C.4)$$

For the case of a square patch, i.e., $\Delta x = \Delta y$, the following is true

$$\ell n\left|\tan\left(\frac{\pi}{4}+\frac{1}{2}\tan^{-1}\frac{\Delta x}{\Delta y}\right)\right| = \ell n(1+\sqrt{2}) . \quad (C.5)$$

APPENDIX D

SOLUTION OF AN INTEGRAL EQUATION WITH ELECTROSTATIC-TYPE KERNEL

In this appendix two methods are discussed for deriving the solution of the integral equation

$$\iint_{\bar{A}} \frac{\sigma}{2\pi|\vec{\rho}-\vec{\rho}'|}\, da' = e^{jn\phi} f(\rho) \quad , \tag{D.1}$$

where $\bar{A}$ is a circular region with radius a. The discussion is mainly based on the analysis done by Sneddon (1957).

The first method to be considered here is the dual integral equation technique, which can be constructed beginning with the Laplace equation in polar coordinates

$$\frac{1}{\rho}\frac{\partial}{\partial\rho}\left(\rho\frac{\partial\psi}{\partial\rho}\right) + \frac{\partial^2\psi}{\partial z^2} + \frac{1}{\rho^2}\frac{\partial^2\psi}{\partial\phi^2} = 0 \quad , \tag{D.2}$$

subject to the following mixed boundary conditions

$$\psi = e^{jn\phi} f(\rho) \qquad \text{on } z = 0,\ 0 \leq \rho \leq a \tag{D.3}$$

and

$$\frac{\partial\psi}{\partial z} = 0 \qquad \text{on } z = 0,\ a < \rho \ . \tag{D.4}$$

A general solution of Equation (D.2) can readily be constructed by applying the method of separation of variables. This solution takes the following form:

$$\psi = e^{jn\phi} \int_0^\infty S(\xi)\, e^{-\xi|z|}\, J_n(\rho\xi)\, d\xi \tag{D.5}$$

where J_n is the nth order Bessel function and $S(\xi)$ is an unknown function determined below. Imposing the mixed boundary conditions (D.3) and (D.4), one arrives at the dual integral equations

$$\int_0^\infty S(\xi)\, J_n(\rho\xi)\, d\xi = f(\rho)\ , \quad 0 \leq \rho \leq a \tag{D.6}$$

$$\int_0^\infty \xi\, S(\xi)\, J_n(\rho\xi)\, d\xi = 0\ .\ a < \rho\ . \tag{D.7}$$

General techniques for solving the above equations have been suggested by Titchmarsh (1937), Mittra (1961) and others. Sneddon (1957) used Titchmarsh's solution and gave the following expression as a general solution of the dual integral equations (D.6) and (D.7):

$$S(\xi) = \sqrt{\frac{2}{\pi}} \left[\xi^{1/2}\, J_{n-1/2}(\xi) \int_0^a \frac{\eta^{n+1} f(\eta)}{\sqrt{a^2 - \eta^2}}\, d\eta + \int_0^a \frac{\zeta^{n+1}}{\sqrt{a^2 - \zeta^2}}\, d\zeta \right.$$

$$\left. \int_0^a (\xi\eta)^{3/2}\, f(\eta\zeta)\, J_{n+1/2}(\xi\eta)\, d\eta \right] \ . \tag{D.8}$$

Obtaining ψ from Equation (D.5), the unknown σ, defined in (D.1), may then be determined as follows:

$$\sigma = -\frac{1}{2} \left[\left.\frac{\partial \psi}{\partial z}\right|_{z=+0} - \left.\frac{\partial \psi}{\partial z}\right|_{z=-0} \right] \ . \tag{D.9}$$

It is important to mention that σ may be interpreted as the charge distribution on an electrified disk with potential distribution $e^{jn\phi}\, f(\rho)$. Substituting (D.5) into (D.9) and simplifying the result, the following equation is obtained:

$$\sigma(\rho, \phi) = e^{jn\phi} \int_0^\infty \xi S(\xi)\, J_n(\rho\xi)\, d\xi \ . \tag{D.10}$$

As an example, the following special case is considered:

$$\iint_{\overline{A}} \frac{\sigma}{2\pi |\vec{\rho} - \vec{\rho}'|}\, da' = \rho^n\, e^{jn\phi} \ .$$

Substituting $f(\rho) = \rho^n$ into (D.8) and simplifying the integrals by using the integral table of Magnus (1954), σ is then determined to be

$$\sigma = \frac{2}{\sqrt{\pi}} \frac{\Gamma(n+1)}{\Gamma(n+1/2)} (a^2-\rho^2)^{-1/2} \rho^n \qquad (D.12)$$

where Γ is the Gamma function.

The second method to be discussed in this appendix is based on applying Copson's formula (Sneddon, 1957). The functional representation of the solution of (D.1) using Copson's formula takes a simpler form than the result obtained by using (D.8). Employing Copson's formula, the solution of Equation (D.1) is determined to be

$$\sigma = -\frac{2}{\pi} e^{jn\phi} \rho^{n-1} \frac{d}{d\rho} \int_\rho^a \left[\frac{1}{\xi^{2n-1}\sqrt{\xi^2-\rho^2}} \frac{d}{d\xi} \int_0^\xi \frac{\eta^{n+1} f(\eta)}{\sqrt{\rho^2-\eta^2}} d\eta \right] d\xi \ . \qquad (D.13)$$

As an example, the following special case is considered

$$\iint_A \frac{\sigma}{2\pi|\vec{\rho}-\vec{\rho}'|} da' = e^{j\phi} \rho^3 \ .$$

Upon substituting $f(\rho) = \rho^3$ and $n = 1$ into (D.13) and evaluating the integrals by using the integral table of Dwight (1965), σ is determined as follows:

$$\sigma = \frac{16}{3\pi} [3\rho(a^2 - \rho^2)^{1/2} - \rho^3(a^2 - \rho^2)^{-1/2}] e^{j\phi} \ .$$

APPENDIX E

GREEN'S FUNCTION OF THE OPERATOR $\frac{d^2}{dx^2} + k^2$

In this appendix the validity of equation

$$\left(\frac{d^2}{dx^2} + k^2\right) \frac{e^{-jk|x-x'|}}{2jk} = -\delta(x-x') \tag{E.1}$$

will be presented via application of some simple properties of the generalized functions (Arsac, 1966).

One can readily verify that the following is true

$$\frac{d}{dx} e^{-jk|x-x'|} = -jke^{-jk|x-x'|} \frac{d}{dx}(|x-x'|)$$

$$= -jk[\theta(x-x') - \theta(x'-x)] \cdot e^{-jk|x-x'|} \tag{E.2}$$

where θ symbolizes the unit step function, i.e.,

$$\theta(x) = \begin{cases} 1 & x > 0 \\ 0 & x < 0 \end{cases} \tag{E.3}$$

Evaluating the derivative of (E.2) results in

$$\frac{d^2}{dx^2} e^{-jk|x-x'|} = [-2jk\delta(x-x') - k^2]\, e^{-jk|x-x'|}. \tag{E.4}$$

In deriving the above equation the following formulas have been used

$$\frac{\partial}{\partial x}\theta(x) = \delta(x) \tag{E.5}$$

and

$$[\theta(x-x') - \theta(x'-x)][\theta(x-x') - \theta(x'-x)] = 1 . \tag{E.6}$$

The validity of (E.1) can now be confirmed by simply substituting (E.2) into the left-hand side of (E.1).

APPENDIX F

CONVERGENCE TEST FOR THE KERNEL OF INTEGRAL EQUATION (6.12)

This appendix is concerned with the numerical behavior of the kernel of integral equation (6.12). Extensive numerical results will demonstrate the behavior of this kernel close to the resonant situations. The validity of applying the approximated Equation (6.18) will also be tested.

The kernel of the integral equation (6.12) may be denoted by $S(\infty)$, such that $S(N)$ is defined as follows:

$$S(N) = \sum_{n=0}^{N} \frac{e^{-jk|\vec{\rho}-\vec{\rho}' + (2nw)\hat{z}|}}{2\pi k|\vec{\rho}-\vec{\rho}' + (2nw)\hat{z}|} \qquad (F.1)$$

As was discussed in Chapter 6, $S(\infty)$ diverges for the values of $w/\lambda = 1/2$, 1, 3/2,..., and converges otherwise. Actually, it can be readily shown that only the real part of $S(\infty)$ diverges and its imaginary part is always convergent.

The behavior of $S(N)$ has been tested for several values of N and different values of w/λ. Throughout the calculation, the value $|\vec{\rho}-\vec{\rho}'|/\lambda = \sqrt{2}$ has been chosen, which is the maximum separation that may exist between the source points and observation points for $1\lambda \times 1\lambda$ aperture. The results of calculating $S(N)$ for different values of N and w/λ are listed in Table F.1. In this table, the numerical values of $S(N)$, for values of w/λ very close to the resonant separation $w/\lambda = 2$, are displayed. The values show that $S(N)$ converges more slowly by getting closer to the resonant separation $w/\lambda = 2$; and exactly at this separation, the series shows a diverging behavior. This result also indicates how close one may actually get to the resonant separations before the

TABLE F-1

KERNEL EVALUATION

$$S(N) = \sum_{n=0}^{N} e^{-jk\left|\vec{\rho}-\vec{\rho}'+(2nw)\hat{z}\right|} \;/\; 2\pi k\left|\vec{\rho}-\vec{\rho}'+(2nw)\hat{z}\right|$$

N / w/λ	20	100	1000	10000
.5	-.2085(-2)*	.3759(-1)	.9577(-1)	.1541(0)
	-j.3422(-1)	-j.4035(-1)	-j.4177(-1)	-j.4192(-1)
.6	.3853(-2)	.3304(-2)	.3203(-2)	.3193(-2)
	+j.1169(-1)	+j.1125(-1)	+j.1112(-1)	+j.1111(-1)
.7	-.7443(-3)	-.1114(-2)	-.1197(-2)	-.1205(-2)
	-j.1451(-1)	-.1453(-1)	-.1456(-1)	-j.1456(-1)
.8	-.1154(-1)	-.1181(-1)	-.1188(-1)	-.1189(-1)
	-j.1814(-1)	-j.1797(-1)	-j.1795(-1)	-j.1794(-1)
.9	-.1684(-1)	-.1702(-1)	-.1707(-1)	-.1708(-1)
	-j.1613(-1)	-j.1571(-1)	-j.1562(-1)	-j.1561(-1)
1.	-.2893(-2)	.1716(-1)	.4627(-1)	.7542(-1)
	-j.3069(-1)	-.3223(-1)	-j.3259(-1)	-j.3263(-1)
1.95	-.1067(-1)	-.1072(-1)	-.1075(-1)	-.1075(-1)
	-j.1094(-1)	-j.1054(-1)	-j.1045(-1)	-j.1044(-1)
1.96	-.1083(-1)	-.1040(-1)	-.1042 (-1)	-.1043(-1)
	-j.1015(-1)	-j.1075(-1)	-j.1064(-1)	-j.1063(-1)
1.97	-.9102(-2)	-.9847(-2)	-.9869(-2)	-.9872(-2)
	-j.1105(-1)	-j.1096(-1)	-j.1081(-1)	-j.1079(-1)
1.98	-.9987(-2)	-.8813(-2)	-.8827(-2)	-.8830(-2)
	-j.1118(-1)	-j.1120(-1)	-j.1098(-1)	-j.1095(-1)
1.99	-.4694(-2)	-.6433(-2)	-.6416(-2)	-.6418(-2)
	-j.9797(-2)	-j.1150(-1)	-j.1115(-1)	-j.1110(-1)

* (-2) means 10^{-2}

TABLE F-1 (CONTINUED)

1.999	.8456(-4) -j.1924(-1)	.8072(-2) -j.1387(-1)	.5303(-2) -j.1172(-1)	.5340(-2) -j.1127(-1)
1.9999	- .1639(-3) -j.2055(-1)	.9889(-2) -j.2030(-1)	.2215(-1) -j.1389(-1)	.1935(-1) -j.1173(-1)
2.	-.2018(-3) -2069(-1)	.9855(-2) -j.2108(-1)	.2441(-1) -j.2117(-1)	.3897(-1) -j.2118(-1)
2.01	-.1124(-1) -j.2900(-1)	-.1282(-1) -j.2696(-1)	-.1281(-1) -j.2741(-1)	-.1282(-1) -j.2745(-1)
2.02	-.1927(-1) -j.2383(-1)	-.1813(-1) -j.2397(-1)	-.1815(-1) -j.2420(-1)	-.1816(-1) -j.2422(-1)
2.03	-.2013(-1 -j.2123(-1)	-.2089(-1) -j.2120(-1)	-.2091(-1) -j.2135(-1)	-.2092(-1) -j.2137(-1)
2.04	-.2293(-1) -j.1923(-1)	-.2244(-1) -j.1874(-1)	-.2247(-1) -j.1885(-1)	-.2247(-1) -j.1886(-1)
2.05	-.2317(-1) -j.1620(-1)	-.2329(-1) -j.1656(-1)	-.2332(-1) -j.1665(-1)	.2332(-1) -.1666(-1)
2.1	-.2277(-1) -j.9094(-2)	-.2290(-1) -j.9249(-2)	-.2293(-1) -j.9286(-2)	-.2293(-1) -j.9290(-2)
2.2	-.1730(-1) -j.4944(-2)	-.1741(-1) -.4972(-2)	-.1744(-1) -j.4980(12)	-.1744(-1) -j.4981(-2)
2.3	-.1362(-1) -j.6012(-2)	-.1372(-1) -j.5968(-2)	-.1374(-1) -j.5960(-2)	-.1375(-1) -j.5959(-2)
2.4	-.1187(-1) -j.8189(-2)	-.1197(-1) -.8037(-2)	-.1199(-1) -j.8004(-2)	-.1150(-1) -j.8001(-2)
2.5	-.1407(-2) -j.1742(-1)	.6642(-2) -j.1767(-1)	.1828(-1) -j.1773(-1)	.2994(-1) -j.1773(-1)

formulation breaks down. In the same table, the behavior of S(N) is tested for values of w/λ different from those of the resonant separations, and good converging behavior is observed. The values of S(10000) will be used as a testing base for determining the correctness of the approximated series (6.18) in the next paragraph.

The approximated series (6.18) is denoted by s(L) and takes the following form:

$$s(L) = \sum_{n=0}^{L} \frac{e^{-jk|\vec{\rho}-\vec{\rho}' + (2nw)\hat{z}|}}{2\pi k|\vec{\rho}-\vec{\rho}' + (2nw)\hat{z}|} - \left[\sum_{n=1}^{L} \frac{e^{-jk(2nw)}}{4\pi nkw} + \frac{1}{4\pi kw} \ln(1-e^{-j2kw})\right] . \qquad (F.2)$$

In Table F.2 the relative error r(L), as defined below, is listed for different values of L and w/λ. The relative error r(L) is defined as

$$r(L) = \frac{|S(10000) - s(L)|}{|S(10000)|} \times 100 . \qquad (F.3)$$

Table 6.A.2 has been divided into four sections. The first section displays the values of r(L) for small values of w/λ such that $.1 \leq w/\lambda \leq .5$. The second section shows r(L) for values of w/λ close to the resonant separation $w/\lambda = 2$, namely, $1.95 \leq w/\lambda \leq 2.05$. The third section exhibits r(L) for values of $2.1 \leq w/\lambda \leq 10.5$. For all the cases mentioned above, except exactly at the resonant separations, Equation (F.2) provides a good approximation to Equation (F.1) when $L \leq 20$. For $L = 20$, the relative error is less than 1 percent, which indicates that rather than summing up (F.1), for instance 10000 times for each value of $|\vec{\rho}-\vec{\rho}'|$, one can only sum them up 20 times and use Equation (F.2). This, of course, provides a very significant saving of computer time. Table F.2 also shows that calculations may be performed with good accuracy for values of w/λ very close to the resonant separations.

TABLE F-2

RELATIVE ERROR

$$r(L) = |S(10000) - s(L)| \times 100/|S(10000)|$$

L / w/λ	5	10	20	40	60	80	100
.5	355.9	352.6	351.8	353.5	351.6	351.6	351.6
.6	24.92	7.215	1.925	.4959	.2229	.1267	.8219(-1)
.7	9.129	2.609	.6930	.1784	.8028(-1)	.4571(-1)	.2978(-1)
.8	4.695	1.351	.3599	.9275(-1)	.4179(-1)	.2385(-1)	.1561(-1)
.9	5.288	1.577	.4258	.1103	.4981(-1)	.2852(-1)	.1876(-1)
1.	333.4	332.7	332.6	332.6	332.6	332.6	332.6
1.95	3.021	.9471	.2634	.6941(-1)	.3199(-1)	.1907(-1)	.1341(-1)
1.96	3.517	1.144	.3244	.7654(-1)	.4656(-1)	.1736(-1)	.1669(-1)
1.97	4.272	1.441	.4099	.1042	.5750(-1)	.4021(-1)	.2245(-1)
1.98	5.554	1.9773	.6323	.1776	.6599(-1)	.2840(-1)	.3490(-1)
1.99	8.246	3.272	1.098	.3810	.1294	.1153	.7719(-1)
1.999	9.231	6.903	3.358	1.539	.9129	.5880	.3932
1.9999	10.06	6.295	4.259	3.201	2.843	2.663	2.555
2.	298.2	298.1	298.1	298.2	298.2	298.2	298.2
2.01	3.562	1.409	.4915	.1258	.8163(-1)	.3475(-1)	.2799(-1)
2.02	2.610	.9199	.2688	.1256(-1)	.4062(-1)	.2745(-1)	.1462(-1)
2.03	2.074	.6762	.1998	.5564(-1)	.2098(-1)	.7992(-2)	.9963(-2)
2.04	1.731	.5378	.1493	.4358(-1)	.1377(-1)	.1315(-1)	.7641(-2)
2.05	1.494	.4541	.1244	.3240(-1)	.14851(-1)	.8854(-2)	.6268(-2)
2.1	.9652	.2760	.7340(-1)	.1897(-1)	.8700(-2)	.5201(-2)	.3695(-2)
2.2	.7666	.2145	.5664(-1)	.1463(-1)	.6730(-2)	.4045(-2)	.2895(-2)
2.3	.8439	.2372	.6276(-2)	.1624(-1)	.7494(-2)	.4529(-2)	.3265(-2)

TABLE F-2 (CONTINUED)

2.4	1.240	.3604	.9660(-1)	.2514(-1)	.1165(-1)	.7084(-2)	.5145(-2)
2.5	299.3	299.3	299.3	299.3	299.3	299.3	299.3
10.	235.8	235.8	235.8	235.8	235.8	235.8	235.8
10.1	.5384(-1)	.1544(-1)	.4132(-2)	.1186(-2)	.7284(-3)	.6183(-3)	.5871(-3)
10.2	.3455(-1)	.9659(-2)	.2567(-2)	.7394(-3)	.4545(-3)	.3853(-3)	.3639(-3)
10.3	.3503(-1)	.9817(-2)	.2617(-2)	.7568(-3)	.4662(-3)	.3952(-3)	.3732(-3)
10.4	.5596(-1)	.1617(-1)	.4374(-2)	.1276(-2)	.7878(-3)	.6672(-3)	.6293(-3)
10.5	221.2	221.2	221.2	221.2	221.2	221.2	221.2

REFERENCES

Abramowitz, M., I. A. Stegun, eds. (1970), Handbook of Mathematical Functions, Dover Publications, Inc., New York.

Andrews, C. L. (1950), "Diffraction Pattern in a Circular Aperture Measured in the Microwave Region," J. Appl. Phys., Vol. 22, pp. 761-767.

Arsac, J. (1966), Fourier Transforms and the Theory of Distributions, Prentice-Hall, Inc., Englewood Cliffs, New Jersey.

Baker, B. B., and E. T. Copson (1953), The Mathematical Theory of Huygen's Principle, Oxford University Press, Amen House, London.

Bethe, H. A. (1944), "Theory of Diffraction by Small Holes," Phys. Rev., Vol. 66, pp. 163-182.

Bouwkamp, C. J. (1953), "Diffraction Theory," Mathematics Research Group, New York Univ., New York, N. Y., EM-50.

Bouwkamp, C. J. (1970), "Theoretical and Numerical Treatment of Diffraction Through a Circular Aperture," IEEE Trans. Antennas Propagat., Vol. AP-18, pp. 152-176.

Bowman, F. (1958), Introduction to Bessel Functions, Dover Publications, Inc., New York.

Brigham, E. O. (1974), The Fast Fourier Transform, Prentice-Hall, Inc., New Jersey.

Chen, K. C., and C. E. Baum (1974), "On EMP Excitations of Cavities with Small Openings," Interaction Note 170. Air Force Weapons Lab., Albuquerque, New Mexico.

Chen, L. W. (1970), "On Cavity Excitation Through Small Apertures," Interaction Note 45. Air Force Weapons Lab., Albuquerque, New Mexico.

Collin, R. E. (1960), Field Theory of Guided Waves, McGraw-Hill, New York.

Collin, R. E. and F. J. Zucker (1969), Antenna Theory, Part I, McGraw-Hill, New York.

Copson, E. T. (1946), "An Integral Equation Method of Solving Plane Diffraction Problem," Proc. Roy. Soc. A 186, pp. 100-118.

Davis, W. A. (1974), "Numerical Solutions to the Problems of Electromagnetic Radiation and Scattering by a Finite Hollow Cylinder," Ph. D. Thesis, University of Illinois, Urbana, Illinois.

Deschamps, G. A. (1972), "Ray Techniques in Electromagnetics," Proc. IEEE, Vol. 60, pp. 1022-1035.

Dwight, H. B. (1965), Tables of Integrals and Other Mathematical Data, Macmillan, New York.

Eggiman, W. H. (1961), "Higher-Order Evaluation of Electromagnetic Diffraction by Circular Disks," IRE Trans. MTT, Vol. 9, No. 5, pp. 408-418.

Flammer, C. (1953), "The Vector Wave Function Solution of the Diffraction of Electromagnetic Waves by Circular Disks and Apertures," I: "The Oblate Spheroidal Vector Wave Function," J. Appl. Phys., Vol. 24, pp. 1218-1223; II: "The Diffraction Problem," pp. 1224-1231.

Grinberg, G. A., and Yu. V. Pimenov (1957), "On the Question of Diffraction of Electromagnetic Waves from Infinitesimally Thin Ideally Conducting Screens," Soviet Phys. JETP, Vol. 2, pp. 2160-2175.

Hamming, R. W. (1973), Numerical Methods for Scientists and Engineers, McGraw-Hill, New York.

Hansen, W. W. (1935), "A New Type of Expansion in Radiation Problems," Phys. Rev., 47, pp. 139-143.

Harrington, R. F. (1961), Time-Harmonic Electromagnetic Fields, McGraw-Hill, New York.

Harrington, R. F. (1968), Field Computation by Moment Methods, Macmillan, New York.

Hollis, J. S., T. J. Lyon and L. Clayton (1970), Microwave Antenna Measurement, Scientific-Atlanta, Atlanta, Georgia.

Jackson, J. D. (1962), Classical Electrodynamics, John Wiley and Sons, Inc., New York.

Javid, M. and P. M. Brown (1963), Field Analysis and Electromagnetics, McGraw-Hill, New York.

Jones, D. S. (1952), "Diffraction by an Edge and by a Corner," Quart. J. Mech. Appl. Math., Vol. 5, pp. 363-378.

Jones, D. S. (1956), "A New Method for Calculating Scattering with Particular Reference to the Circular Disc," Comm. Pure and Appl. Math., Vol. 9, pp. 713-746.

Jones, D. S. (1964), The Theory of Electromagnetism, Pergamon Press, New York.

Jordan, E. C. and K. G. Balmain (1968), Electromagnetic Waves and Radiating Systems, Prentice-Hall, Englewood Cliffs, New Jersey.

Keller, J. B., R. M. Lewis and B. D. Seckler (1957), "Diffraction by an Aperture. II," J. Appl. Phys., Vol. 28, pp. 570-579.

Keller, J. B. (1962), "Geometrical Theory of Diffraction," J. Appl. Phys., Vol. 28, pp. 426-444.

Kirchhoff, G. (1891),"Vonlesungen über math," Physik, 2 (Optik).

Kleinman, R. E. (1967), "Low Frequency Solution of Electromagnetic Scattering Problems," Electromagnetic Wave Theory, ed. J. Brown, pp. 891-905, Pergamon Press, London.

Kuritsyn, V. N. (1961), "Arbitrary Incidence of a Plane Wave on a Conducting Disk," Soviet Phys. JETP, Vol. 5, pp. 744-752.

Liu, Y. P. (1969), "Penetration of Electromagnetic Fields Through Small Apertures into Closed Shields," Interaction Note 48, Air Force Weapons Lab., Albuquerque, New Mexico.

Levine, H. and J. Schwinger (1950), "On the Theory of Electromagnetic Wave Diffraction by an Aperture in an Infinite Plane Conducting Screen," Comm. Pure and Appl. Math., Vol. 3, pp. 355-391.

Li, T. S. (1972), "A Spectral Domain Approach to the Numerical Solution of Electromagnetic Scattering Problems," Ph. D. Thesis, University of Illinois, Urbana, Illinois.

Lin, J. L., W. L. Curtis, and M. C. Vincent (1974), "On the Field Distribution of an Aperture," IEEE Trans. on Antennas and Propagation, Vol. AP-22, pp. 467-471.

Magnus, W. and F. Oberhettinger (1949), Formulas and Theorems for the Special Functions of Mathematical Physics, Chelsea Publishing Co., New York.

Maxwell, J. C., ed. (1879), Electrical Researchers of the Hon. Henry Cavendish, FRS (1971-1981), Cambridge University Press.

Maxwell, J. C. (1890), The Scientific Papers of James Clark Maxwell, ed., W. D. Niven, Dover Publications, Inc., New York.

Meixner, J. and W. Andrejewski (1950), "Strenge Theorie der Beugung Ebener Elektromagnetischer Wellen an Der Volkommen, Leitenden Kreisscheibe Und an Der kreisförmigen Öffnung im Volkommen Ieitenden Schirm," Ann. Phys., Vol. 7, pp. 157-168.

Mentzer, J. R. (1955), Scattering and Diffraction of Radio Waves, Pergamon Press, New York.

Mikhlin, S. G. (1957), Integral Equations, Pergamon Press, London.

Mikhlin, S. G. (1967), Linear Equations of Mathematical Physics, Holt, Rinehart and Winston, Inc., New York.

Mittra, R. (1961), "Solution of a Class of Dual Integral Equations," Technical Report No. 51, Electromagnetics Laboratory, University of Illinois, Urbana, Illinois.

Mittra, R., ed. (1973), Computer Techniques for Electromagnetics, Pergamon Press, Oxford.

Mittra, R. and S. W. Lee (1971), Analytical Techniques in the Theory of Guided Waves, Macmillan, New York.

Mittra, R., Y. Rahmat-Samii, D. V. Jamnejad and W. A. Davis (1973), "A New Look at the Thin-Plate Scattering Problem," Interaction Note 155.

Morse, P. M., and H. Feshback (1953), Methods of Theoretical Physics, Part II, McGraw-Hill, New York.

Muller, C. (1969), Foundations of the Mathematical Theory of Electromagnetic Waves, Springer-Verlag, New York.

Muller, R. (1961), "Theory of Cavity Resonators," in Electromagnetic Waveguides and Cavities, Chapter 2, ed. G. Goubau, Pergamon Press, New York.

Nomura, Y. and S. Katsura (1955), "Diffraction of Electromagnetic Waves by Circular Plates and Circular Holes," J. Phys. Soc. Japan, Vol. 10, pp. 285-304.

Papoulis, A. (1962), The Fourier Integral and its Applications, McGraw-Hill, New York.

Pöggio, A. J. and E. K. Miller (1973), "Integral Equation Solutions for Three Dimensional Scattering Problems," in Computer Techniques for Electromagnetics, Chapter 4, ed., R. Mittra, Pergamon Press, New York.

Rahmat-Samii, Y. (1974), "On the Application of the Theory of Generalized Functions in Constructing the Dyadic Green's Function at the Source Region in Waveguides, Cavities, and in Free Space," 1974 IEEE G-AP International Symposium, Boulder, Colorado.

Rahmat-Samii, Y. and R. Mittra (1974), "Integral Equation Solution and RCS Computation of a Thin Rectangular Plate," IEEE Trans. on Antennas and Propagation, Vol. AP-22, No. 4, pp. 608-610.

Ransom, P. L. (1972), "Evaluation of the Fourier Integral Using the Fast Fourier Transform," Antenna Laboratory Report No. 72-9, University of Illinois, Urbana.

Rayleigh, Lord (1817), "On the Incidence of Aerial and Electric Waves on Small Obstacles in the Form of Ellipsoids or Elliptic Cylinders, on the Passage of Electric Waves Through a Circular Aperture in a Conducting Screen," Phil. Mag., Vol. 44, p. 28.

Robinson, H. L. (1953), "Diffraction Patterns in Circular Apertures Less than One Wavelength in Diameter," J. Appl. Phys., Vol. 24, pp. 35-38.

Ross, R. A. (1966), "Radar Cross Section of Rectangular Flat Plates as a Function of Aspect Angle," IEEE Trans. Antennas and Propagation, Vol. AP-14, pp. 329-335.

Ruck, C. T., ed. (1970), Radar Cross Section Handbook, Plenum, New York.

Sancer, M. I. and A. D. Varvatsis (1970), "Electromagnetic Penetrability of Perfectly Conducting Bodies Containing an Aperture," Interaction Note 49, Air Force Weapons Laboratory, Albuquerque, New Mexico.

Sneddon, I. N. (1957), Elements of Partial Differential Equations, McGraw-Hill, New York.

Sneddon, I. N. (1972), An Introduction to the Use of Integral Transforms, McGraw-Hill, New York.

Sommerfeld, A. (1967), Partial Differential Equations in Physics, Academic Press, New York.

Spiegel, R. S. and D. E. Young (1973), "The Field Computation in a Rectangular Aperture by a Moment Method Solution," 1973 IEEE GAP International Symposium, Boulder, Colorado.

Stackgold, I. (1967), Boundary Value Problems of Mathematical Physics, Vol. I, Macmillan, New York.

Stevenson, A. F. (1953), "Solution of Electromagnetic Scattering Problems as Power Series in the Ratio (Dimensions of Scatterer)/Wavelength," J. Appl. Phys., Vol. 24, pp. 1134-1142.

Stratton, J. A. (1941), Electromagnetic Theory, McGraw-Hill, New York.

Suzuki, M. (1956), "Diffraction of Plane Electromagnetic Waves by a Rectangular Aperture," I.R.E. Trans. on Antennas and Propagation, Vol. AP-4, pp. 149-155.

Tai, C. T. (1971), Dyadic Green's Functions in Electromagnetic Theory, Intext Educational Publishers, Scanton, Pennsylvania.

Taylor, C. D. (1971), "Electromagnetic Pulse Penetration through Small Apertures," Interaction Note 74.

Tesche, F. M. (1972), "On the Singularity Expansion Method as Applied to Electromagnetic Scattering from Thin-Wires," Interaction Note 102.

Titchmarsh, E. C. (1937), Introduction to the Theory of Fourier Integrals, Oxford, New York.

Ufimtsev, P. Ya. (1962), Method of Edge Waves in the Physical Theory of Diffraction, Air Force Systems Command, Foreign Technology Division, Document ID No. FTD-HC-23-259-71 (1971). (Translation of Method Krayevykh Voiln fizicheskoy teorii difraktsii, Sovetskoye Radio, 1962.)

Uslenghi, P. L. E. (1972), "High-Frequency Scattering Methods," Scientific Report, Department of Information Engineering, University of Illinois at Chicago Circle.

Van Bladel, J. (1961), "Some Remarks on Green's Dyadic for Infinite Space," IRE Trans. Antennas Propagation, Vol. 9, pp. 563-566.

Van Bladel, J. (1964), Electromagnetic Fields, McGraw-Hill, New York.

Van Bladel, J. (1972), "Small Apertures in Cavities at Low Frequencies," AEÜ, pp. 481-486.

Van Bladel, J. (1974), Summer 1974 Lecture Notes, University of Wisconsin, Madison, Wisconsin.

Werner, P. (1963), "On the Exterior Boundary Value Problem of Perfect Reflection for Stationary Electromagnetic Wave Fields," J. Math. Anal. Appl., Vol. 7, pp. 348-396.

Wilcox, C. H. (1956), "An Expansion Theorem for Electromagnetic Fields," Comm. Pure Appl. Math., Vol. 9, pp. 115-134.